EVIDENCE FOR A LUMINAL, CALCIUM-MEDIATED CROSS TALK BETWEEN SERCA1 PUMPS AND RyR1 CALCIUM RELEASE CHANNELS IN HEAVY SARCOPLASMIC RETICULUM (HSR) MEMBRANES

BY

CHRIS G. PALAHNIUK

A Thesis
Submitted to the Faculty of Graduate Studies
in Partial Fulfillment of the Requirements
for the Degree of

MASTERS OF SCIENCE

Department of Oral Biology, and
The Division of Stroke and Vascular Disease
University of Manitoba
Winnipeg, Manitoba

THE UNIVERSITY OF MANITOBA

FACULTY OF GRADUATE STUDIES

*****

COPYRIGHT PERMISSION PAGE

Evidence for a Luminal, Calcium-Mediated Cross Talk Between Serca1 Pumps and RyR1 Calcium Release Channels in Heavy Sarcoplasmic Reticulum (HSR) Membranes

BY

Chris G. Palahniuk

A Thesis/Practicum submitted to the Faculty of Graduate Studies of The University of Manitoba in partial fulfillment of the requirements of the degree of Masters of Science

TABLE OF CONTENTS

Acknowledgments

First and foremost I'd like to thank (over and over) my life partner and endless source of love, encouragement, support, and happy thoughts. Noriko, I could not have finished the beast of burden without you. My appreciation is also extended to my lab confidante and good friend Bernard Abrenica. Bernie, as we both know, it has been an absorbing ride. The many 'coffee' excursions always kept me going when I thought perhaps I couldn't. Thanks for your ear. Thanks be to the gods! Tom Cook deserves a big pat on the back side for putting up with my interesting laboratory techniques and results. His guidance (especially on beer breaks) helped shape my confidence in my lab skills and abilities. Thanks old fella. I'd also like to thank my supervisor, James Gilchrist, for all the in depth conversations and guidance during my Masters career. You were right, it was a maturation process. Finally thanks go out to my committee, Larry Hryshko and Raj Bhullar, for all the important comments and insight you had in the process leading up to completion.

Table of Abbreviations

The common abbreviations used in this document are listed in the following table.

Abbreviation	Unabbreviated Terminology
CICR	Ca^{2+}-induced Ca^{2+} release
HSR	heavy sarcoplasmic reticulum
SERCA1	sarco-endoplasmic reticulum Ca^{2+} ATPase
RyR1	ryanodine receptor/Ca^{2+} release channel
CSQ	calsequestrin
DHPR	dihydropyridine receptors
Tg	thapsigargin
CPA	cyclopiazonic acid
CG2	Calcium Green-2
MF2	Mag-Fura 2
CTC	chlortetracycline

Abstract

The potential for luminal Ca^{2+} to modulate the activity of both SERCA1 pumps and RyR1 channels was examined in isolated skeletal muscle heavy sarcoplasmic reticulum vesicles. A synchronous assay was developed using Calcium Green-2 to monitor extravesicular Ca^{2+} and NADH oxidation as an indicator of SERCA1 activity. Results from these assays demonstrated that SERCA1 pumps responded with near-maximal activity (4200 nmol/mg/min for Ca^{2+}-induced activation, 4400 for ryanodine-induced activation) to RyR1-mediated Ca^{2+} leak states. Cytosolic Ca^{2+} alone was shown to insufficiently stimulate SERCA1 activity. Threshold luminal Ca^{2+} loading (~150 nmol/mg) of HSR membranes both sensitized the RyR1 to activation and back-inhibited the SERCA1 such that the pump was sensitized to treatment with sub-stoichiometric concentrations of thapsigargin. Similar treatment of membranes with sub-stoichiometric thapsigargin or cyclopiazonic acid collapsed steady state, outwardly directed, Ca^{2+} gradients demonstrating that maintenance of such gradient was dependent upon active, basal SERCA1 activity. Decreasing the rate of Ca^{2+} gradient formation, with thapsigargin or cyclopiazonic acid, during active Ca^{2+} sequestration resulted in activated RyR1 channels and increased SERCA1 catalytic activity.

To better determine how Ca^{2+} was distributed in the lumen of HSR membranes two luminal fluorophores, Mag-Fura 2 and chlortetracycline were employed. The data indicated that Mag-Fura 2 reported on a shallow, free, ionomycin insensitive, SERCA1-sensitive, and rapidly exchangeable luminal Ca^{2+} pool. The maximum determined ceiling of this free Ca^{2+} pool was ~50 μM. On the other hand, chlortetracycline probably reported on Ca^{2+} in the mM range. This luminal Ca^{2+} probe was also shown to undergo

2.5-fold fluorescence enhancement in the presence of the luminal Ca^{2+} binding protein, calsequestrin. In Ca^{2+} transport assays, Ca^{2+} was shown to enter the free Ca^{2+} pool before binding to calsequestrin. Ca^{2+}-induced Ca^{2+} release was accompanied by large increases in the free Ca^{2+} pool coinciding with large decreases in the bound Ca^{2+} pool. The evidence provided here demonstrates that the chlortetracycline, bound, luminal Ca^{2+} compartment is sensitive to open states of the RyR1. The Mag-Fura 2, free, luminal Ca^{2+} compartment responded with fluorescence increases upon activation of SERCA1 pumps. Together it becomes clear that minimized free luminal Ca^{2+}, due to the presence of basal levels of SERCA1 activity, facilitated the accumulation of Ca^{2+} in the RyR1-associated bound luminal Ca^{2+} pool. This luminal Ca^{2+} exchange appeared important for the generation of high, outwardly directed Ca^{2+} gradients and the sensitization of RyR1 channels to activation. Therefore the activities of both the SERCA1 and the RyR1 appear intertwined through a luminal, Ca^{2+} mediated, cross talk, such that the formation of SERCA1-mediated luminal Ca^{2+} gradients required for RyR1-mediated Ca^{2+} releases is dependent upon the distribution of Ca^{2+} between free and bound luminal Ca^{2+} compartments.

List of Figures

LITERATURE REVIEW

RESULTS

Introduction

Skeletal muscle contraction is initiated by the release of Ca^{2+} from the terminal cisternae of the sarcoplasmic reticulum. It is now generally accepted that four dihydropyridine receptors (DHPR's) on the transverse tubular membrane are in alignment with every second ryanodine receptor (RyR1) on the terminal cisternal membrane (16). Each DHPR is associated with a single RyR1 monomer. The current proposal for the transfer of signal across the triadic gap has aligned DHPR's functionally controlling Ca^{2+} release from their RyR1 counterparts, but unaligned RyR1's are activated through secondary Ca^{2+}-induced Ca^{2+} release (CICR) mechanisms. The observation that not all RyR1's are located at the triadic junction but also along flanking regions of the jSR, also referred to as corbular jSR, supported this secondary CICR hypothesis of skeletal muscle SR Ca^{2+} release (7, 208).

Muscle relaxation occurs by the sequestration of Ca^{2+} in the longitudinal SR where sarco-endoplasmic reticulum Ca^{2+}-ATPase (SERCA) pumps are uniformly distributed (103). Yet there is also evidence that SERCA pumps are located on the corbular jSR, in close proximity to the RyR1 channels (133). Transport of Ca^{2+} occurs with the binding of Ca^{2+} to high affinity binding sites accessible from the cytosol. Subsequent conformational changes accompany the transition of these binding sites from high to low affinity, which are now orientated towards the SR lumen. Luminal low affinity Ca^{2+} binding sites and their Ca^{2+} occupation under conditions of increased luminal Ca^{2+} have been implicated in back-inhibition of the SERCA1 pump (122). Specific inhibitors of the SERCA family of Ca^{2+} pumps have also been characterized. Thapsigargin (Tg) and cyclopiazonic acid (CPA) are two inhibitors that have been shown

to preferentially bind the Ca^{2+} free enzyme and slow the forward reaction at low concentrations while irreversibly inhibiting the pump at higher concentrations with a 1:1 binding stoichiometry (137, 213, 224). Dettbarn and Palade (54a) have recently demonstrated that Tg- and CPA-induced Ca^{2+} effluxes from HSR vesicles were inhibited by ruthenium red.

Studies of skeletal muscle SR Ca^{2+} release have been advanced with early findings that different fractions of the SR could be isolated (176). Both triadic (containing t-tubular membranes and jSR membranes) and heavy sarcoplasmic reticulum (HSR) (containing just jSR) membranes have been characterized (40, 270). The presence of DHPR receptors (on triadic membranes), the RyR1, the luminal Ca^{2+} binding protein calsequestrin (CSQ), SERCA1 pumps and possibly the full complement of junctional proteins (on triadic and HSR membranes) have made vesicles useful for studying SR Ca^{2+} uptake and Ca^{2+} release under quasi-physiological conditions (51a). The phenomenon of CICR was first described by Endo using skinned muscle fibers (63). These early observations demonstrated that a minimum level of Ca^{2+} load was required for CICR and that Mg^{2+} was an inhibitor of the Ca^{2+} release process. Subsequently, CICR has been observed in HSR vesicles, with increased RyR1 activation in the presence of μM Ca^{2+}, mM ATP and low μM ryanodine (79, 178) and RyR1 inhibition by mM Mg^{2+} and Ca^{2+} , μM ruthenium red (248), and high μM ryanodine (233). Indeed, the specific binding of the plant alkaloid, ryanodine, to the Ca^{2+} release channel proved useful for initial isolation of the RyR1 and incorporation into planar lipid bilayers (120, 126, 209).

Single channel studies of the RyR1 incorporated into lipid bilayers have been useful in establishing and identifying RyR1 channel modulators that influenced the gating characteristics of the protein in isolation. However, the results of these studies have sometimes been contradictory. Of importance, the influence of luminal/*trans* Ca^{2+} has been shown to decrease (160), increase (95, 243), or bimodally (273) influence single channel open probability. Increased RyR1 activity, including bimodal increases followed by decreases in channel activity, were thought to occur either by (a) luminal Ca^{2+} acting at luminal Ca^{2+} binding sites (95) or (b) luminal Ca^{2+} fluxes through the RyR1 having access to cytosolic high affinity activation/low affinity inactivation Ca^{2+} binding sites (273).

One explanation for varied results from single channel studies has been the absence of accessory proteins implicated in formation of protein complexes at the SR junctional face membrane and possible control of RyR1-mediated Ca^{2+} release (51a, 170a). A protein complex at the skeletal muscle jSR is thought to exist in vivo, consisting of the anchoring membrane proteins junctin and triadin, the luminal Ca^{2+} binding protein, calsequestrin, and the Ca^{2+} release channel, RyR1 (294). This complex may modulate activation of the RyR1 through Ca^{2+} binding and altered affinities of these proteins for one another. The consequences of these protein-protein interactions, as well as the influence of proteins like calmodulin and FKBP12, upon RyR1 function remains to be fully determined. Therefore for the study of SR Ca^{2+} release an intact a preparation as possible appears physiologically appropriate.

As with single channel experiments the influence of luminal Ca^{2+} upon RyR1 activation in vesiculated SR preparations has not been well established. Ikemoto has

suggested that the Ca^{2+} gradient across HSR membranes is an important regulator of the coordination between Ca^{2+} uptake and Ca^{2+} release (118, 226). In these studies there was a luminal Ca^{2+} load dependence to Ca^{2+} release and increases in luminal Ca^{2+} were shown to favor Ca^{2+} release and back inhibit Ca^{2+} uptake. The influence of luminal Ca^{2+} in favoring back inhibition of the SERCA1 pump has been previously characterized (122). Other studies have suggested there may be a role for luminal Ca^{2+} cycling between the RyR1 and SERCA1 (170a). These studies supported the coordination between activation of RyR1, reduced luminal Ca^{2+} and activation of SERCA1. Ikemoto has demonstrated a transient rise in luminal Ca^{2+} that precedes Ca^{2+} release and suggested a change in Ca^{2+} binding to CSQ may mediate these luminal changes (118, 225). These observations were further supported with the increased sensitivity of RyR1's to ryanodine treatment upon luminal Ca^{2+} loading of HSR membranes (90). Distinctions between free luminal Ca^{2+} and bound luminal Ca^{2+} (to CSQ) have also raised the possibility of a direct interaction of CSQ on the RyR1 and/or the RyR1 on CSQ for mediating luminal Ca^{2+} effects upon the Ca^{2+} release channel (54).

Discrepancies in the literature pertaining to luminal Ca^{2+}, as well as an absence of information regarding Ca^{2+} control mechanisms on the corbular jSR, where RyR1's and SERCA1's are both present in close proximity, led to the hypothesis that rates of Ca^{2+} gradient formation across HSR membranes governed by SERCA1 activity impact the manner in which RyR1 channels are activated. Furthermore, we propose that the sequestration of luminal Ca^{2+} influences states of SERCA1 pumps and RyR1 channels such that luminal Ca^{2+} is a means by which pumps and channels communicate. Using HSR membranes, an assay system was developed that allowed synchronous monitoring

of SERCA1 catalytic activity and cytosolic Ca^{2+} transients. The use of Calcium Green-2 as the cytosolic Ca^{2+} probe and NADH fluorescence as an indicator of SERCA1 ATP hydrolysis through a coupled enzyme assay led to the finding that formation of RyR1 Ca^{2+} leak states were accompanied by activation of SERCA1 pumps. In these experiments luminal Ca^{2+} proved important for sensitizing the RyR1 to activation by cytosolic Ca^{2+}. Luminal Ca^{2+} was further shown to sensitize both the SERCA1 to Tg inhibition, and the RyR1 to ryanodine activation.

Not only was luminal Ca^{2+} important for modulation of Ca^{2+} release and Ca^{2+} sequestration but the rate at which it was sequestered to the lumen proved equally important. When SERCA1 pumps were slowed by Tg treatment or by rapid Ca^{2+} loading, the efflux of Ca^{2+} from the lumen was favored. The requirement of threshold luminal Ca^{2+} concentrations for CICR led to the incorporation of the luminal Ca^{2+} indicators, Mag-Fura-2 and chlortetracycline, into well-defined Ca^{2+} transport protocols. These luminal indicators were important in the identification of two distinct luminal Ca^{2+} pools. Our data indicates that CTC reports on a CSQ-bound luminal Ca^{2+} compartment while MF2 reports on a shallow, free, possibly RyR1 associated, luminal Ca^{2+} pool. Increases in MF2 and decreases in CTC fluorescence accompanied RyR1 activation, while the movement of Ca^{2+} from the MF2-visible Ca^{2+} compartment into the CTC-visible compartment occurred during RyR1 inactivation. These results indicate that the SERCA1 and RyR1 may be intimately regulated by a luminal Ca^{2+} cross talk governed by formation of Ca^{2+} gradients and the binding of Ca^{2+} to luminal Ca^{2+} buffers like CSQ.

Literature Review

'the molecular mechanism of the Ca2+ release process in excitation-contraction coupling in muscle is one of the most important unsolved problems in muscle physiology and cell biology'. (192)

I. A Brief Historical Perspective

IA. *An ultra-structural description of muscle contraction: the role of Ca^{2+} in cross bridge formation*

The functional unit of skeletal muscle is a sarcomere. A skeletal muscle can be morphologically described as consisting of parallel groupings of multinucleated muscle cells referred to as muscle fibers. Muscle fibers, in turn, are made up of bundles of myofibrils, the basic contractile element of muscle fibers. Sarcomeres are the repeating units of myofibrils as seen through microscopic analysis. Differential light and dark areas can be observed on the surface of muscle fibers as well as repeating in a similar fashion on myofibrils. The terms *A band* and *I band* have been used to describe the repeating dark and light areas, respectively (see Plate 1(B)). The lighter area within the *A band* has been called the *H zone* which is separated by a central darker line, the *M line*. The *I band* contains a dark central line, the *Z line*, and a sarcomere is the area between two repeating *Z lines*. Myofibrils appear as they do microscopically due to ultrastructural organization of components of the sarcomere. The *A band* contains myosin thick filaments that either have no overlap (*H zone*) or overlap (dark outer areas) with actin

thin filaments. The *I band* is where thin filaments originate, at the *Z line*, extending in both directions to overlap with myosin thick filaments in two adjacent sarcomeres (60).

Observations made with the light microscope and later the electron microscope, were important in deducing how these gross morphological regions interacted during muscle contraction. Initial studies showed that *I bands* and *H zones* became compressed while *A bands* remained unchanged as a sarcomere shortened. Electron micrographs demonstrated that as sarcomeres were stretched or shortened the *A* and *I bands* did not undergo changes in length but did change the extent to which they overlapped. These observations resulted in the sliding-filament theory of muscle contracture which stated that sarcomere shortening/muscle contracture was a consequence of actin thin filaments sliding over the myosin thick filaments and being drawn closer to the *M line*. It was shortly there-after that sliding was shown to be functionally controlled by the attachment of myosin heads to the actin thin filaments and that pivoting of the myosin head group actively pulled the thin filaments closer to the *M line*. In the late 1960's, there was much debate over the role of Ca^{2+} in muscle contraction which resulted in theories about the involvement of a so-called 'relaxing factor' which was released following contraction. It was not until the discovery of a protein complex consisting of troponin T, C and I and the definitive Ca^{2+}-binding properties of these subunits that led to the general acceptance of the role of Ca^{2+} in contraction. Experiments with isolated actomyosin (isolated actin + isolated myosin) showed that it retains the ability to hydrolyze ATP. When tropomyosin and troponin were added back to actomyosin, the ATPase activity was subsequently inhibited. The addition of Ca^{2+} removed this inhibition. Thus, tropomyosin and troponin were postulated to associate in such a manner that they blocked the linkage between the

heavy meromyosin globular protein heads (site of ATPase activity) and the actin thin filaments. These findings were instrumental in showing that Ca^{2+} was involved in cross bridge formation. Tropomyosin was found to directly overlay or block the myosin binding site on actin. When the troponin C subunit binds Ca^{2+}, a resultant change in the interactions between troponin T, C, and I, further results in the repositioning of tropomyosin. This in turn, unveils a binding site on the actin filaments for the attachment of the myosin globular heads. The hydrolysis of ATP causes the pivoting of the myosin heads and ultimately muscle shortening (59).

IB. ***The role of the sarcoplasmic reticulum in E-C coupling***

In the early 1900's, different terminology represented the *Z line, A band, and I band* that were just now gaining popularity to describe the morphological characteristics of muscle fibers using microscopic techniques (245). The comparison between earlier observations and current definitions of the dark and light zones of skeletal muscle are shown in Plate 1 (A) and (B). Also noted in (A) are early observations of the sarcoplasmic reticulum (SR). It was first observed in various muscle fiber types using rudimentary silver staining techniques in the late 1800's and early 1900's, designated in Plate 1 (A) with the letter b. It was initially described as a delicate lattice work at the A-I junction and at the time was called the transverse reticula (278). Yet, staining and microscopic techniques of the time failed to allow wide spread confirmation of its existence. The SR was re-discovered in 1953 by Bennet and Porter using electron microscopy techniques (11). These later descriptions detailed an organization of tubules and vesicles between the myofibrils that were limited by simple, smooth (no attached

particles) membranes, and had no observable internal structure. Observations that the SR repeated in phase with each sarcomere originally implicated it as significant to muscle contraction. By 1957 the existence of a three unit group was recognized opposite the A-I band junction and an example of an electron micrograph of the structure is shown in Plate 1 (C) (75). It was noted that the outer two groups were contiguous with the SR, that they appeared as 'foot processes', and that they 'pushed' against the middle group (214). The three unit group was referred to as a triad. Two years later the middle group was noted as distinct from the SR groups. This 'transverse' group was also realized to be continuous with the plasma membrane (8). Andersson-Cedergren suggested at this time that the T group may conduct the stimulus for muscle contraction.

In a paper in 1947 titled "The action of various cations on muscle contraction", Heilbrunn and Wiercinski found the uniqueness of the Ca^{2+} ion was that it alone caused muscle contraction (106). Meanwhile, there were proposals that the underlying ion in muscle contraction may actually be K^{+} (260). Using both isolated fibers and minced muscle tissue, the Heilbrunn group demonstrated that only the addition of Ca^{2+} caused an immediate and pronounced shortening of their skeletal muscle preparations. The authors noted "*that the shortening which the calcium ion initiates when it comes in contact with muscle protoplasm is not a simple phenomenon involving just a protein and an ion. Rather there is growing evidence that a complicated clotting mechanism is involved and that the addition of calcium is just the first step in a long chain of events*" (260). Indeed, the overall mechanism for Ca^{2+} control by the SR has proved to be a *long chain of events,* difficult to fully deduce.

By 1960 it was generally accepted that Ca^{2+} was key for muscle contraction yet the SR had not been implicated as the Ca^{2+} controlling system. Research efforts had been concentrated in unraveling the protein machinery that was involved in actual contraction. Because of the similarities to the endoplasmic reticulum (ER) in other cells, it was thought the SR may be important in metabolite sequestration and transport (207). As had been previously done with the ER from various cell types, attempts were made to fractionate skeletal muscle and the SR in order to better determine its function (189). These experiments were the first to make the connection between the SR and the mechanical events of contraction. From these earliest attempts at obtaining triadic or heavy SR vesicles it was suggested that the SR was responsible for releasing a 'relaxing factor' that led to muscle relaxation. Then Ebashi (57) described how fragments of the SR and T system, also called muscle microsomes, bind Ca^{2+} in the presence of ATP. It was then proposed that the binding of Ca^{2+} by the SR may be the relaxing factor for skeletal muscle relaxation.

In the early 1960's studies involving Ca^{2+} and the SR gained prominence and two main observations were of critical importance. First, SR microsomal fractions contained an ATP-driven Ca^{2+} pump which was different from the actomyosin ATPase and effectively removed Ca^{2+} from the actomyosin systems causing muscle relaxation (58, 284). Second, Ca^{2+} oxalate precipitation (i.e. Ca^{2+} compartmentalization) in relaxed skeletal muscle fibers occurred principally in the SR lateral sacs of the triads (46, 102). This final observation led Costantin et al. to suggest that Ca^{2+} sequestration and compartmentalization in the lateral sacs of the SR, in close proximity to the T-tubule,

may be an indication that the release of Ca^{2+} from the SR is the signal for skeletal muscle contraction.

To further correlate the electrical events of T-tubule depolarization with the Ca^{2+} transients thought to cause muscle contraction and the Ca^{2+} transients with the actual mechanical event of contraction, Ashley and Ridgeway (9) used an intracellular electrode to record membrane potential, the photoprotein aequorin to record Ca^{2+} transients, and a force transducer to record isometric tension in a single, isolated depressor muscle of the acorn barnacle (Plate 2). The simultaneous recording allowed these three events to be correlated. These experiments demonstrated that depolarization of the membrane preceded the rise in cytosolic Ca^{2+} which in turn occurred prior to the development of isometric tension. Although this study did little in explaining how the Ca^{2+} transient was controlled by the SR, it did show that the Ca^{2+} signal was transient and that rises in Ca^{2+} were both intimately controlled by membrane depolarizations, and intimately related to the generation of tension. The authors did propose that Ca^{2+} release and Ca^{2+} removal from the cytosol were SR-controlled events. The use of aequorin, which the investigators extracted themselves from *Aequorea forskalea,* seemed to be the precursor to the advent of many Ca^{2+} sensitive probes.

By the early 1970's the control mechanisms of Ca^{2+} release from the SR were still unknown and the Ca^{2+} release channel had not been identified. Still working with isolated single fibers and a Ca^{2+} binding, metallochromatic dye, murexide, Endo (63) observed that Ca^{2+} release from the SR was an all or none process. Furthermore it was identified that an intrinsic property of the SR was that Ca^{2+} itself promoted the release of Ca^{2+}. Mg^{2+} was also shown to inhibit Ca^{2+} release from the SR. Importantly, the process

of Ca^{2+}-induced Ca^{2+} release (CICR) was described with the conclusion that it may indeed be the mechanism which explained the regenerative nature of muscle contraction following depolarization. The importance of determining the protein composition of the SR and the role of proteins like the Ca^{2+} release channel and the Ca^{2+}-ATPases in Ca^{2+} sequestration and release is presented in the following section.

II. The proteins involved in SR Ca^{2+} uptake, temporary Ca^{2+} storage and Ca^{2+} release

II.A. *The Sarco-endoplasmic Reticulum Ca^{2+} ATPase (Ca^{2+} pump)*

The sarco/endoplasmic reticulum Ca^{2+}-ATPase family of enzymes are ATP-driven Ca^{2+} pumps that actively translocate Ca^{2+} across cellular membranes (252). There are three genes that encode the SERCA pump isoforms SERCA1a and 1b, SERCA2a and 2b, and SERCA3a, 3b and 3c (156). Distribution of the SERCA protein products are shown in Table 1. The SERCA isoforms 1a (1b) and 2a are the only isoforms localized to the SR in the noted muscle cell types whereas other isoforms appear localized to the ER and outer membrane of the nuclear envelope in the tissue types specified in the table (133).

Table 1. Distributions of SERCA protein gene products.

SERCA ISOFORM	Location	Role
SERCA1a	adult fast-twitch skeletal muscle	muscle relaxation
SERCA1b	neonatal fast-twitch skeletal muscle	muscle relaxation
SERCA2a	cardiac muscle slow-twitch skeletal muscle	muscle relaxation
SERCA2b	smooth muscle brain	

SERCA3a	platelets lymphoid cells salivary glands endothelial cells purkinje neurons	
SERCA3b,3c	kidney pancreas	possibly cell proliferation

The role of SERCA1 in SR Ca^{2+} sequestration and ultimately skeletal muscle relaxation was not determined until the 1960's. The first reports of an ATPase on the SR membrane were made using particulate fractions from skeletal muscle referable to fragmented SR. Ebashi found that when these early forms of SR vesicles were given a continuous supply of ATP they had the ability to concentrate Ca^{2+} inside the membranes (58). Some years later, the Ca^{2+}-ATPase, mw 102,000 daltons, was the first protein to be isolated from skeletal muscle SR (163, 165). It was determined that the enzyme was the sole transporter of Ca^{2+} in the SR. Furthermore the Ca^{2+}-ATPase had sites for Ca^{2+} and Mg^{2+} binding, was phosporylated in the ATP to ADP exchange reaction, and that activity was abolished in the presence of Ca^{2+} chelators like EGTA.

The location of SERCA1 pumps along the SR membrane initially became evident from the proportion of SERCA1 pumps found in different isolated subsections during fractionation of the SR in early vesicle preparations. In an early paper by Meissner (176), three distinct 'types' of SR vesicles were recovered from 25 - 45% sucrose gradients as summarized in Table 2. The protein components of each type of SR vesicle are listed with the proportion of those proteins being Ca^{2+} pump represented as % Ca^{2+} pump. The nomenclature light (L), intermediate (I), and heavy (H) SR are now accepted terminology for referring to fractionated sarcoplasmic reticulum.

Table 2. Initial characterization of vesicles isolated from the skeletal muscle sarcoplasmic reticulum.

Vesicle	Location on Gradient	% Ca^{2+} Pump	Other Proteins	Appearance
LSR	28-32%	90%	-	empty sacs
ISR	32-39%	-	-	-
HSR	39-43%	55-65%	Ca^{2+} binding protein(25%) M55 protein (7%)	filled with electron dense material

It appeared from Meissners' study that the majority of SERCA1 was contained in longitudinal sections of the SR, yet large amounts of enzyme were recovered from the terminal cisternal, HSR fractions. Immunocytochemical studies have corroborated these early attempts at localizing SERCA pumps and found that the majority of Ca^{2+} pumps were indeed located at longitudinal SR membranes but that pumps were also found on the flanking regions of the terminal cisternal SR (133) alongside Ca^{2+} release channels. HSR vesicles were subsequently characterized further and shown to contain numerous other proteins (also further characterized) found in native SR. Characterization of the ISR fraction in the above study was neglected but it is now known that this fraction contains many of the proteins found in the HSR fraction but at a lesser extent.

The operational mechanisms of SERCA1 pumps from skeletal muscle SR has long been an area of intense research. The Ca^{2+} pump works on energy transduction where the chemical energy of ATP is converted to the translocation of Ca^{2+} across a membrane with the formation of an outwardly directed Ca^{2+} gradient. Early studies showed that ATP hydrolysis during a single SERCA1 pump cycle transported 2 Ca^{2+} ions into the lumen of the SR (103). Basic schemes were developed to include the binding of Mg^{2+}, the phosphorylation of the SERCA pump, and the translocation of Ca^{2+}

ions (5, 77, 114) as shown in Plate 3. Briefly, the SERCA enzyme (E) has 2 high affinity Ca^{2+} binding sites on the cytoplasmic side of the enzyme and been suggested to bind Ca^{2+} with a K_D of about 2 μM (241). The binding of Ca^{2+} to these sites is cooperative such that the binding of Ca^{2+} to the first site facilitates binding to the second Ca^{2+} transport site (125). The binding of both Ca^{2+} ions to these sites is a requirement for catalysis of ATP and subsequent transport (12). Ca_2-E is then phosphorylated by ATP in the presence of Mg^{2+} (23). Once the SERCA1 pump has been phosphorylated, a change in conformation of the enzyme occludes the Ca^{2+} ions from both the cytosol and lumen of the SR. The Ca_2-E-P configuration of the pump is inherently unstable and the Ca^{2+} ions are rapidly moved to the lumen and dissociate from the enzyme. The E-P state of the pump now has 2 low affinity Ca^{2+} binding sites facing the lumen of the SR. The bound Mg^{2+} and Pi are removed by hydrolytic cleavage of the enzyme and the SERCA pump returns to the E formation with the two Ca^{2+} binding sites once again positioned facing the cytosol.

The transport of 2 Ca^{2+} ions per Ca^{2+}-ATPase cycle requires an optimal pH between 6.5 and 6.8. Above or below these pH values, ATPase activity was markedly reduced. This possibly occurs by protonation of the enzyme at lower pH and the binding of Ca^{2+} being inhibited by H^+ ions (83, 230) and by proton limitation at higher pH (123). These effects of H^+ upon the Ca^{2+}-ATPase are thought to arise from a proton countertransport with Ca^{2+} making the SERCA1 similar to Ca/H- and Na/K-ATPases (291, 293) Another requirement for optimum SERCA pump activity is cytosolic Mg^{2+} concentrations of ~1-2 mM (15). Mg^{2+} binding to SERCA1 is still in debate as some believe that Ca^{2+} occupation of the high affinity sites decreases the affinity of the enzyme for Mg^{2+} (83) while others believe Mg^{2+} has a higher affinity for the enzyme in the

presence of Ca^{2+} (217). Higher concentrations of Mg^{2+} have been shown to have an inhibitory effect upon the catalytic turnover of the pump by locking the enzyme in a dead-end complex by binding to the low-affinity luminal Ca^{2+} binding sites (15).

Ca^{2+} itself has been shown to inhibit the Ca^{2+}-ATPase. While μM Ca^{2+} concentrations in the cytosol were shown to activate SERCA1 activity by promoting binding to the high-affinity Ca^{2+} binding sites, mM Ca^{2+} concentrations appear to inhibit enzymatic activity (290). It has been suggested that these high Ca^{2+} concentrations cause the formation of CaATP complexes that bind to the catalytic site instead of MgATP. Elevated luminal Ca^{2+} concentrations have also been shown to reduce SERCA1 activity possibly by back-inhibition of Ca^{2+} release to the SR lumen from the low-affinity Ca^{2+} binding sites (54, 108, 122). The suggested mechanism of SERCA back-inhibition according to the scheme in Plate 3 has the luminal low-affinity Ca^{2+} sites remaining saturated and unable to release the bound Ca^{2+} to the lumen. This in turn decreases the rate of Pi release and decreases the rate of enzyme turnover (53, 113). Interestingly, it is under similar conditions of high luminal Ca^{2+} loads that may promote SERCA1 pump reversal (169, 170). In terms of the transport cycle scheme (Plate 3), SR vesicles that were initially loaded with Ca^{2+} would have 2 Ca^{2+} ions bound luminally to the low-affinity Ca^{2+} binding sites on the SERCA1 pump. Because the Pi has not been removed, the enzyme may favor the binding of ADP and the Ca^{2+} ions would efflux through the pump to the cytosol with the concomitant synthesis of ATP. If the phosphorylated intermediate was allowed to relieve itself of the two luminal Ca^{2+} ions it would form the E-P formation of the enzyme and subsequently only react with water, proceeding with the forward reaction of the SERCA1 cycle (130, 182). Indeed, the initial reports of pump

reversals were thought to be a mechanism by which the skeletal muscle SR released stored Ca^{2+} required for muscle contraction.

The SERCA1 family of Ca^{2+} pumps are inhibited by several recently identified compounds. The first is the sesquiterpene lactone, thapsigargin (Tg), derived from the plant *Thapsia garganica*. Tg was found to specifically inhibit the SERCA pump isoforms with a binding stoichiometry of 1:1 and an IC_{50} of about 20 nM (157, 124). Further studies have shown that Tg binds to the SERCA pump with a dissociation rate constant of 0.0052 s^{-1} (52). The SERCA1 pump appears to be inhibited by Tg in the E (Ca^{2+} absent) formation of the enzyme and more specifically in the low affinity state for Ca^{2+} (284a). During active SERCA1 turnover in the presence of Ca^{2+} and ATP, Tg was reported to slowly inhibit catalytic turnover since it specifically interacts with the Ca^{2+} absent form of the enzyme in the Ca^{2+} transport cycle. When SERCA1 pumps were treated with Tg in the absence of Ca^{2+}, the Ca^{2+} transport cycle was arrested in a dead-end complex (182). The binding of Tg to the pump has also been shown to inhibit the binding of ATP. If the reaction cycle was allowed to proceed, Tg was shown to be ineffective at blocking Ca^{2+} binding to the Ca_2-E formation and that the enzyme could then be phosphorylated (even in the presence of Tg) forming the E-P state from the Ca_2-E. Because of the binding characteristics of Tg, sub-stoichiometric Tg concentrations were shown to reduce both the catalytic rate and the Ca^{2+} loading rate of the SERCA1 pump possibly by binding to those enzymes in the E formation while other SERCA1 pumps proceeded through the Ca^{2+} transport cycle (137, 224).

A second SERCA1-specific inhibitor is cyclopiazonic acid (CPA), a mycotoxin produced by *Aspergillus flavus* and *Penicillium cyclopium* (92, 124). In much the same

manner as Tg, CPA binds to the SERCA1 pump with a 1:1 stoichiometry but with an IC_{50} in the 400 nM range. As with Tg, CPA preferentially binds and inhibits the Ca^{2+} absent (E) form of the enzyme but the mode of action of CPA appears to be as a competitive inhibitor of ATP binding to the pump (233). In contrast, others report that CPA acts in a similar manner to Tg by blocking the E to Ca_2-E transition and thus inhibiting ATP binding (251). It is agreed that CPA inhibits the SERCA1 to a lesser extent than Tg and, unlike Tg, CPA-induced inhibition is fully reversible (213, 251). Plenge-Tellechea et al. have also shown that catalytic turnover rates of the enzyme and Ca^{2+} loading at sub-stoichiometric CPA concentrations reflect the combined contribution of enzyme turnover with and/or without CPA inhibition.

The SERCA1 is thought to operate as a monomeric enzyme in the SR membrane with neighboring SERCA1 pumps acting in concert. Indeed, isolation of the Ca^{2+}-ATPase and study of the monomeric form has shown that the pump operates with the full Ca^{2+} transport cycle outlined above and transports Ca^{2+} (105, 161). Yet, recent evidence has suggested that the Ca^{2+}-ATPase may in fact operate as oligomeric unit of enzymes, even in isolated SR vesicles (14, 42, 168). In studies in the Thomas laboratory (168), the finding that only 50% of the total ATPases present were phosphorylatable led the investigators to suggest that ATPase/ATPase interactions may account for this loss in activity. Further evidence came from cryo-electron microscopy images of the SERCA1 leading the authors to describe the arrangement of pumps in the membrane as 'dimer ribbons' (271).

Cryo-electron microscopy and site-directed mutagenesis studies were important for deduction of possible Ca^{2+} associated portions of the SERCA pump as well as

structural changes that may occur during Ca^{2+} transport (199). These studies suggest that 70% of the SERCA1 protein is cytoplasmic and that this portion resembles the head and neck of a bird. The 'head' of the pump is suggested to be the domain that interacts with other Ca^{2+}-ATPases as well as containing binding sites for ATP. The neck connects the membrane and cytosolic portions of the enzyme and is thought to convey conformational change to the head of the SERCA pump. The neck is connected to the transmembrane segments of the SERCA pump and the images were thought to correlate to earlier findings that there were 10 transmembrane helices (17). Site-directed mutagenesis studies have identified 4 of these helices as being important for Ca^{2+} binding and Ca^{2+} translocation across the SR membrane (35, 218). Ca^{2+} binding to these segments appear to result in large conformational changes to the cytosolic domains in the SERCA molecule possibly to allow ATP hydrolysis and subsequent phosphorylation required for Ca^{2+} transport (199). Where Ca^{2+} ions cross through the SERCA pump and the SR membrane, and indeed whether the SERCA pump operates in vivo as a monomer or oligomer remains to be determined.

II.B. Sarcolipin

Sarcolipin is a proteolipid of 6 kDa first shown to copurify with the SERCA1 from skeletal muscle sarcoplasmic reticulum (166). Expression of the protein follows the expression of the SERCA1 in that it is most abundant in fast-twitch skeletal muscle (198). Cloning of the gene for sarcolipin revealed similarities in gene make-up between sarcolipin and phospholamban, another integral membrane protein that co-expresses with SERCA2a in cardiac and slow-twitch muscles (197, 287). Homology of protein

sequences of sarcolipin and phospholamban led to speculation that sarcolipin regulated SERCA1 activity in a similar fashion to the way phospholamban regulated SERCA2a activity. Phospholamban is known to inhibit the SERCA2a by decreasing enzyme affinity for Ca^{2+}. This inhibition can be reversed by phosphorylation of phospholamban or under conditions where cytosolic Ca^{2+} becomes elevated (141). Coexpression of sarcolipin and SERCA1 in HEK-293 T-cells showed that sarcolipin decreased the affinity of the SERCA1 for Ca^{2+} at low Ca^{2+} concentrations but increased Ca^{2+} sequestration rates by SERCA1 at higher Ca^{2+} concentrations (196). The investigators also noted that sarcolipin was not phosphorylatable and that the way in which sarcolipin interacts with the SERCA1 may be different from the interactions between phospholamban and the SERCA2a. This is preliminary evidence that the SERCA1 may be modulated by a phospholamban-like membrane protein, sarcolipin.

II.C. The Ca^{2+} Release Channel/Ryanodine Receptor

During the mid-1970's, the same time that Meissner was characterizing light and heavy sarcoplasmic reticulum vesicles containing (as was known at the time) only three main proteins (a Ca^{2+}-ATPase, a Ca^{2+} binding protein and M55 protein) (176), the concept of a channel large enough to conduct Ca^{2+} from the SR lumen to sites of cross bridge formation was almost unimaginable. Ca^{2+} release channels began to be identified morphologically as the 'feet' structures in HSR vesicles because of their similarity to the feet of triadic junctions and because of the capabilities of HSR vesicles to release Ca^{2+} (28, 85, 86). The root alkaloid isolated from the *Ryania speciosa* plant, ryanodine, proved pivotal for the identification of the Ca^{2+} release channel. The early observations that

ryanodine had Ca^{2+} agonist or antagonist actions in isolated SR vesicles (70, 233) led researchers to suggest that "ryanodine may interact with an SR Ca^{2+} channel and either open it or close it depending on experimental conditions" (258). The subsequent findings that ryanodine bound with high affinity to a receptor localized to the junctional SR membranes led to the isolation and further characterization of the Ca^{2+} release channel now known as the ryanodine receptor (79, 178, 209, 211).

The Ca^{2+} release channel/Ryanodine receptor (RyR) was purified from rabbit skeletal muscle (120, 126, 209) and from canine cardiac muscle (6, 112) in the late 1980's. The isolated channels were shown to carry Ca^{2+} current and were gated into open states by various ligands helping identify them as Ca^{2+} release channels (247, 248). The Ca^{2+} release channel is the largest membrane spanning channel in the body. Actual dimensions of 27x27x14 nm have been suggested. These studies also indicated that the RyR has a central pore of about 1-2 nm that radiates into four smaller channels in the cytoplasmic quatrefoil foot structures (216, 280). Although the RyR appears as a quatrefoil, the channel is actually made up of four equal monomeric subunits that have a sedimentation coefficient of 30S and a molecular weight of 565 kDa (147). The RyR1 polymer has a molecular weight of 2.3 mDa.

Cryo-electron microscopy studies have indicated that only 20% of the monomeric protein was membrane associated constituting the pore-forming portion of the channel. The remaining 80% of the monomer formed the cytoplasmic foot (215). The membrane topology of the RyR is still under some debate. The membrane-associated C-terminal 20% is thought to have either four transmembrane segments (93), or 10-12 transmembrane segments (281) according to site specific antibody studies or cryo-

electron microscopy studies, respectively. The rest of each monomer (80% of the protein) upstream to the N-terminus embodies the large cytosolic foot structures that have come to typify the RyR/Ca^{2+} release channel. Recent studies have shown that two domains make up each cytosolic monomeric foot (234) and that there appears to be a 4° shift in the foot structures in relation to the membrane upon RyR channel opening (203). Binding sites for adenine nucleotides (238), cytosolic Ca^{2+} (36), ryanodine (26), calmodulin (265), FKBP12 (279), as well as phosphorylation sites (255), have been predicted from primary structure but further investigations are required.

The Ca^{2+} release channel has three isoforms encoded by three genes giving a skeletal muscle RyR1 (265), a cardiac muscle RyR2 (205) and a more widely distributed RyR3 (99). Although RyR3 was first isolated from the brain, later studies revealed that the RyR2 was actually most abundant in this tissue (175). Furthermore, RyR1 is also found in some areas of the brain. Other evidence has suggested the RyR3 isoform may also be found alongside RyR1 channels at the triadic junction in skeletal muscle (188). Sequence homology between the three isoforms from one species show that RyR1 and RyR2 are 67% homologous, RyR1 and RyR3 are 67% homologous, and RyR2 and RyR3 are 70% homologous (99). The specificity for each receptor isoform for the tissues in which they are found is indicative of the specificity of function of RyR within these tissues. For example, the RyR2 is more sensitive to activation and less sensitive to inactivation by various modulators (like Ca^{2+}) than the RyR1 (180). This immediately suggests that the control mechanisms for SR Ca^{2+} release are different in cardiac and skeletal-type muscle. For the purposes of this review, control of the RyR1 will be the primary focus.

RyR1 Modulation

RyR1 channel function can be studied using a variety of different methods. Of the most popular *in vitro* methods, SR vesicles, isolated RyR channels and [^{3}H]-ryanodine binding studies have all been used to speculate upon how the RyR1 functions *in vivo*. The first of these methods utilizes vesicular derivatives of the SR. SR vesicles are prepared by fractionation of skeletal muscle components which yields an SR fraction that can be further separated by sucrose density centrifugation. The resultant SR vesicles can be (1)triadic in nature (junctional or jSR), that is both RyR1 and T-tubule DHPR are present and 'connected' in the isolated membrane fraction (270), or (2)solely heavy(H) SR vesicles containing membrane derivatives from the junctional SR devoid of T-tubule 'contamination' (40). To obtain jSR membranes a high salt wash is omitted during isolation procedures since this step results in osmotic disruption of the triad and thus results in isolation of HSR vesicles. The study of Ca^{2+} release from HSR vesicle preparations can be carried out with radiolabelled Ca^{2+} and determining residual $^{45}Ca^{2+}$ after stimulation of Ca^{2+} release and vesicle filtration (187, 256). Additionally, Ca^{2+} release and Ca^{2+} sequestration can be monitored spectroscopically using a variety of Ca^{2+} indicators. Metallochromatic Ca^{2+} indicators such as murexide, arsenazo III, and antipyrylazo III have historically been the most popular for measurement of extravesicular Ca^{2+} (90, 195, 206). The Ca^{2+}-sensitive antibiotic, chlortetracycline, was another common Ca^{2+} indicator for measuring luminal Ca^{2+} signals but has lost popularity as of recently (33, 34, 69, 181). A variety of newer extravesicular Ca^{2+} fluorophores like Indo-1, Fura, Fluo-3, Mag Fura-2, and Calcium Green-2 (91, 146, 225, 226) have also been used to examine Ca^{2+} release from skeletal muscle SR. In these

studies, HSR membranes can be actively or passively loaded with Ca^{2+} and release of Ca^{2+} can be stimulated with a variety of RyR antagonists, including Ca^{2+} itself.

A second and more recent method for examining Ca^{2+} release and RyR1 regulation has been single channel ion flux measurements of isolated RyR1 channels. Either RyR1's from HSR vesicles or the purified RyR1 can be incorporated into Mueller-Rudin-type planar lipid bilayers (111, 147, 249). The RyR incorporates into the bilayer with polarity such that the cytosolic 'feet' are in the *cis* chamber while the luminal portion of the protein faces the *trans* chamber (44). The current flowing through the channel is recorded and the opening and closing events are examined to give conductance and the open probability (P_O) of the RyR (44). Once a RyR channel has been incorporated and identified, effectors of the Ca^{2+} release channel can be tested by addition to the *cis* or *trans* chambers and their influence upon conductance and P_O can be established. Isolated RyR1 receptors have been important for determining subconductance states of the channel, although the physiological relevance of such sub-states has been questioned. One noted problem of single channel studies is that they remove the RyR from an environment where protein-protein interactions are key to its' modulation (111). Regardless, these studies have increased the body of knowledge pertaining to the biophysics and pharmacology of the RyR1.

A third method for examining RyR1 modulation is by [^{3}H]-ryanodine binding both to isolated single channels and to HSR membranes. Radiolabelled ryanodine was first used in laboratories where ryanodine could be radiolabelled on site (211), but has more recently become commercially available. Ryanodine has been described to bind preferentially to the open state of the RyR (107, 178). It has also been shown that

ryanodine itself can activate the Ca^{2+} release channel by binding to high affinity sites presumably located on the cytoplasmic domains of the protein. These binding sites appear to be accessible preferentially when the channel is in an open state (178). This preference of binding has allowed [^{3}H]-ryanodine to be used to probe the 'openess' of the ryanodine receptor under experimental conditions where the channel is thought to be activated or inactivated. The K_D for ryanodine binding to the RyR1 has been calculated to be between 20 and 200 nM. Furthermore, HSR vesicle preparations are thought to specifically bind ~10 pmol [^{3}H]-ryanodine per mg of membrane protein (79).

Ryanodine has proven to be one of the most important compounds for the study of SR Ca^{2+} release. The identification that ryanodine effects were Ca^{2+} release channel-mediated came with vesicle experiments where ryanodine was shown to increase the amount of Ca^{2+} loaded into HSR membranes while SERCA1 pump activity remained unaffected (131). Subsequent Ca^{2+} release studies showed that ryanodine activated the Ca^{2+} release channel and that this activation was inversely related to free cytosolic Ca^{2+} concentrations. Ryanodine was also shown, following activation, to subsequently and irreversibly inhibit the RyR1 in a time and concentration-dependent manner (104, 150). Stimulation of the RyR1 channel with Ca^{2+}, adenine nucleotides or caffeine increased ryanodine binding to the RyR1 (39). Furthermore, ryanodine binding correlated with Ca^{2+} release channel activation/inactivation induced by increased cytosolic Ca^{2+} concentrations (180, 211). These results were substantiated with single channel experiments showing that μM ryanodine locked the isolated Ca^{2+} release channel in an partially open subconductance state while increased ryanodine concentrations (mM) inhibited the RyR1 (22, 110, 223). In these studies, the ryanodine modified and partially

open RyR1 was insensitive to modulators that normally activate the release channel like Ca^{2+} and ATP and was also unresponsive to inhibition by Mg^{2+} and ruthenium red. Ryanodine is thought to initially bind to high-affinity sites on the RyR1 leading to (submaximal) channel activation while increased ryanodine concentrations begin to saturate low-affinity RyR-inactivation binding sites (21, 178, 212). Evidence such as this has indicated that the Ca^{2+} release channel must activate before it is capable of being inactivated (76). The number of low affinity and high affinity ryanodine binding sites is still under some debate (148, 283).

The methods used for studying Ca^{2+} release from the skeletal muscle RyR1 have been important for describing the way in which opening and closing of this large membrane-spanning channel is possibly modulated. The gating control mechanism of the RyR1 have proved to be multifactorial and very complex, making modeling of the channel difficult. Divalent cations, adenine nucleotides, lipid metabolites, phosphorylation, and numerous luminal and cytosolic proteins are all endogenous mechanisms by which the Ca^{2+} release channel has been reportedly controlled. For the purposes of this review, with the exception of the above mentioned, ryanodine, and ruthenium red, the endogenous modulators of the RyR1 will be the primary focus.

In early results obtained with $^{45}Ca^{2+}$ efflux studies, the RyR1 was known to be activated by μM Ca^{2+} concentrations but inhibited at higher cytosolic Ca^{2+} (138, 177). Results with [^{3}H]-ryanodine showed that binding was enhanced in the presence of μM Ca^{2+} but became inhibited with Ca^{2+} concentrations in the mM range (39, 180, 210). These findings were later confirmed with single channel experiments that demonstrated that nM Ca^{2+} concentrations had little effect on the P_O, μM Ca^{2+} concentrations greatly

increased P_O, and mM Ca^{2+} concentrations decreased the P_O of the RyR1 (160, 248). The bell-shaped Ca^{2+} activation curve for Ca^{2+} activation of the RyR1 suggested that the channel has high-affinity Ca^{2+} activation sites and low affinity Ca^{2+} inactivation sites.

The rates at which Ca^{2+} alone caused Ca^{2+} efflux from SR vesicles led Meissner to propose that the effects of Ca^{2+}-induced efflux could approach physiological relevance only in the added presence of mM ATP (177). These results were corroborated in single channel experiments which demonstrated that full activation of the RyR1 required both μM Ca^{2+} and mM ATP (248). Furthermore, the presence of physiological Mg.ATP concentrations narrowed the Ca^{2+} concentration required for maximal RyR1 activation (179). Augmenting the above results was the observation that isolated triads could compartmentally synthesize ATP which was not accessible to the bulk cytoplasm, and therefore may preferentially be available for activation of the RyR1 or use by other components of the triad (100).

The mechanism of Ca^{2+}-induced Ca^{2+} release (CICR) from skeletal muscle SR was first proposed by Endo using skinned muscle fibers (61, 62). These early experiments and others that followed suggested that a critical luminal Ca^{2+} load was required before CICR could be stimulated (65, 91, 118, 195). The influence of luminal or *trans* Ca^{2+} upon SR vesicle Ca^{2+} release and RyR1 single channels, respectively, has to date yielded conflicting results. The data collected have indicated that increases in luminal Ca^{2+} may, (1) increase RyR1 activity (56, 118, 243), (2) decrease RyR1 activity (78, 146, 160), or (3) bimodally affect RyR1 activity (95, 273). The differences in results have been attributed to differences in the methods of study of luminal Ca^{2+}, ranging from skinned fibers (146), triadic preparations (56, 118) and single channel studies (243, 273).

Also the possibility that luminal Ca^{2+} effects upon states of the RyR1 could be indirectly governed by the luminal Ca^{2+} binding protein, calsequestrin, has been suggested (90, 136). Other proposed mechanisms of luminal Ca^{2+} control of the RyR1 include luminal Ca^{2+} sensing sites on the RyR1 (95, 195) or the preferential access, by luminal Ca^{2+}, to Ca^{2+} inactivation sites and minor access to Ca^{2+} activation sites on the cytoplasmic/*cis* side of the Ca^{2+} release channel (289). This latter Ca^{2+} flux control hypothesis of the RyR1 would explain the bimodal influence of luminal Ca^{2+} upon the RyR1 activation identified in the study of Tripathy and Meissner (273).

Free Mg^{2+}, uncomplexed with ATP, has been shown to inhibit Ca^{2+} release by inhibition of the Ca^{2+} release channel (139, 142, 177). The inhibition of the RyR1 by Mg^{2+} was dependent upon Ca^{2+} concentration in such a manner that lower Mg^{2+} concentrations were required for channel inhibition if less Ca^{2+} was present in the medium (177). Furthermore, the presence of adenine nucleotides decreased the observed Mg^{2+} inhibition possibly due to complexing with ATP which have been conversely shown to activate the RyR1 (179). In single channel studies, mM Mg^{2+} was shown to decrease the P_O of the RyR1 (222). Mg^{2+} also inhibited [^{3}H]-ryanodine binding to the Ca^{2+} release channel (211). Suggested possible mechanisms of Mg^{2+} inhibition have included competing with Ca^{2+} for the RyR1 Ca^{2+} activation sites, binding to the low-affinity Ca^{2+} inactivation sites, or by blockage of the actual ion conduction pathway in the pore forming segment of the Ca^{2+} release channel (45, 142, 179).

As mentioned previously, Ca^{2+} release studies have shown that adenine nucleotides activate the RyR1 even in the presence of Mg^{2+} (177, 193, 288). Furthermore, mM adenine nucleotide appeared to be a requirement for full activation of

the RyR1 and that, in order of decreasing potency, AMP-PCP, cAMP, ADP, ATP, and AMP were all able to activate the release channel (179, 186). These results were confirmed using RyR1 single channel experiments where μM Ca^{2+} concentrations along with mM adenine nucleotides increased the length of time the channel was in the open state (147, 248). Interaction of adenine nucleotides with the Ca^{2+} release channel has been suggested to occur at a different binding site than Ca^{2+} or Mg^{2+}. However, the possibility that ATP binding at its site allows interactions with the Ca^{2+} or Mg^{2+} binding sites on the channel has not been ruled out. ATP has been shown to bind to the RyR1 with a 1:1 stoichiometry (238).

Several protein kinases have been suggested to use the RyR1 as a substrate. Calmodulin-dependent protein kinase II (CaMK) was shown to be located and bound to junctional SR membranes (41) and able to phosphorylate the skeletal muscle Ca^{2+} release channel (138). cAMP-dependent protein kinase (PKA) and cGMP-dependent protein kinase (PKG) were also shown to phosphorylate the RyR1 with stoichiometries in the 0.3 to 0.9 moles per receptor monomer range (255), but these findings have been challenged (254). Phosphorylated states of the RyR1 have been shown to either activate (107), inactivate (282) or have no effect (41) on RyR1 function. In one study specifically, phosphorylation of the skeletal muscle Ca^{2+} release channel by exogenous CaMK removed Mg^{2+} inhibition of the RyR1, while in the absence of Mg^{2+} phosphorylation by endogenous CaMK inhibited the channel (98a). Studies involving the phosphorylation of RyR2 have more clearly indicated a role for PKA, PKG and CaMK in regulation of the cardiac isoform of the receptor (254). Phosphorylation of the cardiac RyR2 by PKA, PKG or protein kinase C (PKC) promoted Ca^{2+} release and increased [^{3}H]-ryanodine

binding to the channel (261). Furthermore, phosphorylation increased RyR2 activation responses to Ca^{2-} in single channel experiments (275). These results are suggestive that phosphorylation may also have an important role physiologically in skeletal muscle RyR1 regulation but this requires further study.

The RyR1 has been shown to be regulated by a number of endogenous proteins of the SR. The possible role of each protein in SR Ca^{2+} handling will be dealt with in more detail in the specified sections that follow. Briefly: FKBP12 has been shown to stabilize the open or closed states of the RyR1, removing the appearance of subconductance states in single channel studies; calmodulin (mM) inhibits the RyR1; Ca^{2+} bound states of calsequestrin may impact states of the RyR1, or vice-versa, either by direct interaction between the two proteins or via accessory proteins like triadin or junctin; annexin IV (nM) decreases the open probability of isolated RyR1.

Non-endogenous modulators of the Ca^{2+} release channel have been well characterized and have become useful for studying RyR function. The aforementioned ryanodine, as well as caffeine and ruthenium red have proven helpful in elucidating the experimental modes of RyR-regulation of Ca^{2+} release from the SR.

Caffeine has been one of the most widely used compounds for eliciting SR Ca^{2+} release (62, 65, 177, 288). In Ca^{2+} release experiments, caffeine was shown to increase the sensitivity of the RyR1 to cytosolic Ca^{2+} and increase [^{3}H]-ryanodine binding confirming a Ca^{2+} release channel effect (39, 110). Caffeine is thought to act differently than the adenine nucleotides (242) but the mechanism of RyR1 modulation has not been deduced.

Ruthenium red is one of the most widely used RyR channel inhibitors. Ruthenium red has been shown to block Ca^{2+} release from isolated skeletal muscle SR vesicles (177, 185, 201). In ryanodine binding experiments, ruthenium red effectively decreased [^{3}H]-ryanodine binding (IC_{50} of about 20 nM) indicative of Ca^{2+} release channel closure (162, 211). Furthermore, treatment of membranes with ruthenium red effectively slowed ryanodine dissociation from the channel indicative of an alteration of RyR1 conformation. Ruthenium red (μM concentrations) was subsequently shown to decrease the open probability of single channel RyR1 in bilayer experiments (21, 222, 248).

II.D. FKBP12

The FK-506 binding protein, FKBP12, has a MW of 12 kDa and has been shown to associate with the RyR1 at a ratio of 1 FKBP12 protein for each channel monomer (43, 129). A similar association of the RyR2 with FKBP12.6 has been shown (149, 269). FKBP12 is found in the cytosol of most cells, and at an expected concentration of 3 μM in the myoplasm. Therefore an exchange of free and RyR1-bound FKBP12 may occur and this interchange may be one of the many regulatory mechanisms of RyR1 activation/inactivation. FKBP12 has been shown to bind to the RyR1 with an EC_{50} of 0.3 μM (270) and to remain associated with the RyR1 even in isolated vesicular SR preparations. FKBP12 appears to stabilize the RyR1, removing the appearance of subconductance states originally thought to be physiologically relevant in early in RyR1 single channel experiments (19, 174). In more recent single channel studies, the presence of FKBP12 inhibited the *cis* to *trans* current (cytosolic to luminal) without affecting the

trans to *cis* (luminal to cytosolic) current (37, 159). In experiments involving the removal of FKBP12 from the RyR1, the modified channel was shown to be more sensitive to Ca^{2+} and caffeine and less sensitive to Mg^{2+} (270). RyR1-bound FKBP12 appears to have a role in modulating the way in which RyR1 monomers associate with one another and possibly assists in stabilizing closed states of the Ca^{2+} release channel.

II.E. Calsequestrin

Early attempts to unravel the Ca^{2+} control mechanisms of the SR in relation to muscle contraction, it was noted that if the Ca^{2+}-ATPase was able to sequester Ca^{2+} into the SR, then a storage system for that Ca^{2+} was probably required. Initial attempts were made to identify Ca^{2+} binding sites on the ATPase. It was recognized that although the enzyme could form in membranes there was little storage or binding capacity of these membranes (163). These observations led MacLennan and Wong to isolate a protein that was copurified with the Ca^{2+}-ATPase but remained in the soluble fraction during isolation procedures (167). These initial findings showed that the purified protein, named calsequestrin (CSQ), had a MW of approximately 44,000 Da, was possibly hydrophobically bound to the interior membrane of the SR, was soluble when not membrane bound, was highly anionic, and bound between 625 and 835 nmol Ca^{2+} per mg of protein. On the assumption that two carboxyl groups may bind one Ca^{2+} ion, it was suggested CSQ may have the capacity to bind upwards of 1270 nmol Ca^{2+} per mg of protein. Ca^{2+} binding was saturable and found to occur with a sigmoidal shaped Ca^{2+} concentration versus Ca^{2+} bound curve. The dissociation constant of Ca^{2+} binding to CSQ in this study was found to be 40 μM. Subsequent studies have shown that CSQ is a

Ca^{2+} binding protein with a high-capacity for binding Ca^{2+} at 40 to 50 mol of Ca^{2+} per mol of CSQ and that it binds Ca^{2+} with moderate affinity with a Kd of about 1 mM (145, 164). CSQ was proposed to buffer free luminal Ca^{2+} levels in the SR to about 1 to 10 mM (259). The driving force for Ca^{2+} binding to CSQ has been suggested to be unrelated to changes in enthalpy but predominately controlled by increases in entropy upon Ca^{2+} association (145).

In mammals, two genes produce a cardiac and a skeletal muscle isoform of calsequestrin (80, 231). The amino acid sequences of rabbit cardiac and skeletal isoforms were 68% identical. The amino acid sequence also shows that CSQ contains groupings of acidic residues (glu and asp) thought to be Ca^{2+} binding sites, although the sites show no uniformity in distribution or inclusion in Ca^{2+} binding domains. Analysis of the secondary structure of CSQ predicted that the protein contained highly helical segments yet NMR studies have demonstrated that α-helices may only be 5-10% of the CSQ structure (1). Other studies indicate that CSQ may incrementally form α-helices upon Ca^{2+} binding to the protein (244). Several reports have confirmed that CSQ undergoes drastic conformational changes due to the binding of Ca^{2+} and that these changes effectively bury hydrophobic segments of the protein (24, 117, 184).

CSQ has been shown to be concentrated at the luminal terminal interface of triads in skeletal muscle SR (28, 87, 135). This localization of CSQ is thought to make temporary Ca^{2+} storage in the SR spatially close to the sites of SR Ca^{2+} release at the terminal cisternae. The specific localization of CSQ was an initial indication that the luminal Ca^{2+} binding protein may modulate RyR1 function (47, 49). Evidence for coupling between RyR1 opening/Ca^{2+} release and the binding affinity of CSQ was shown

by transient increases in intraluminal free Ca^{2+} prior to expected decreases as Ca^{2+} exited the luminal space (118). Furthermore, Ca^{2+} binding to CSQ was shown to result in conformational changes in the RyR1 channel and, consequently, dissociation of CSQ from RyR1 abolished those changes (115). Ca^{2+} binding to CSQ and the induced changes to RyR1 were also shown by a reduced sensitivity of the RyR1 to ryanodine treatment in SR vesicles under high luminal Ca^{2+} loads (90). Single channel experiments demonstrated that CSQ added back to the *trans* (luminal) face of the RyR increased the open probability of the channel (136). In electron microscopy studies, CSQ was shown to periodically appear attached to the terminal cisternal SR membrane by adjoining strands or fibers (47, 87). Other results have suggested that CSQ proteins may cluster or form conglomerates with one another in a Ca^{2+} dependent fashion (268).

Another junctional SR membrane glycoprotein, triadin, has been implicated in anchoring CSQ to the luminal face of RyR-enriched terminal cisternae (94). The luminal interactions between CSQ and triadin were demonstrated to be Ca^{2+} dependent such that increased Ca^{2+} binding decreased the association of CSQ to triadin. It was suggested from this study that the cytosolic domain of triadin bound to the RyR1. Junctin has also been implicated as a member of this terminal cisternal anchoring protein complex, having been shown to interact not only with CSQ but also with triadin (132). Accordingly, it has been proposed that a quaternary protein complex consisting of RyR, triadin, junctin and CSQ may be specifically located at the terminal junction in the lumen of the SR (294). The exact mechanism of RyR1 control by, and the interactions between, these four luminal SR proteins remains to be determined.

CSQ has been shown to be phosphorylated by casein kinase II (25). It has also been shown that the SR lumen contains a protein phosphatase that may dephosphorylate CSQ as well as other luminal SR proteins (204). Isolation of CSQ from the SR results in acquisition of CSQ in various states of phosphorylation indicating that the phosphorylation/dephosphorylation process has relevance *in vivo* (276, 277). Recent evidence has suggested that it is the dephosphorylated state of CSQ, not the phosphorylated state, which increases RyR1 open probability and possibly Ca^{2+} release (259). Furthermore, it appears that the phosphorylation state of CSQ had no influence on the Ca^{2+} binding characteristics of the protein (25).

One possible mechanism for the control of Ca^{2+} binding to CSQ is the relationship Mg^{2+} binding to the luminal protein may have upon Ca^{2+}-bound CSQ states (145). Ca^{2+} binding to CSQ was shown to decrease in the presence of Mg^{2+} and that Mg^{2+} did not occupy Ca^{2+} binding sites. Ca^{2+} binding to CSQ resulted in the release of protons from the protein while Mg^{2+} binding had no such effect. Krause et al. proposed that during SR Ca^{2+} release CSQ would have a higher number of Mg^{2+} binding sites than Ca^{2+} binding sites. At SR Ca^{2+} uptake, the Ca^{2+} binding sites would outnumber the Mg^{2+} binding sites. Upon Ca^{2+} binding, the pH of the luminal environment would decrease due to Ca^{2+} binding-dependent proton release from CSQ. These changes in affinity for Ca^{2+} and Mg^{2+} may in turn influence the binding of CSQ to junctional proteins and as such may be responsible for the interactions between CSQ and Ca^{2+} release channels.

II.F. Triadin

As mentioned above, skeletal muscle SR terminal cisternae were found to be enriched with the 95 kDa glycoprotein, triadin (18). The protein was found to be at a 1:1 ratio with the RyR1 (81) and evidence suggests that it binds directly to the Ca^{2+} release channel (32, 94). Similarly to the RyR1, triadin has been shown to be a substrate for CaMK (49).

Triadin is a monomer (95 kDa) that forms self-aggregates in native SR membrane to become a large, disulfide-bonded polymer (~3000 kDa) (89). In this capacity, triadin is thought to be a major component in linking the DHPR to the RyR1, or, in linking CSQ to the RyR1. In support of the former, triadin was found to associate with the DHPR from the T-tubule and in overlay experiments also bind the RyR1 (32, 71). The proposed membrane topology of triadin also supports a DHPR/RyR1 interaction because of a pronounced cytoplasmic loop that may form the possible connections with both DHPR and RyR1 (72). In support of the latter, it was found that CSQ interacts with the luminal component of triadin in a Ca^{2+}-dependent manner. The binding of triadin to the RyR1 in these studies was conversely shown to occur through the luminal domains of the protein (94). The proposed interaction with CSQ is also thought to be controlled in the luminal regions of triadin which consist of groupings of basic residues that would possibly form connections with the negatively charged CSQ (144). As mentioned previously, these described interactions have led to the proposal that a quarterary protein complex consisting of RyR, CSQ, triadin and junctin exists in the terminal cisternae of the SR and in someway modulates the activation/inactivation of the Ca^{2+} release channel (294).

Ohkura et al. (200) have shown that triadin inhibited [^{3}H]-ryanodine binding while CSQ conversely enhanced [^{3}H]-ryanodine binding to isolated RyR1 channels. Triadin-induced inhibition of ryanodine binding was then abolished when both CSQ and triadin were added to the *trans* experimental chamber. These data further demonstrated that it was the triadin polymer that resulted in inhibition of [^{3}H]-ryanodine binding, not the monomeric protein. CSQ was also shown to block the formation of triadin polymers. The investigators suggested that these results confirmed the CSQ/triadin interaction and that the RyR1 control may be regulated by a mechanism in which Ca^{2+}-bound CSQ would bind to triadin resulting in disassembly of the triadin polymer into monomers and ultimately removal of triadin-induced inhibition of the Ca^{2+} release channel. This would signal the activation of Ca^{2+} release.

A more recent study has ruled out any direct interactions between the RyR1 and triadin as well as CSQ and triadin (89). The investigators used two-dimensional gel electrophoresis techniques to show that triadin is in close proximity to the RyR1 and CSQ, but was not functionally connected to either. It was suggested that triadin may help stabilize the membrane at the triadic junction thereby indirectly supporting a CSQ:RyR1 interaction.

II.G. Junctin

Junctin is a membrane-spanning, 26 kDa, CSQ-binding protein concentrated at the junctional SR (132). Studies have shown that junctin preferentially bound Ca^{2+} free CSQ and may provide a means by which CSQ would remain anchored near RyR1 release sites during Ca^{2+} release events. Affinity chromatography and co-immunoprecipitation

studies indicated that junctin also associated with both triadin and the Ca^{2+} release channel in a Ca^{2+} -independent manner (294).

II.H. Calmodulin

Calmodulin (CaM) is a 17 kDa, E-F hand Ca^{2+} binding protein found in many cell types including the myoplasm of skeletal muscle cells. For skeletal muscle SR, the primary effect of CaM appears to be RyR1 inhibition. CaM has been shown to block Ca^{2+} release in $^{45}Ca^{2+}$ efflux experiments (178) as well as decrease the P_O of RyR incorporated into planar lipid bilayers (250). It was demonstrated that the CaM inhibition of Ca^{2+} release channels was due to the direct binding of CaM. Either two (265), or three (295), binding sites on the RyR1 have been suggested. Other reports have demonstrated that the binding of CaM to the RyR1 was Ca^{2+}-dependent such that four CaM molecules bound per release channel monomer at nM Ca^{2+}, while only one CaM bound per release channel monomer at μM Ca^{2+}. The influence of CaM on Ca^{2+} release channels was thus biphasically dependent upon cytosolic Ca^{2+} concentrations such that nM Ca^{2+} resulted in RyR1 stimulation by CaM while μM to mM Ca^{2+} resulted in the expected inhibition of the channel (119, 274). The physiological relevance of the interactions between CaM and RyR1 were supported by observations that CaM-induced inhibition of the channel was reversible and incomplete (partial) (250). CaM may also have a role in the phosphorylation/dephosphorylation control of the Ca^{2+} release channel as the activity of CaMK II in phosphorylation of the RyR1, and of the phosphatase, calcineurin, in dephosphorylation, required CaM as a cofactor (41, 254).

II.I. Sarcolumenin

First identified by affinity chromatography and monoclonal antibody studies from the skeletal muscle SR, the protein identified as sarcolumenin had a MW of 150 kDa, was phosphorylated by casein kinase II, and found to bind $^{45}Ca^{2+}$ (204, 236). The protein was assumed to have little direct interaction with the RyR1 but phosphorylation of sarcolumenin was shown to decrease [^{3}H]-ryanodine binding, although a mechanism was not suggested (204). Sarcolumenin was found in all the isolated, light, intermediate and heavy, SR fractions but primarily located in the light fraction. Since it was found in all isolated SR fractions but concentrated in the light SR fraction it was postulated that sarcolumenin may shuttle Ca^{2+} from the longitudinal SR, where Ca^{2+}-ATPases sequester Ca^{2+}, to the terminal cisternae, where Ca^{2+} is released. Phosphorylation/dephosphorylation is thought to control the protein-protein interactions of sarcolumenin although they remain to be determined.

II.J. Histine-rich Ca^{2+} binding protein

The histine-rich Ca^{2+} binding protein (HCP, MW 160 kDa) was identified along with sarcolumenin (204, 237). In experiments similar to sarcolumenin, HCP was shown to be phosphorylated by casien kinase II as well as the 60 kDa membrane bound calmodulin-dependent protein kinase (51). HCP was also described to decrease [^{3}H]-ryanodine binding to the RyR1 in the phosphorylated form. Unlike sarcolumenin, HCP was located primarily in heavy SR fractions, although weak interactions with the RyR were expected (50). A role for HCP in SR Ca^{2+} handling remains to be determined.

II.K. S100A1

The S100 family of proteins has been shown to be involved in a variety of cell functions including cell cycle progression and cell differentiation (227). S100A1 is the family member associated with skeletal muscle. It has a MW of 10 kDa, is cytosolic, is an E-F hand Ca^{2+}-binding protein, and can form dimers and trimers (272). It has also been shown to potentiate CICR from skeletal muscle SR (74, 171). It was demonstrated that S100A1 binds directly to the RyR1, independent of free Ca^{2+} concentrations (272). However, nM concentrations of S100A1 were shown to increase the P_O of isolated RyR1 at nM cytosolic Ca^{2+}, but not at mM cytosolic Ca^{2+}. S100A1 may also interact with other proteins found at the triadic junction. It was proposed that S100A1 proteins may be cytosolic Ca^{2+} sensors and that Ca^{2+} binding to the protein may cause interaction and opening of the RyR1. The actual role of S100A1 in E-C coupling or regulation of SR Ca^{2-} release remains to be determined.

II.L. Porin

The finding that SR luminal proteins may undergo phosphorylation/dephosphorylation cycles has led to the suggestion that ATP transport into the lumen is required for phosphorylation to occur. In a recent report, evidence for an ATP-transporting protein on the SR membrane, not unlike the voltage-dependent anion channel (VDAC) of the mitochondria, was reported (236). The investigators demonstrated that [α-^{32}P]-ATP was transported into the SR lumen and that the transport was inhibitible with specific anion transport inhibitors like 4,4'-diisothiocyanostilbene

2,2'-disulfonic acid (DIDS). Furthermore, a 35 kDa and a 30 kDa protein from the SR membrane were shown to cross react with monoclonal antibodies raised against B-lymphocyte VDAC. The investigators suggested that these two proteins are two different isoforms of porin. A postulated role for porin in SR membranes for allowing metabolic intermediates as well as anions and cations access to the SR luminal space was suggested. The importance of porin in SR Ca^{2+} control remains to be determined.

II.M. Annexin VI

Annexin VI is a 67 kDa, luminal Ca^{2+} and phospholipid binding protein that was shown to increase the P_O of single channels at the *trans*/luminal face of RyR1. The protein was shown to be localized to the terminal cisternae of skeletal muscle SR and to be present in isolated HSR membrane fractions. Inhibition was observed at nM concentrations of annexin VI and occurred in a Ca^{2+}-dependent manner (55). It was not determined whether annexin VI associated with other luminal proteins or was phosphorylated.

III. Excitation-contraction coupling in skeletal muscle

Skeletal muscle contraction initiates with depolarization of the plasma membrane. This depolarizing signal travels through invaginations of the membrane to t-tubules that are in close proximity to SR terminal cisternae also referred to as junctional SR. The t-tubule and its' two opposing terminal cisternae have been designated a triad. The end result of depolarization is Ca^{2+} release from the SR and muscle contraction. Ca^{2+} release from the junctional SR has been positively shown through confocal microscopy (64).

The Ca^{2+} release channel has been well documented as the site of SR Ca^{2+} release that spans the junctional gap between the triadic SR and t-tubule membranes (16, 69). On the t-tubule membrane it is generally accepted that there are voltage-sensing proteins that convey the depolarization signal to the RyR1 on the SR membrane. The dihydropyridine-sensitive L-type Ca^{2+} channels (DHPR) were identified as voltage sensors with evidence of charge movement and subsequent muscle contraction (219, 229).

There are several current and debated models of how the depolarization signal of the t-tubule is conveyed to the junctional SR membrane to stimulate Ca^{2+} release required for muscle contraction. The first is a direct coupling model which proposes that there are connections between DHPR and RyR, either through the two proteins themselves or via accessory proteins like triadin. The second is a Ca^{2+} release that is elicited by the movement of a Ca^{2+} releasing agent, like Ca^{2+}, from the DHPR to the RyR in the junctional gap between the triadic membranes. A third is a model which combines a direct coupling scenario with a secondary CICR in uncoupled RyR's. There is evidence supporting components of each model of E-C coupling which will be sequentially presented below.

Some biochemical information has been presented with co-immunoprecipitation and chemical cross-linking experiments that demonstrates a direct interaction between DHPR and RyR1 (173, 188a). The large cytoplasmic domains of the RyR1 were thought to be the connections required for mechanical coupling (16). In the most basic form of the theory, direct interactions of DHPR's would inhibit Ca^{2+} release from the RyR1. Depolarization signals would induce readjustments to the interactions between the triadic

proteins and thus remove DHPR-induced inhibition (220, 221). In this regard, DHPR's would act like voltage sensors, responding and communicating depolarization signals though coupled interactions with RyR1 channels. Several conformational sequences of the DHPR have been postulated as the sites of interaction with the RyR1 (267), but more recently, other proteins like triadin have been implicated in connecting the DHPR to the sites of SR Ca^{2+} release (32, 140).

Information on the spatial organization between DHPR's and RyR1's came with the development of a transgenic mouse line that is lacking in functional DHPR's and called dysgenic mice. More specifically these mice were born with DHPR's that were missing the $\alpha 1$ subunit (88, 262) which has been shown to be important for the voltage sensing, channel, and binding of Ca^{2+}-antagonist properties of the DHPR (10). In skeletal muscle freeze fracture studies, DHPR have been shown to congregate into groups of four molecules (16). Four DHPR's were shown to interact with one RyR1 molecule, with each DHPR protein aligning itself with one of the four monomers that constitutes a complete RyR1 unit. Furthermore, a group of four DHPR was shown to interact only with alternate RyR1's such that every second Ca^{2+} release channel would not associate with a DHPR cluster. In the dysgenic mouse, DHPR groupings were absent but could be fully restored by the transfection of the DHPR cDNA (262). A second transgenic mouse line, called dyspedic because the offspring lack 'foot' proteins/RyR1, was important in showing that membrane triads still formed between t-tubules and the SR membranes that were missing Ca^{2+} release channels. Furthermore, this model demonstrated that CSQ still targeted to the terminal cisternal SR. However the DHPR's appeared to be randomly distributed on the t-tubular membrane when RyR1's were absent on the SR membrane

(263, 264). This data suggested that DHPR's cluster in groups of four because of some association with RyR1 monomers, although the investigators did not assume the data required direct interactions between the two (194).

The demonstration that E-C coupling was absent from either the dysgenic (lacking functional DHPR) (4) or the dyspedic (lacking RyR) (20) mice but could be restored by transfecting the DHPR or the RyR respectively, was an indication of the importance for both proteins in the skeletal muscle E-C coupling process. Moreover, when the cardiac $\alpha 1$ subunit of the DHPR was transfected into dysgenic skeletal muscle, RyR1's responded like cardiac RyR2's (see E-C coupling in cardiac muscle), that is, they became conditional upon cytosolic Ca^{2+} for CICR (256). Furthermore, a specific region of the RyR1 was required to re-establish a RyR-$\alpha 1$ DHPR connection in dyspedic mice (151, 292). The corresponding region on the cardiac RyR2 did not associate with the skeletal muscle DHPR. Lu, Xu and Meissner (153, 154) have also shown that the $\alpha 1$ subunit of the DHPR increased [^{3}H]-ryanodine binding and the P_O of the skeletal muscle RyR1 but not the cardiac RyR2. Phosphorylation of the $\alpha 1$ subunit by PKA resulted in removal of the previous RyR1 activation, further attesting to the importance of phosphorylation/dephosphorylation in regulating E-C coupling. Together these data indicate that direct coupling between the DHPR of the t-tubular membrane and RyR1 of the skeletal muscle junctional SR membrane is important for E-C coupling in skeletal muscle.

It is understood that the skeletal muscle RyR1 is responsive to Ca^{2+} and can be activated in a CICR mechanism (82). This led to initial proposals that in skeletal muscle

E-C coupling, it was Ca^{2+} that was the signal for Ca^{2+} release from the junctional SR and muscle contraction. Supporting evidence for the proposal came from the studies of cardiac E-C coupling (see later). In these studies an influx of Ca^{2+} from the DHPR into the vicinity of RyR2 results in CICR from the SR and cardiac muscle. Modeling of cardiac CICR maintains that the build-up of Ca^{2+} ions in the vicinity of the RyR2 may both activate and inactivate the channel. Unfortunately in skeletal muscle, the t-tubule and SR terminal cisternae appear too intimately associated to allow a similar build-up of Ca^{2+} ions in the junctional space at the cytosolic mouth of the RyR1. It was then proposed that Ca^{2+} ions coming from DHPR's in response to depolarization were released into a very restricted space such that immediate and confined interaction with the RyR1 was favored (48, 109). This hypothesis stemmed from observations that depolarization-induced Ca^{2+} release was not abolished by the use of Ca^{2+} buffers like BAPTA, suggesting that if Ca^{2+} was signalling Ca^{2+} release from the SR it was in a BAPTA inaccessible space. Further evidence for the restricted space model of Ca^{2+} activation of RyR1 came from studies of the RyR2 which found that a single Ca^{2+} ion could activate Ca^{2+} release (73, 228). Extrapolating their findings from cardiac SR Ca^{2+} release, under the assumption that skeletal muscle RyR1 requires four Ca^{2+} ions for activation (240), Fan and Palade suggested that the arrangement of four DHPR about each RyR1 raises the possibility that each DHPR could release one Ca^{2+} ion into the vicinity of each RyR1 monomer resulting in channel activation (73). Furthermore, in the dyspedic mouse model, it was demonstrated that DHPR's only operated as Ca^{2+} conducting channels when RyR1's were present on the opposing SR membrane (194). Unfortunately, kinetic models of Ca^{2+}-induced Ca^{2+} release from RyR1 in restricted

spaces were identical to similar models that used direct DHPR-RyR1 interactions and so it was difficult to substantiate such a model.

The observation that not all RyR1's are associated with DHPR's has led to suggestions that aligned RyR1's are activated by direct coupling with apposing DHPR whereas unaligned RyR1's may be activated through secondary CICR mechanisms (7, 208). In support of this hypothesis, single fiber studies showed that caffeine increased the sensitivity of Ca^{2+} release and slowed the reaccumulation of released Ca^{2+} consistent with a CICR mechanism (143). Again an important assumption with this theory of E-C coupling is that Ca^{2+} concentrations in the immediate vicinity of terminal cisternal RyR1 channels would be magnitudes higher than Ca^{2+} concentrations in the cytosol. Moreover, a large number of RyR1 may in fact reside on the flanking regions of the junctional SR, spatially separate from interactions with DHPR (134). In this case, a secondary CICR mechanism would be necessary for inclusion of these RyR1 channels in SR Ca^{2+} release.

IV. Excitation-contraction coupling in cardiac muscle

Unlike in skeletal muscle, the basic mechanism for SR Ca^{2+} release in cardiac muscle E-C coupling is better understood. Cardiac E-C coupling is under the control of Ca^{2+} transients. Early experiments by Fabiato using skinned cardiac muscle preparations demonstrated that SR Ca^{2+} release responded to increases in bathing Ca^{2+} concentrations (66, 67, 68). The response of SR Ca^{2+} release was graded and dependent upon the rate of presentation of trigger Ca^{2+}. Therefore, increases in trigger Ca^{2+} increased the amount of Ca^{2+} released up to the point at which μM trigger Ca^{2+} inhibited SR Ca^{2+} release. This demonstrated a Ca^{2+} activation and a Ca^{2+} inactivation of cardiac SR Ca^{2+} release that

resembled the bell shaped Ca^{2+} responses of single-channel experiments (6, 112). Furthermore, if trigger Ca^{2+} was increased slowly, there was no observable SR Ca^{2+} release, resulting only in net SR Ca^{2+} uptake. Conversely if trigger Ca^{2+} was increased rapidly net SR Ca^{2+} release occurred. Another factor for demonstrating a solely Ca^{2+}-dependent response was an experiment showing that photolysis of caged Ca^{2+} resulted in SR Ca^{2+} release regardless of T-tubule membrane potential (190, 191). Other single channel experiments showed that Ca^{2+}-dependent inactivation of the RyR2 occurred following Ca^{2+}-dependent activation if *cis* Ca^{2+} was increased to low mM Ca^{2+} concentration or decreased to low nM Ca^{2+} concentrations (228). Equally compelling evidence for CICR was an experiment that showed removal of cytosolic Ca^{2+} resulted in cessation of cardiac muscle contraction, regardless of SR Ca^{2+} content (246).

The Ca^{2+} stimulus for cardiac SR Ca^{2+} release is thought to originate from the DHPR on the T-tubular membrane (13, 27, 29, 191). Experiments have demonstrated that cardiac SR Ca^{2+} release was blocked if the inward Ca^{2+} current was shut off by inhibition of the DHPR channel (285). The L-type Ca^{2+} channels appeared to inactivate in a similar fashion to the RyR2, that is, increased local Ca^{2+} concentrations were effective in arresting Ca^{2+} currents carried by DHPR's (121). Thus, it appears that cardiac muscle contraction arises when the t-tubular membrane becomes depolarized resulting in activation of L-type Ca^{2+} channels (DHPR's), the entry of Ca^{2+} into the cardiac muscle cell in the vicinity of RyR2's and the subsequent activation of SR Ca^{2+} release through a CICR mechanism.

The structure of the triadic junction in cardiac muscle is fundamentally different from that of skeletal muscle. As previously mentioned, skeletal muscle displays a

complex arrangement of DHPR into four units that appear to align themselves with a single RyR1. In cardiac muscle the DHPR were found to cluster at the triadic junctions but were not arranged with one another nor were they aligned in any fashion with RyR2's (30, 235, 257). This arrangement of cardiac triads in no way negates an intimate association between DHPR and RyR2's. Indeed, in attempts to model experimental results from cardiac E-C coupling studies, Stern was required to assume that Ca^{2+} influx through the DHPR's would preferentially contact RyR2's on the SR membrane (and not enter the bulk cytosol) allowing activation for the proposed calcium-synapse model of cardiac CICR (253). In support of a confined and local increase in Ca^{2+} concentration at the triadic gap were voltage-clamp experiments that suggested Ca^{2+} may increase to mM concentrations between t-tubule and SR membranes (127).

As suggested, activation and inactivation of RyR2-mediated CICR is by nature Ca^{2+}-dependent. The inactivation of the RyR2 by rising Ca^{2+} concentrations appears to occur on a time scale too slow to be considered physiological (98, 275). It has therefore been suggested that inactivation of CICR may be regulated by the removal of Ca^{2+} from the triadic space. The sequestration of Ca^{2+} by the Ca^{2+}-ATPases on the SR membrane is the likely candidate in this process. This would spatially separate the sequestered Ca^{2+} from the terminal release sites of the SR possibly allowing RyR2 inactivation (228). The other mechanism, also implicated in maintaining steady state SR Ca^{2+} content, is the Na/Ca exchanger which is located on the sarcolemmal membrane but spatially separated from the junctional face (3). The Na/Ca exchanger transports one Ca^{2+} ion from the cytoplasm for 3 Na^{+} ions into the cytoplasm. There is evidence that the Na/Ca exchanger balances the influx of Ca^{2+} from the DHPR's, which activates CICR, with the efflux of

that trigger Ca^{2+}. The implication is that under normal circumstances the trigger Ca^{2+} is kept constant and therefore the Ca^{2+} released and re-sequestered by the SR is also maintained. It has been shown that the SR requires a specific Ca^{2+} load for the triggering of Ca^{2+} release, such that at low SR loads increased trigger Ca^{2+} was required for CICR and at high Ca^{2+} loads Ca^{2+} release may occur without cytosolic triggers (101, 202). These results suggest that the Na/Ca exchanger and Ca^{2+}-ATPase may have dual functions of inactivation of CICR mechanisms and maintaining the SR Ca^{2+} load at constant levels.

In agreement or disagreement with Ca^{2+}-dependent inactivation of the CICR mechanism is the recent modal gating behavior of RyR2 inactivation which has been suggested to be release channel adaptation (96, 97). The initial observation in single channel studies was that the fast release of caged Ca^{2+} triggers caused RyR2 activation and slow inactivation with maintained *cis* Ca^{2+} concentrations. The subsequent observation that RyR2 reactivation by the addition of further Ca^{2+} was functionally different from Ca^{2+}-dependent inactivation was suggested to be RyR2 adaptation (96). The mechanism by which RyR2's adapt to sustained Ca^{2+} triggers is unresolved, but multiple Ca^{2+} binding sites beyond the simple high affinity activation/low affinity inactivation sites have been suggested (38) The proposal that the RyR2 undergoes adaptation has not been supported by results from other laboratories (228).

It is clear that cardiac E-C coupling is dependent upon Ca^{2+} triggers and CICR from the SR. However, the gating controls of DHPR's, RyR2's and the inevitable inactivation of the Ca^{2+} trigger signal/CICR remain to be determined.

Plate 1. In **(A)**, early descriptions of silver stained sarcoplasmic reticulum (SR) are shown. In the upper figure, *K* represents the line of Krause which has since been termed the *Z line*. The ball-like structures (labeled *a*) on either side of the *Z-line* were considered to be elements of the SR. The lower figure shows repeating *Z lines* (*K*) with the darker staining SR (labeled *b*) on either side of the *Z lines* resting where, according to current descriptions, the A and I bands meet. The connecting lines (labeled *d*) between two SR lines were thought to represent the longitudinal SR (taken from 245). Panel **(B)** shows an electron micrograph of the ultra-structural organization of a skeletal muscle sarcomere and labeled with the current terminology of the *Z-line*, *A* and *I bands*, and the *H-zone* (taken from 60). Shown in Panel **(C)** is an electron micrograph of a longitudinal section of toadfish striated muscle showing the sarcoplasmic reticulum. The triads are shown at the A-I junction and are identified with the central, circular T-tubule surrounded by two adjacent SR terminal cisternae. The separation between the terminal and longitudinal SR is clearly evident in the image. The arrows refer to the region of the SR at the position of the *Z-line* (taken from 75).

Plate 2. This figure correlates the electrical events of membrane depolarization with Ca^{2+} transients and the mechanical event of muscle contraction from an isolated *Balanas* fiber from a barnacle. The uppermost trace (1) is the membrane depolarization response of the fiber to an electrical stimulus event of 3.5 V (shown in trace 4) as recorded with an intracellular electrode. The injection of the fiber with the Ca^{2+} sensitive protein, aequorin, allowed the recording of the cytosolic Ca^{2+} transient response to the same stimulus (trace 2). A force transducer was used to monitor the development of tension during the time period after the stimulus (trace 3). The elapsed time was 1000 msec. (Taken from 9).

PLATE 2

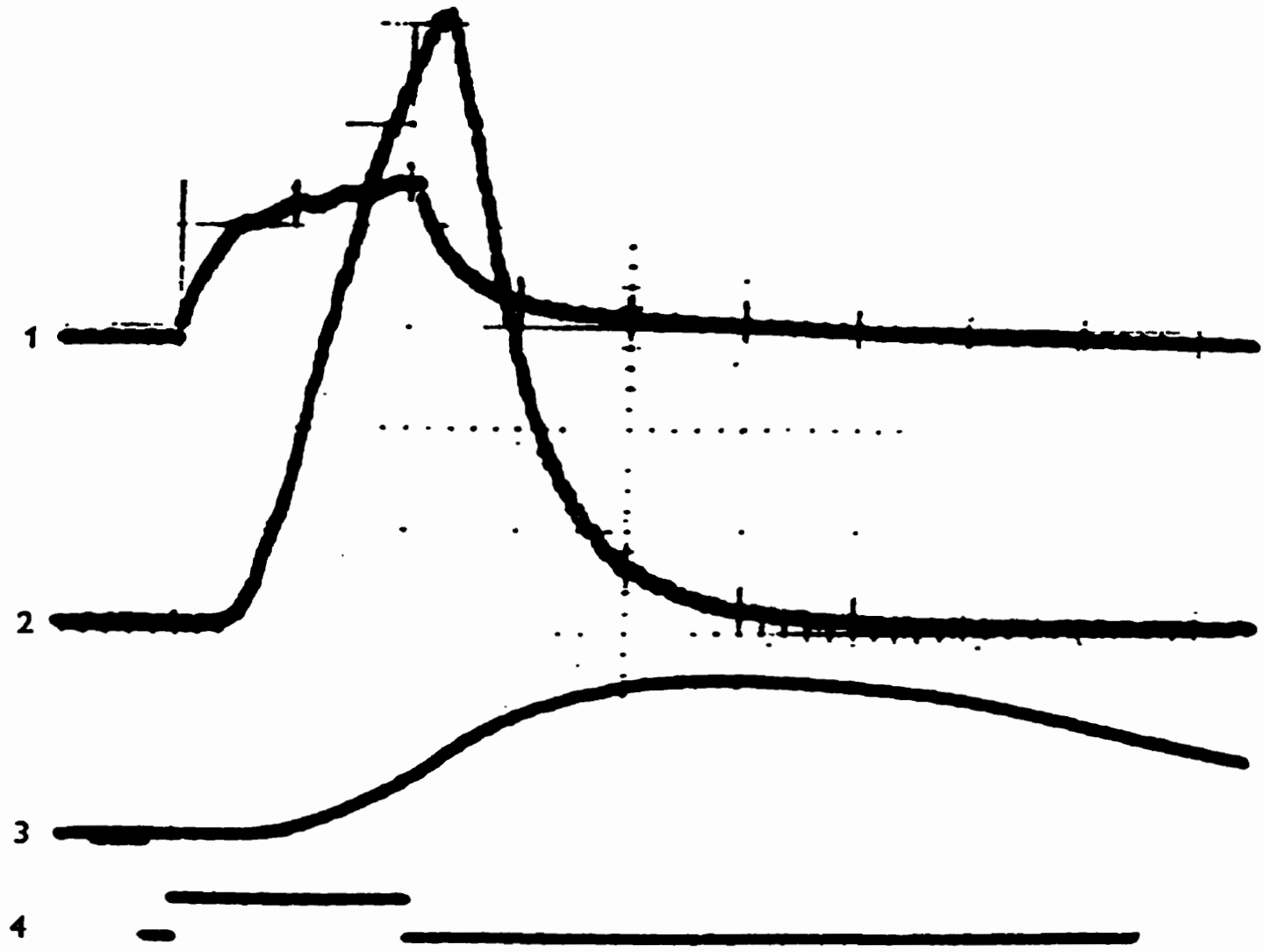

Plate 3. A schematic representation of the transport of 2 Ca^{2+} ions from the cytosol to the SR lumen by the SERCA pump. 1. Binding of 2 Ca^{2+} ions to the transport sites on the E (Ca^{2+} absent) form of the ATPase. 2. Binding of Mg^{2+} and ATP and the subsequent phosphorylation of the Ca^{2+} bound enzyme. 3. The events in 2. allow conformational changes such that the 2 Ca^{2+} ions are shuttled from the cytosol, to the interior of the SERCA protein, and finally to luminally positioned low affinity Ca^{2+} binding sites. The Ca^{2+} ions are released to the SR lumen. 4. The phosphorylated Ca^{2+} free enzyme is hydrolyzed such that the Mg^{2+} and phosphate are removed and the SERCA pump returns to the E form with the Ca^{2+} binding sites facing the cytosol. (taken from 182)

PLATE 3

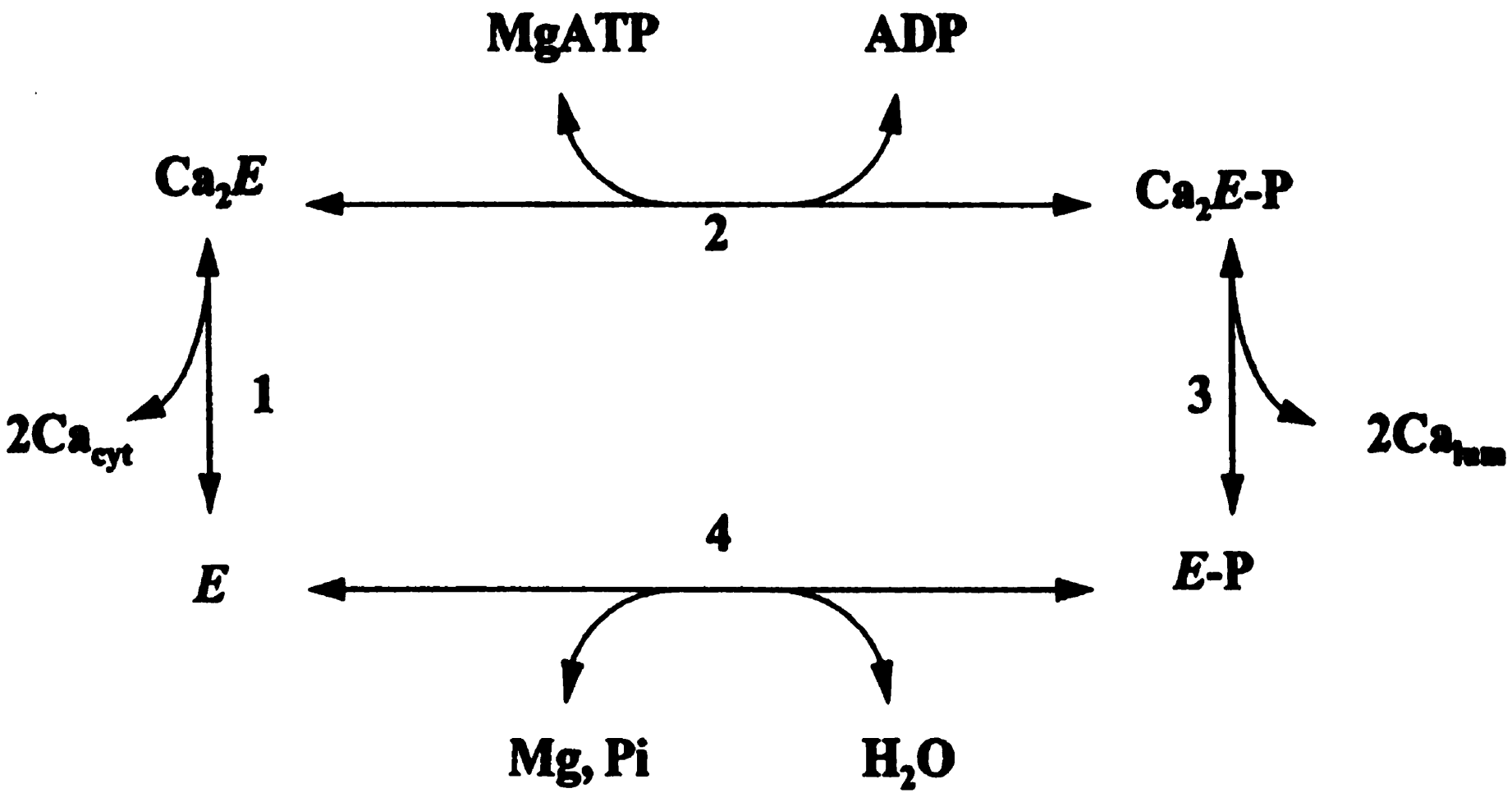

Experimental Procedures

Materials

Creatine phosphate (CP), creatine phosphokinase (CPK), pyruvate kinase (PK), phosphoenolpyruvate (PEP), adenosine triphosphosphate (ATP), and nicotinamide adenine dinucleotide (reduced, NADH) were acquired from Boehringer Mannheim. Lactate dehydrogenase (LDH), ryanodine, ionomycin, cyclopiazonic acid (CPA) were purchased from Calbiochem. Thapsigargin was purchased from L.C. Laboratories. The fluorophores Mag-Fura 2, Mag-Fura 2-AM, and Calcium Green-2, as well as Calcium Sponge-S, were all acquired from Molecular Probes. All electrophoresis reagents were obtained from Bio-Rad. All other chemicals were of analytical grade and were obtained from Sigma.

Isolation of HSR Membranes

Isolation of membranes was done as previously described (90) with modifications. Immediately following sacrifice of an anaesthetized White New Zealand rabbit, the longissimus dorsi muscle was excised with a scalpel in sections approximately 2" squared. Connective tissue was removed to minimize contamination. The sectioned muscle was compressed between a custom Wollenburg clamp fashioned with 3 inch square aluminum plates (0.5 cm thick) and immediately submerged in liquid nitrogen. This formed fast-frozen discs of between 5 and 10 g each. Frozen samples were bagged, labeled and stored at -70° until required.

All steps in the isolation of SR vesicles were performed at 4° C (in cold room) and with plasticware unless otherwise stated. A ceramic mortar was secured within a bed of ice and precooled with liberal amounts of liquid nitrogen. The frozen muscle sections were weighed to a total of 180 g. The muscle was ground, one or two sections at a time, to a fine powder with the mortar and pestle under liquid nitrogen. The powdered tissue was added slowly to 900 mls of homogenization buffer (300 mM sucrose, 20 mM imidazole, pH 7.4) containing 1 mM PMSF, 1 mM DTT, 2 μM leupeptin, 0.5 mM Tris-ATP, and 0.5 mM EGTA. The powdered muscle was then stirred into a thick slurry. Aliquots of approximately 200 mls were transferred into a Waring (250 ml) stainless steel commercial blender and gently homogenized at slow speed with a 40 secs on - 40 secs off - 40 secs on protocol. The blended material was transferred into 250 ml Nalgene centrifuge bottles and centrifuged in a JA-14 rotor for 10 mins at 10,000 rpm.

The pinkish supernatant was then filtered through 4-ply cheesecloth and the pellet and colloidal material were discarded. The filtered material was aliquoted into centrifuge tubes and centrifuged in a JA-17 rotor at 17,000 rpm for 1.5 hrs following which the supernatant was discarded while the pellet was saved. Approximately 500 μl of homogenization buffer containing 1 mM PMSF, 1 mM DTT and 2 μM leupeptin was added to each centifugation tube. Gentle agitation with a rubber policeman was used to free the pellet from the bottom of the tube. The loose pellets were transferred, 3 at a time, to a 5 ml Wheaton Potter-Elvehjem glass tissue grinder and gently homogenized to an even consistency with a teflon pestle. The final volume of all the homogenized pellets was approximately 12 mls. Two ml aliquots were loaded slowly onto the top of 25 to 45

% sucrose gradients. Gradients were made, prior to isolation, by consecutive freezing of 7 ml layers (25, 30, 35, 40, 45 % sucrose containing 5 mM imidazole at pH 7.4 and DTT/leupeptin) in a disposable thin-walled Beckman centrifuge tube and stored indefinitely at -70° C. One day before required, the gradients were thawed overnight at 4° C. The loaded SR proteins were separated on the gradients by centrifugation in a SW28 swinging bucket rotor at 23,000 rpm for between 24 and 27 hrs.

The gradients were removed and each visible layer of material was pipetted into a separate receptacle. "Intermediate" SR vesicles formed thick bands in the 35-40% region of the gradients while "heavy" SR vesicles were banded in the 40-43% region. Volumes of approximately 40 mls for each fraction were collected. ISR and HSR fractions were diluted 2 fold with 5 mM imidazole (pH 7.4) and KCl was added, slowly, to a final concentration of 150 mM. This was a Ca^{2+} wash step which decreased amounts of contaminating Ca^{2+} in the membrane preparations and has also been shown to rupture triadic connections still present in HSR membranes. Vesicles were washed for 1 hour at 4° C under gentle stirring.

Washed vesicles were centrifuged for 1 hour at 19,000 rpm in a JA-20 rotor. The supernatant was discarded while the pellets were resuspended (as described earlier) in 300 mM sucrose/50 mM diK^+ PIPES (pH 7.4) containing DTT and leupeptin. The final volume was approximated to about 5 mls and the final concentration of vesicles was consistently found to be between 30-40 $mg \cdot ml^{-1}$. SR vesicles were aliquoted into 500 µl eppendorf tubes, frozen in liquid nitrogen and stored at -70° C until needed.

Protein Determination

SR vesicle protein concentrations were determined by the method of Harrington (101a) using bovine serum albumin as a standard.

SDS-PAGE

Sodium dodecyl sulfate polyacrylamide gel electrophoresis (SDS-PAGE) of HSR membranes was performed as previously described (91a). Briefly, SR proteins were resolved on 3-13 % denaturing analytical 1.5 mm SDS-PAGE slab gels. Proteins (1000 $\mu g.ml^{-1}$) at a final of 100 μg, were solubilized in SDS-PAGE sample buffer containing 187.5 mM Tris-HCl (pH 8.8), 2 % SDS, 10 % glycerol, 5 % 8-mercaptoethanol and 0.02 % bromophenol. Proteins were stained with either Coomassie Brilliant Blue R-250 or Stains-All.

Luminal Loading of HSR Membranes with Mag-Fura-2, AM

The calcium-sensitive fluorophore, Mag-Fura-2, AM was reconstituted in DMSO at a final stock concentration of 1 mM. Briefly, freshly isolated HSR vesicles were resuspended in transport buffer containing 300 mM sucrose, 50 mM di·K^+-PIPES, supplemented with 4 μM Leupeptin, 2 mM DTT, at pH 7.4 (TB1).

Loading of 5 mg/ml HSR vesicles with 5 μM Mag-Fura-2, AM was performed by incubation in TB1 at 25 °C for 30 min, with moderate stirring and in complete darkness. Following incubation, vesicles were diluted (in TB1) and aliquoted under low-light conditions into ultracentrifuge tubes at a final volume of 25 ml/tube. HSR vesicles were concentrated by ultracentrifugation in a Beckman 50.2 Ti rotor for 30 min at 4° C and

148 000 x *g*. The supernatant was discarded and the vesicles were washed by gently resuspending the pellets in 20 ml total volume of TB1 and stirred as above. After washing, vesicles were again concentrated by ultracentrifugation as above. HSR pellets were then carefully resuspended in 1 ml/tube of TB1, aliquoted, flash-frozen in liquid nitrogen, and then stored in a lumino-protective container at –70° C.

Loading of HSR Vesicles with Chlortetracycline

Chlortetracycline (CTC), HCl was reconstituted in 10 ml of transport buffer at a final concentration of 1 mM and then aliquoted, frozen, and stored at –30° C. Immediately before each experiment was performed, freshly thawed HSR vesicles (500 $\mu g.ml^{-1}$) were loaded with 40 μM CTC in 3 mls TB. Low light and constant stirring were also employed during loading. Proper loading required > 5 minutes to allow for adequate equilibration of CTC across the HSR vesicular membrane. CTC transport to the lumen of HSR membranes was facilitated by the SERCA1-mediated co-transport of Ca^{2+} (181). Initiation of Ca^{2+} transport and Ca^{2+} loading of CTC-loaded HSR membranes occurred as described below.

Assay of Ca^{2+} transport

All Ca^{2+} fluorescence measurements were performed with a Photon Technology International Quantimaster ™ steady state spectrofluorometer with a Deltaram upgrade. Experiments were carried out in a quartz cuvette (3 ml) thermostatically regulated to 25° C and under constant mixing with a magnetic flea. Data acquisition occurred through Windows©-based Felix software.

Monitoring of extraluminal Ca^{2+} transients was performed with either Calcium Green-2 (Ex 506 nm/Em 531 nm) or Mag-Fura 2 (cell impermeant) (Ex1 340, Ex2 380/Em 510). Ca^{2+} transport assays were performed as follows: HSR membranes (100-1000 $\mu g.ml^{-1}$, as indicated) were pre-incubated for > 5 minutes in quartz cuvette containing transport buffer (TB = 300 mM sucrose, 50 mM dipotassium Pipes (pH 7.0), 0.8 μM Calcium Green-2 or Mag-Fura 2, and 17.5 $u.ml^{-1}$ CPK. All assays were initiated with the combined addition of 1 mM Mg.ATP and 10 mM CP. The CP/CPK enzyme system was important for constant ATP regeneration as consumed by the SERCA1 pump. All additions were made through an overhead injection port which allowed uninterrupted assays.

Synchronous determinations of NADH fluorescence (Ex 410 /Em 451 nm), expected to indicate ATP consumption by the SERCA1, were performed with Calcium Green-2. With synchronous assays, HSR membranes (100-1000 $\mu g.ml^{-1}$) were preincubated in TB containing 0.8 μM Calcium Green-2, 400 μM NADH, and 17.5 $u.ml^{-1}$ LDH and PK. In this case, Ca^{2+} transport was initiated by the combined addition of 1 mM Mg.ATP and 10 mM PEP. The coupled enzyme reaction has PEP converted to pyruvate with ADP being regenerated to ATP. In the next step of the pathway, pyruvate is converted to lactate with the concommitant consumption of NADH.

Luminal Ca^{2+} transients were monitored identically as described for extraluminal indicators except that Mag-Fura 2-loaded (Ex1 340 nm, Ex2 380 nm/Em 510nm) or chlortetracycline-incubated (Ex 440 nm/Em 510 nm) HSR membranes (500 $\mu g.ml^{-1}$, unless otherwise indicated) were used for fluorescence determinations.

Post-acquisition data manipulation

Fluorescence curves collected in Felix were subsequently exported to Prizm software for analysis and subsequent presentation of traces. Conversion of Calcium Green-2 and Mag-Fura 2 to [Ca^{2+}] and NADH to [NADH] or ATPase activity were performed as outlined in 'Results'.

Isolation of calsequestrin

Calsequestrin was separated from isolated HSR membranes as described previously (24). Briefly, HSR membranes containing approximately 10 mg calsequestrin (assumed that calsequestrin comprises 25 % of HSR protein) were diluted in homogenization buffer (300 mM sucrose, 20 mM imidizole, pH 7.0) containing 1 mM DTT and 2 μM leupeptin to 10 mls. Proteins were centrifuged at 50 000 x g in a Beckman 70iTi rotor for 30 minutes. The pellets were resuspended in 20 mls of ice cold sodium carbonate (100 mM at pH 11) and incubated on ice for 30 minutes. Proteins were centrifuged a second time as described above. The supernatant was transferred into a 15 cm strip of dialysis membrane and dialyzed overnight in 1 L of PC buffer (50 mM MOPS, 500 mM NaCl and 1 mM DTT, pH 7.0). The dialyzed protein was run on a 5 ml butyl-sepharose column and eluted with PC buffer containing 10 mM $CaCl_2$.

Results

A. Characterization of HSR membranes and Calcium Green-2, NADH Calibration

Isolation of skeletal muscle SR membranes by sucrose density centrifugation yields fractionated SR vesicles with differential protein compositions (see 'Experimental Procedures') as previously identified (90, 91, 176). To verify the current vesicle preparations, 1 mg/ml HSR and ISR membranes were resolved on 3-13 % SDS-PAGE gradient gels and stained with either Coolmassie-R250 or Stains-All. Figure 1, Panel A, shows that HSR vesicles (lanes 1 and 3) contain RyR Ca^{2+} channels, SERCA pumps, and the luminal Ca^{2+} binding protein CSQ as identified by the positions on the gels relative to molecular weight markers. On the other hand, ISR vesicles (lanes 2 and 4) were virtually devoid of RyR and CSQ when visualized with the same Coolmassie (lanes 1 and 2) and Stains-All (lanes 3 and 4) protein-stains. The presence of RyR1, SERCA1, triadin and absence of SERCA2 in HSR vesicles was further confirmed by antibody identification. In Panel B the immunoreactive staining to RyR1 (lane 1) and triadin (lane 2) are seen. In Panel C, mainly SERCA1 (lane 1), not SERCA2 (lane 2), was recognized in HSR membranes. When HSR vesicles were resolved under electron microscopy (EM) (Panel D) at 60 000x magnification, the protruding RyR1 'feet' proteins could be visualized. The inset to Panel D shows that these 'feet' appeared to align with other RyR1 channels on neighboring vesicles forming vesicle conglomerates. The EM observations were correlated with confocal microscopy using fluorescent species of ryanodine and thapsigargin (data not shown). These three-dimensional images also showed large conglomerates consisting of numerous individual HSR vesicles. The localized ryanodine

fluorescence, indicative of RyR presence, was directly overlaid with thapsigargin fluorescence, indicative of SERCA presence. These images provided further evidence that any given vesicle contains both RyR1 channels and SERCA1 pumps.

SR vesicles are known to both passively and actively accumulate Ca^{2+} and can be stimulated to release the accumulated Ca^{2+} through the presence of RyR1 channels (90). The use of extravesicular Ca^{2+} probes to monitor real-time ATP-dependent, SERCA1-mediated Ca^{2+} sequestration and RyR1-mediated Ca^{2+} release have also been documented (91). In this study, we have for the majority, utilized Calcium Green-2 (CG2), and to a lesser extent Mag-Fura-2 (MF2), as extravesicular fluorescent Ca^{2+} indicators. CG2 is a long wavelength Ca^{2+} indicator that is excited by visible light, is responsive to Ca^{2+} in the low μM range and undergoes large increases in fluorescence emission due to Ca^{2+} binding (Molecular Probes booklet). CG2 is excited at 506 nm and emissions are collected at 531 nm. The reported Kd is 550 nM. To verify the Kd under current conditions employed for monitoring active Ca^{2+} transport, CG2 (0.8 μM) was calibrated in transport buffer (TB = 300 mM sucrose, 50 mM diK^+ PIPES, pH 7.0, 25° C) containing Ca^{2+}:EGTA at increasing free Ca^{2+} concentrations from 0 to 1 mM and emission scans were collected. Fluorescence values obtained from the scans were plotted against the log[Ca^{2+}] to acquire the Hill Plot shown in Figure 2, Panel B. Emission scans were performed in both the presence (open symbols) and absence (closed symbols) of 250 $\mu g.ml^{-1}$ HSR protein. A slightly higher Kd of 579 nM was obtained and used for conversion of CG2 traces to Ca^{2+} concentrations as shown in Equation 1.

Equation 1:

$$[Ca^{2+}] = 579 * (F - F_{MIN}) / (F_{MAX} - F)$$

where: 579 = Kd

F = fluorescence intensity

F_{MIN} and F_{MAX} = fluorescence minimum and maximum

The synchronous monitoring of SERCA1 catalytic activity and Ca^{2+} transport was performed with a coupled enzyme reaction in which the reduction of NADH was followed as an indication of ATP hydrolysis (see 'Experimental Procedures'). Calibration of NADH fluorescence signals (Ex_{377}/Em_{451} nm) is shown in Figure 2, Panel A. A series of emission scans were collected using TB and increasing NADH concentrations (0 to 1 mM). The normalized maximum fluorescence was plotted against NADH concentration in a relationship that was well described by the second order polynomial shown in Panel A. Only data up to 400 μM NADH are shown as fluorescence emissions at NADH concentrations above this value were decreased when compared with the 400 μM values, probably due to fluorescence quenching of the NADH signal. Thus a maximum of 400 μM NADH was used for assaying Ca^{2+} transport. This concentration of NADH was sufficient for resolving SERCA1 catalytic activity within time-restrained sections of Ca^{2+} transport assays but became limiting for events occurring outside the window of NADH consumption (see later Figures). On the other hand, loss of NADH supply was not limiting for the regeneration of ATP required for sustained Ca^{2+} transport and maintenance of luminal to cytosolic Ca^{2+} gradients because recycling of ADP to ATP occurred in the initial step of the coupled enzyme reaction. For ATP regeneration, 10 mM PEP (or 10 mM CP in conditions where NADH was not utilized)

was added in combination with ATP to initiate Ca^{2+} transport and for sustained supplies of ATP. Equation 2, as derived from the second order polynomial curve fit shown in Panel A, was used to convert NADH fluorescence to NADH concentrations.

Equation 2:

$$[NADH] = 0.0466 + 0.00422F - 4.91e^{-6}F^2$$

where:F = fluorescence intensity

B. Extravesicular Ca^{2+} transients and the coordination between SERCA1 catalytic activity and RyR1 channel opening.

NADH fluorescence changes (Ex_{377}/Em_{451}) were initially monitored to elucidate the dependence of SERCA1 catalytic activity/NADH reduction upon the cytosolic free Ca^{2+} concentrations during active HSR membrane Ca^{2+} transport (Figure 3). These experiments were performed with Ca^{2+}:EGTA buffers to effectively clamp extravesicular Ca^{2+} at the concentrations desired. NADH fluorescence traces were converted to ATPase activity with the assumption that nmols NADH reduced would be equivalent to nmols ATP consumed by the SERCA1 pump. Thus NADH consumption curves were converted to nmol NADH reduced/mg HSR protein/min and plotted against the log of the EGTA clamped free cytosolic Ca^{2+} concentrations. Control SERCA1 activities at each Ca^{2+} condition were compared to those activities in which 50 μM ryanodine was present and expected to result in opened RyR1 receptors, as well as where ionomycin was present resulting in HSR membrane leaks. Figure 3 demonstrates (1) increased maximal SERCA1 activation with ionomycin- (open squares) or ryanodine- (closed triangles) induced membrane Ca^{2+} leaks and (2) increased steepness of the Ca^{2+}-dependent

activation curve in the face of ryanodine- (closed triangles) induced activation of Ca^{2+} release channels. Increased free cytosolic Ca^{2+} appeared to only partially activate SERCA1 catalysis when compared to situations that favored HSR membrane Ca^{2+} leaks, which, in turn, resulted in near-maximal catalytic activity. The possibility that RyR1 channel activation may induce SERCA1 activation preliminarily indicated that Ca^{2+} release may somehow be coupled to Ca^{2+} sequestration.

The dependence of SERCA1 activity upon increased cytosolic Ca^{2+} loads was further examined with the synchronous monitoring of CG2 and NADH fluorescence. These experiments were done, in the absence of high concentrations of cytosolic buffers like EGTA, under quasi-physiological conditions which allowed free exchange of added boluses of Ca^{2+} between the extravesicular space and the lumen of the SR vesicles. Although HSR vesicles are KCl washed during isolation procedures (see 'Experimental Procedures') the membranes were not devoid of Ca^{2+} and upon dilution into TB medium, a sustained and passive efflux of Ca^{2+} was always seen with CG2 (data not shown). Analysis of HSR membranes with atomic absorption spectroscopy revealed an endogenous source of Ca^{2+}, probably CSQ and other bound luminal stores, such that 250 $\mu g.ml^{-1}$ HSR vesicles had approximately 10 μM associated, contaminating, Ca^{2+}.

The data in Figure 4, Panel A, reflect conditions where 0, 15 μM, and 17.5 μM exogenous Ca^{2+} was added to 500 $\mu g.ml^{-1}$ HSR membranes, in addition to endogenous Ca^{2+}, prior to Mg.ATP stimulation of SERCA1-mediated Ca^{2+} sequestration. Under conditions where no exogenous Ca^{2+} was added (0 condition), the addition of Mg.ATP resulted in a rapid removal of Ca^{2+} from the cytosol to the SR lumen and the maintenance of steady state extravesicular Ca^{2+} at about 50 nM. The corresponding NADH trace (0,

Panel B) revealed that little NADH was consumed during the initial phase of Ca^{2+} transport and that basal rates of NADH consumption were required (330 nmol NADH/mg HSR protein/min) to maintain the steady state outward Ca^{2+} gradient. No changes to these profiles were observed until increases in added exogenous Ca^{2+} approached 15 μM. This level of Ca^{2+} pre-load resulted in a slower removal of Ca^{2+} from the cytosol (Panel A) accompanied by burst SERCA1 catalytic activity which transitioned to near-basal levels (Panel B). The inflection point of this transition coincided with the completed removal of extravesicular Ca^{2+} to steady state levels at the 25 second time point. Although this finding may indicate Ca^{2+} pump cycling in order to reduce an increased cytosolic Ca^{2+} load, the transitory nature of the NADH signal in this case may reflect the influence of added exogenous Ca^{2+} upon the RyR1. This is based upon the findings in Figure 3 and can be explained by bursts in SERCA1 activity being indicative of Ca^{2+} pumping against RyR1 leak states, while return to basal SERCA1 activity indicative of RyR1 channel closure. Increases in added Ca^{2+} by only 2.5 μM in Figure 4, to a total of 17.5 μM exogenous Ca^{2+} pre-load, resulted in a much suspended removal of extravesicular Ca^{2+} (Panel A) accompanied by a sustained near-maximal activation of SERCA1 catalysis (Panel B) beyond the limited supply of NADH (4200 nmol/mg/min).

This apparent dependency of SERCA1 activity upon RyR1 channel opening was further examined with the use of the plant alkaloid, ryanodine, which is known to (a) bind preferentially to the open state of the RyR1 (107), (b) lead to activation of RyR1 (178), and (c) inactivate the RyR1 with prolonged incubation (150). The use of ryanodine to evoke RyR1 channel opening was important for removing the added influence of added high exogenous Ca^{2+} concentrations upon SERCA1 activation. In

Figure 4, HSR membranes (250 μg.ml^{-1}) were pre-treated with increasing concentrations of ryanodine and initial Mg.ATP-dependent Ca^{2+} sequestration was monitored with CG2 (Panel C) and NADH fluorescence (Panel D). At ryanodine concentrations of 5 μM, initial Ca^{2+} uptake appeared only slightly reduced compared to controls. Surprisingly, this ryanodine pre-treatment resulted in burst SERCA1 catalytic activity, followed by a resumption to levels that were 2 fold faster than controls (790 nmols/mg/min compared to 360 nmols/mg/min). Under these conditions it seemed that the biphasic increase in SERCA1 activity was a direct result of RyR1 channel opening which was followed by an apparent, sustained, RyR1 channel Ca^{2+} leak state induced by ryanodine. When ryanodine concentrations were further increased to 50 μM, Ca^{2+} sequestration rates were greatly reduced (Panel C) while the corresponding rates of SERCA1 (Panel D) increased 13 fold over controls (4800 nmols/mg/min) with the available supply of NADH being consumed within seconds.

RyR1-mediated Ca^{2+} release from HSR membranes can be implied from the observed large, cytosolic Ca^{2+} transients during sequential Ca^{2+} pulse loading experiments where HSR Ca^{2+} fluxes are monitored by cytosolic Ca^{2+} indicators. Furthermore, the luminal Ca^{2+}-dependence of Ca^{2+}-induced Ca^{2+} release (CICR) can be indirectly assumed and quantitated from these pulse loading experiments. In Figure 5, 500 μg.ml^{-1} HSR vesicles were subjected to well-defined Ca^{2+} transport protocols while Ca^{2+} transients were recorded with either CG2 (Panel A) or MF2 (cell-impermeant, Panel B). In both cases, Ca^{2+} transport was initiated by the combined addition of 1 mM Mg.ATP/10 mM CP at the curved arrow. Sequential 5 μM Ca^{2+} pulses were added (both Panel A and B) resulting in small cytosolic Ca^{2+} transients indicative of rapid Ca^{2+}

sequestration by the HSR membranes. Large cytosolic Ca^{2+} transients are identified after the sixth (Panel A) or seventh (Panel B) 5 μM Ca^{2+} addition and were assumed to be RyR1-mediated CICR. Furthermore, if HSR membranes required five or six Ca^{2+} additions to be sequestered, and thus luminally loaded, before CICR was elicited than threshold Ca^{2+} loading for 500 $\mu g.ml^{-1}$ HSR membranes can be calculated to be between 150 to 180 nmol Ca^{2+}/mg HSR, respectively.

The large cytosolic Ca^{2+} transients, noted during Ca^{2+} pulse loading, do not themselves reveal whether RyR1 channels are activated during these events. It is also not clear from these experiments whether RyR1 channels became activated at other points during Ca^{2+} pulse loading. In Figure 5, Panel C, ryanodine was employed to probe RyR1 channels at the peak of cytosolic Ca^{2+} transients and during the rapid re-sequestration phase of CICR. In this experiment HSR membranes (250 $\mu g.ml^{-1}$) were Ca^{2+} pulse-loaded and CICR was evoked. At these HSR vesicle concentrations, the number of 5 μM Ca^{2+} additions required for CICR was halved but the luminal Ca^{2+} load dependency of CICR (120 nmol Ca^{2+}/mg HSR) was similar to that required for 500 $\mu g.ml^{-1}$ HSR membranes. Ryanodine (250 μM) was added at the peak of the CICR Ca^{2+} transient (trace 1), when Ca^{2+} re-sequestration was partially complete (trace 2), and when Ca^{2+} re-sequestration was close to full completion (trace 3). Ryanodine addition was ineffective for RyR1 channel reactivation, noted in trace 1 and 2 by the stimulation of further, large cytosolic Ca^{2+} transients upon ryanodine addition, only when Ca^{2+} re-sequestration was nearing full completion. Indeed, RyR1 channel activation in trace 3 occurred only with the subsequent addition of a 5 μM Ca^{2+} pulse. The balance between RyR1 activation and inactivation revealed by comparing traces 2 and 3, suggested that the entire population of

RyR1 channels may undergo differential inactivation. Thus, complete Ca^{2+} sequestration would involve closure of some RyR1 channels and partial Ca^{2+} accumulation by these vesicles before all RyR1 channels inactivated. The data in Panel C implicate RyR1 channel activation as governing the large increases in cytosolic Ca^{2+} transients, but also inactivation of RyR1 channels leading to completed Ca^{2+} re-sequestration.

The sensitivity of CICR upon luminal thresholds and trigger pulses of Ca^{2+} shown in Figure 5 may reflect the sensitivity of RyR1 channels to Ca^{2+} distributions across HSR membranes. This was further examined with Ca^{2+} pulse loading of 250 $\mu g.ml^{-1}$ HSR vesicles in experiments where the concentrations of the Ca^{2+} pulse additions were varied (Figure 6). In a series of highly reproducible traces, HSR membranes were incrementally presented with 2.5, 3.33, 4.16, 5, 6.67, 7, 8.33, 10, 13.33, and 16.67 μM Ca^{2+} and CG2 and NADH responses were recorded. Although all conditions are not shown, information from all 10 Ca^{2+} loading experiments were used to composite the figure in Panel D. Shown in Figure 6 are the 2.5 (Panel A), 5 (Panel B) and 10 μM (Panel C) Ca^{2+} pulse conditions. Taking into account the chelation of Ca^{2+} by the presence of 1 mM Mg.ATP, calculations indicated that these Ca^{2+} additions would be expected to raise cytosolic free Ca^{2+} concentrations to 0.54, 1.08, and 2.19 μM respectively. Panels A through C demonstrate that the presence of active SERCA1 pumps reduced the level of actual free Ca^{2+}, as recorded with CG2, produced by each Ca^{2+} bolus. However, in all cases, successive Ca^{2+} additions resulted in increases in observed free extravesicular Ca^{2+} that approached or surpassed these expected calculations.

In Panel A, repeated pulses of 2.5 μM Ca^{2+} produced no net Ca^{2+} release. The Ca^{2+} load requirements for CICR for 250 $\mu g.ml^{-1}$ HSR membranes was shown in Figure 5

to be approximately 120 nmol Ca^{2+}/mg HSR. HSR vesicles in Panel A were sufficiently loaded with 3 fold more Ca^{2+} (360 nmol Ca^{2+}/mg HSR by the final Ca^{2+} pulse addition), to levels where CICR should have been facilitated. The absence of Ca^{2+} release under these conditions suggests that a minimal level of cytosolic Ca^{2+} was also required, but not attained, by 2.5 μM Ca^{2+} pulse additions. The extravesicular Ca^{2+} transients recorded with CG2 increased with each successive 2.5 μM Ca^{2+} addition and the rate of removal of Ca^{2+} additions appeared to decrease. Although burst activation of SERCA1 pumps was not observed, the rate of NADH consumption, as Ca^{2+} pulse additions continued, did increase in a nonlinear fashion. This contrasted to the linear rates seen with steady-state basal SERCA1 activity in Figure 4.

When Ca^{2+} pulse additions were increased to 5 μM (Figure 6, Panel B), the initial two pulses were rapidly sequestered by SERCA1 pumps with little concomitant activation of ATP catalysis. However, distinct burst activations of SERCA1 catalytic activity were observed on the third and fourth Ca^{2+} additions. The cytosolic free Ca^{2+} concentrations where these activations are seen were 0.75 and 0.5 μM respectively. The Ca^{2+} load at these points of SERCA1 activation can therefore be calculated to include the Ca^{2+} pulses previously accumulated as well as the portion of the current Ca^{2+} pulse presumed sequestered at the point of activation. Thus, Ca^{2+} loads of 86 and 100 nmol Ca^{2+}/mg HSR protein were required at the observed SERCA1 activations at 0.75 and 0.5 μM free Ca^{2+}, respectively. This contrasted with the luminal Ca^{2+} load of 330 nmol Ca^{2+}/mg HSR protein attained with no net Ca^{2+} release in Panel A. Furthermore, when a single bolus of 10 μM Ca^{2+} was added (Panel C), an extravesicular free Ca^{2+} of >1.5 μM was required before activation of SERCA1 pumps was observed. In Panel B, RyR1

activation and net Ca^{2+} release is supported by the large increase in cytosolic Ca^{2+} at the fourth 5 μM Ca^{2+} pulse. However, when the free cytosolic Ca^{2+} concentrations required for activation of SERCA1 pumps are compared between Panel B and C, it becomes clear that cytosolic Ca^{2+} alone did not activate SERCA1 catalysis. Thus, even small RyR1 channel openings may have profound influences upon SERCA1 catalytic cycles, requiring high ATP consumption when pumping against membrane Ca^{2+} leaks. In Panel D, the entire range of incremental Ca^{2+} pulse addition experiments, where the total luminal Ca^{2+} load and the cytosolic free Ca^{2+} concentrations for burst NADH consumption/SERCA1 activation were calculated and plotted, is shown. The inverse relationship between luminal Ca^{2+} and cytosolic Ca^{2+} required for burst SERCA1 activations compiled in Panel D, further suggest that the regulation of both RyR1 opening/Ca^{2+} leak states and SERCA1 activation may occur through the effects of luminal Ca^{2+} loads upon these proteins.

C. Rates of SERCA1 catalytic activity and influence of ryanodine, thapsigargin, and cyclopiazonic acid upon Ca^{2+} gradient formation.

As shown in Figure 6, Panel A, each successive 2.5 μM Ca^{2+} pulse appeared to both increase the level of Ca^{2+} temporarily remaining in the cytosol, as well as, decrease the rate at which this Ca^{2+} transient was removed from the cytosol. These phenomenon may simply be a result of the same mechanism, that is a slowing of the rate at which SERCA1 pumps remove Ca^{2+} from the cytosol under steady state conditions, in the absence of RyR1 Ca^{2+} leaks. This in turn may affect RyR1 activation and Ca^{2+} leaks states as luminal Ca^{2+} loading was increased. To test this idea further, HSR membrane

concentrations were increased to 1 mg/ml. This effectively created a large Ca^{2+} sink to Ca^{2+} source ratio, making the driving force for Ca^{2+} sequestration far greater than the forces governing Ca^{2+} efflux. In Figure 7, the relationship between the rate of presentation of 5 μM Ca^{2+} pulses is shown. These rates of presentation were more or less arbitrarily chosen, with Panel A illustrating slow presentation (21 additions in 1000 seconds), while Panel B conversely showing a more rapid presentation (14 additions in <400 seconds), of Ca^{2+} pulse loading. The attainment of luminal threshold and CICR with rapid Ca^{2+} pulse additions in Panel B, but not with slowed Ca^{2+} pulse additions in Panel A, demonstrated that not only was there a luminal Ca^{2+} requirement for CICR but a mechanism by which luminal Ca^{2+} may be made available for release. Indeed, even with a series of more rapid Ca^{2+} additions (Panel A, section 2), the sensitivity of HSR membranes to CICR was lost. Panel B also showed that, following CICR, slower timed additions of Ca^{2+} were insufficient to elicit further Ca^{2+} release. To resolve the mechanism by which HSR membranes were 'pumped up' for CICR with rapid additions of Ca^{2+} in Panel B, the removal rate (i.e. the rate at which Ca^{2+} was removed from the cytosol to the vesicle lumen) of the first (Panel C, solid symbols) and the thirteenth (Panel C, open symbols) Ca^{2+} pulses were examined. The removal rate of the thirteenth Ca^{2+} addition was calculated to be ~3 fold slower than the removal rate of the first Ca^{2+} addition ($k = 0.378$ and $1.098\ s^{-1}$, respectively). Thus, attainment of threshold luminal Ca^{2+} loading and CICR may involve luminal Ca^{2+} influences upon SERCA1 removal of subsequent triggering Ca^{2+} pulses. Since slowed Ca^{2+} additions did not produce a similar effect, rapid 'pumping up' of HSR membranes for CICR is possibly related to the rate at

which Ca^{2+} is sequestered to the lumen of the vesicles and possibly how this relates to the compartmentalization of Ca^{2+} into bound or free luminal Ca^{2+} pools.

The effects of increased luminal Ca^{2+} loads were further examined with ryanodine, and the SERCA-specific inhibitor, thapsigargin (Tg). It was known from previous studies that Tg (1) binds to SERCA with a 1:1 stoichiometry, (2) preferentially binds to the Ca^{2+} unbound form of the enzyme, and (3) at sub-stoichiometric concentrations effectively decreased the catalytic turnover and Ca^{2+} translocation rates of the SERCA pump (124, 224, 284a). Figure 8 demonstrates the efficacy of ryanodine (Panel A and B) and Tg (Panel C and D) upon HSR Ca^{2+} transport at low (Panel A and C) and high (25 μM exogenous, Panel B and D) Ca^{2+} loads. At low luminal Ca^{2+} loads, neither the addition of 500 μM ryanodine, nor 500 nM Tg, influenced the steady state distribution of Ca^{2+} across the HSR membranes. When the vesicles were subsequently presented with exogenous Ca^{2+}, rates of initial cytosolic Ca^{2+} removal were reduced in a similar manner to Figure 4. Following completion of Ca^{2+} sequestration, luminal Ca^{2+} loads (150-160 nmol Ca^{2+}/mg HSR) were near threshold as seen with Ca^{2+} pulse loading experiments in Figure 5. The addition of either 500 μM ryanodine or 500 nM Tg under these conditions induced Ca^{2+} release in a multiphasic manner. The initial burst increase of cytosolic Ca^{2+}, that was immediately followed by a slower fluorescence incline, eventually transition into a rapid increase in cytosolic Ca^{2+} to maximal CG2 fluorescence values previously observed with CICR. The feed-forward appearance of both the Tg and ryanodine Ca^{2+} effluxes is indicative of an initial, small, drug-induced membrane Ca^{2+} leak that itself induced a secondary CICR. The ryanodine and Tg concentrations used in Figure 8 were chosen to potentiate observed effects. Indeed, higher concentrations of Tg

required no luminal Ca^{2+} loading to elicit Ca^{2+} releases (1-5 μM, data not shown, see also Figure 12). Conversely, ryanodine-induced Ca^{2+} releases from HSR membranes were invariably dependent upon a minimal level of luminal Ca^{2+} loading. Interestingly, at the sub-stoichiometric Tg concentration (500 nM) chosen in Figure 8, the Tg-induced Ca^{2+} release (Tg-ICR) was followed by Ca^{2+} re-sequestration. This finding may be related to the proportion of SERCA1 pumps to Tg concentration employed, and therefore may reflect partially inhibited SERCA1 pumps that initially were unable to maintain steady state Ca^{2+} gradients required for maintenance of closed RyR1 channels. The ability of HSR membranes to re-sequester Ca^{2+} under conditions where SERCA1 pumps were partially inhibited suggested an intimate relationship between the SERCA1 driving force for Ca^{2+} sequestration and the ability of pumps to inactivate RyR1 channels.

The sensitization of RyR1 channels to ryanodine at threshold luminal Ca^{2+} loads was possibly due to the influence of luminal Ca^{2+} upon the channel. Furthermore, in Figure 4, ryanodine pretreatment of HSR membranes and activation of RyR1 channels was accompanied by increased SERCA1 activity. To further examine the possible interdependence of SERCA1 pumping and RyR1 activation by ryanodine, HSR membranes undergoing active Ca^{2+} transport were treated with 250 μM ryanodine (Figure 9). In Panel A, HSR vesicles (250 $\mu g.ml^{-1}$) were incrementally loaded with 2.5 μM Ca^{2+} pulses following Mg.ATP-dependent initiation of Ca^{2+} transport. Membranes were loaded to threshold luminal Ca^{2+} loads (150 nmol Ca^{2+}/mg HSR) as indicated by previous Ca^{2+} loading protocols as well as the increased Ca^{2+} transient and activation of SERCA1 catalysis following the sixth-2.5 μM Ca^{2+} pulse. The addition of ryanodine was made subsequent to the inflection point where burst SERCA activity returned to near-

basal levels. Under these conditions, ryanodine induced a robust Ca^{2+} release with a dramatically decreased rate of Ca^{2+} re-sequestration. The dual effects of ryanodine to activate and subsequently inactivate RyR1 channels was dually demonstrated by the impotency of a final addition of 2.5 μM Ca^{2+} to elicit Ca^{2+} release following the initial ryanodine-induced Ca^{2+} release. Panel B is the segment of the trace in Panel A from 185 to 215 seconds which clearly demonstrated that the initial phase of RyR1 activation by ryanodine was accompanied by a >6 second period where NADH fluorescence increased prior to normal NADH consumption indicative of burst SERCA1 catalytic activity. Similar NADH pathway reversals have been observed with both ethanol- and Ca^{2+}-induced Ca^{2+} release (data not shown) and only under conditions where the requirement of threshold luminal Ca^{2+} loading had been achieved. NADH fluorescence increases appear to represent a luminal Ca^{2+} influence upon SERCA1 activity. In this case, activation of the RyR1 channel by ryanodine may have resulted in altered luminal Ca^{2+} distributions that ultimately affected the SERCA1 pump. Indeed, the effects of luminal Ca^{2+} appeared to either slow (see Figure 7) and/or reverse (Figure 9, Panel B) the forward reaction of the enzyme. However, the possibility that the reversals are a peculiarity of the coupled enzyme pathway cannot be ruled out.

The increased sensitivity of SERCA1 pumps upon treatment by Tg with threshold luminal Ca^{2+} loading was identified with the experiments in Figure 8. The possible role luminal Ca^{2+} has upon SERCA1 pumps was more extensively examined by Tg treatment of HSR membranes (500 $\mu g.ml^{-1}$) undergoing active, Mg.ATP-dependent Ca^{2+} transport and monitoring both CG2 and NADH fluorescence changes (Figure 10). Panel A shows that 750 nM Tg treatment following Mg.ATP addition and initial Ca^{2+} sequestration had

little effect on steady state cytosolic:luminal Ca^{2+}. Furthermore, basal rates of SERCA1 catalytic activity/NADH consumption (300 nmol NADH/mg HSR/min) were unaltered from controls (see 0 condition Figure 4). However, the sequential addition of three-5 μM Ca^{2+} pulses at ~1150 seconds resulted in a decreased luminal Ca^{2+} requirement for CICR (60 nmol exogenous Ca^{2+} /mg HSR compared with ~150-180 nmol exogenous Ca^{2+} /mg HSR in controls). The extraluminal Ca^{2+} transients in Panel A were greatly increased (compare to the three-5 μM Ca^{2+} additions in Panel B) indicating that for each addition of Ca^{2+} a greater proportion of the Ca^{2+} pulse remained in the cytosolic space. This further indicated that normal rates of Ca^{2+} sequestration had been reduced by previous Tg treatment of the HSR membranes. The reduced luminal Ca^{2+} loads required for CICR in the presence of substoichiometric Tg concentrations may therefore be related to the inability of partially inhibited SERCA1 pumps to effectively remove cytosolic Ca^{2+}.

Figure 10, Panel B, shows that an increased luminal Ca^{2+} load with three-5 μM Ca^{2+} additions (to 90 nmol exogenous Ca^{2+}/mg HSR) had little effect upon the efficacy of HSR membrane treatment with 750 nM Tg. Steady state levels of cytosolic Ca^{2+} following Tg addition were observed to increase slightly when compared to Panel A, while NADH consumption rates seemed to transiently decrease at the point of Tg addition. Interestingly, the overall rate of NADH consumption in Panel B was 2 fold higher than observed in Panel A. The increased luminal Ca^{2+} load in Panel B, and the energy requirements for maintaining that load of Ca^{2+} luminally may result in increased NADH consumption. When luminal Ca^{2+} loads were increased to 120 nmol exogenous Ca^{2+}/mg HSR (Panel C), the addition of 750 nM Tg resulted in a fairly rapid but multiphasic release of intraluminal Ca^{2+} stores as observed in Figure 8. Comparison of

the rates of cytosolic Ca^{2+} removal following TgICR (Panel C) and CICR in the presence of Tg (Panel A) showed that there was a 5 fold decrease (k = 0.05033 and 0.2701 s^{-1}, respectively) in Ca^{2+} re-sequestration following TgICR. The multiphasic nature of the Ca^{2+} release profile and the transition from a slow to rapid Ca^{2+} release (compare with Figure 8) further indicated that the initial action of Tg to inhibit the SERCA1 pump may result in a slow Ca^{2+} leak that feeds-forward to a CICR. The activation of SERCA1 catalytic activity with Tg-ICR also appeared non-linear, transitory and coordinated with the multiphasic rise in cytosolic Ca^{2+}. Catalytic activity of the SERCA1 pump transitioned from (1) near-basal (450 nmol NADH/mg HSR/min) before and at the time of Tg addition, (2) to a slowed increase in NADH consumption (1125 nmol NADH/mg HSR/min) as the fast phase of Ca^{2+} release was occurring, (3) followed by near-maximal activation (2250 nmol NADH/mg HSR/min) only after extraluminal Ca^{2+} had reached maximal CG2 fluorescence. However, burst SERCA1 activation observed with Tg-ICR were almost 2 fold less than control activation during CICR (compare 2250 with 4200 nmol NADH/mg HSR/min from Figure 4). The lowered near-maximal activity, together with sustained increases in extraluminal Ca^{2+} required for near maximal activation of SERCA1 pumps in the presence of Tg, indicated that sub-stoichiometric Tg concentrations may uncouple the activation of SERCA1 pumps from activation of RyR1 channels seen in previous Ca^{2+} loading protocols (Figure 6).

Tg effects upon SERCA1 activation/inhibition were further examined in Figure 11. In these experiments, HSR membranes (500 $\mu g.ml^{-1}$) were pretreated with increasing Tg concentrations at low (0 exogenous, Panel A and B) and high (17.5 μM exogenous, Panel C and D) cytosolic Ca^{2+} conditions and initial Ca^{2+} uptake was monitored with

CG2 (Panel A and C) and NADH (Panel B and D). With low cytosolic Ca^{2+}, Mg.ATP-dependent initial Ca^{2+} uptake in the absence of Tg was rapid with concomitant basal rates of SERCA1 catalysis (360 nmol NADH/mg HSR/min) which maintain steady state luminal:cytosolic Ca^{2+} levels. Rates of removal of endogenous, contaminating Ca^{2+} were drastically reduced with Tg pretreatments of 0.67 and 0.75 μM (Panel A). The NADH consumption rates for these slowed Ca^{2+} uptakes were biphasically increased with near-maximal activations (1800 and 1350 nmol NADH/mg HSR/min, respectively) reverting to near-basal rates of SERCA1 activity (405 and 477 nmol/mg HSR/min, respectively) upon sequestration of cytosolic Ca^{2+}. Increased Tg pretreatments of 2 μM resulted in complete inhibition of cytosolic Ca^{2+} transport and the return of NADH consumption rates to close to control values (450 compared to 360 nmol NADH/mg HSR/min for control) although the trace appeared strikingly non-linear in comparison. Surprisingly, ATP hydrolysis by SERCA1 pumps occurred even in the 2 μM Tg condition which may indicate alternate, non-SERCAases or Tg-resistant SERCA1 pumps present in the membrane preparation.

In Figure 11, Panel C, cytosolic Ca^{2+} was increased to 17.5 μM (exogenous) before initiation of Ca^{2+} uptake. In control, Tg absent conditions, this Ca^{2+} preload resulted in a slowed Ca^{2+} removal from the cytosol (Panel C) with a biphasic NADH consumption profile (Panel D) indicating SERCA1 activation (4050 nmol NADH/mg HSR/min) which sharply reverted to near basal inactivation (840 nmol NADH/mg HSR/min) upon completion of Ca^{2+} sequestration. Sharp and abrupt transitions in NADH traces between activated pumps and partially inactivated SERCA1 pumps due to completion of Ca^{2+} sequestration were absent from Tg induced transitions in SERCA1

activity (compare trace 0, Panel D with trace 0.75, Panel B). Under conditions of increased Ca^{2+} preload, 0.5 and 0.75 μM Tg pretreatment resulted in greatly protracted Ca^{2+} sequestration profiles (Panel C). In both cases SERCA1 activity (Panel D) was near-maximal and, in the 0.5 μM Tg pretreatment, sustained beyond sequestration of cytosolic Ca^{2+} as seen with CG2. The rates of NADH consumption were 1800 and 2400 nmol NADH/mg HSR/min for the 0.5 and 0.75 Tg conditions. These results again suggested an uncoupling of SERCA1 inactivation from the inactivation of RyR1 channels that ultimately resulted in removal of Ca^{2+} from the cytosol. Ca^{2+} sequestration by HSR membranes was completely arrested in the presence of Tg pretreatments of 1 and 5 μM. NADH consumption rates were 872 and 370 nmol NADH/mg HSR/min, respectively.

The impact of Tg treatment upon Ca^{2+} gradient formation and HSR Ca^{2+} release led to further investigation with a second specific SERCA1 inhibitor, cyclopiazonic acid (CPA). In Figure 12, HSR membranes (250 $\mu g.ml^{-1}$) were pretreated with increasing CPA concentrations and initial Ca^{2+} sequestration was monitored synchronously with CG2 (Panel A) and NADH fluorescence changes (Panel B). Mg.ATP-dependent rates of initial Ca^{2+} sequestration (Panel A) were not significantly altered with CPA concentrations of 5 or 10 μM but were completely arrested with concentrations in the higher μM range (100 μM). In the 5 and 10 μM conditions, CPA pretreatment did not prolong the initial removal of endogenous cytosolic Ca^{2+} as was observed with Tg (compare with Figure 11, Panel A), but did significantly alter steady state Ca^{2+} gradients. Comparison of control and CPA treated CG2 traces reveal relatively slow CPA-induced Ca^{2+} leak states that were dependent upon CPA concentration and completion of initial sequestration of contaminating Ca^{2+}. The cytosolic Ca^{2+} transients differed greatly

between 5 and 10 μM CPA. In the former, Ca^{2+} release rates were slow and after maximal Ca^{2+} release the fluorescence curve smoothly transitioned to decreased rates of cytosolic Ca^{2+} removal. In the latter, Ca^{2+} release rates were more rapid, maximal Ca^{2+} transients were more sustained, and Ca^{2+} re-sequestration was markedly slower than the 5 μM CPA condition.

In Panel B, the corresponding SERCA1 catalytic rates for each CPA pre-treatment from Panel A are shown. At the uppermost CPA concentration (100 μM) where initial Ca^{2+} sequestration was arrested, NADH consumption was inhibited and slower than control conditions (379 compared with 440 nmol NADH/mg HSR/min, respectively). Under CPA conditions where Ca^{2+} releases were observed following initial Ca^{2+} sequestration, rates of NADH consumption became concomitantly more rapid (compare the 5 and 10 μM CPA with the control and 100 μM CPA conditions at about 50 seconds). The SERCA1 rates were 554 and 628 nmol NADH consumed/mg HSR/min for 5 and 10 μM CPA pre-treatments, respectively. The rates of NADH consumption were unlike those seen with Tg in that no robust activations, nor transitions from rapid to near-basal rates with increased cytosolic Ca^{2+}, were observed with CPA.

The CPA-induced Ca^{2+} leak states shown in Figure 12, Panel A, suggested that the action of CPA upon SERCA1 inhibition was characteristically different from SERCA1 inhibition when Tg was employed (Figure 11, Panel A). Indeed, CPA has been suggested to be a competitive inhibitor of SERCA pumps, competing with ATP binding to the enzyme (232). Furthermore, SERCA inhibition by CPA has been reported as less potent and more reversible than Tg. Figure 12, Panel C, directly compared the potency of 20 μM Tg and CPA to induce Ca^{2+} release from low Ca^{2+}-loaded HSR membranes

(500 μg.ml^{-1}). The Tg-ICR was rapid and considerably more monophasic when compared to CPA-ICR. Furthermore, Tg was also more effective in completely discharging luminal Ca^{2+} stores (~2 μM cytosolic Ca^{2+}) than CPA (~1.35 μM cytosolic Ca^{2+}) which was additionally evident from the increased fluorescence signals following ionomycin treatment of the membranes. The multiphasic nature of the CPA-ICR again suggested that slow Ca^{2+} leaks may feed-forward to a regenerative CICR. To further examine the effects of CPA upon Ca^{2+} release, HSR membranes (500 μg.ml^{-1}) were treated with CPA at low (0 exogenous) or high (25 μM exogenous) luminal Ca^{2+} loads in a fashion similar to Figure 8. In Figure 12, Panel D, 5 μM CPA was shown to potently elicit Ca^{2+} release at threshold luminal Ca^{2+} loads (150 nmol Ca^{2+}/mg HSR) but not under conditions of low, endogenous Ca^{2+} load. The Ca^{2+} leak state induced by CPA was once again multiphasic, with a slow monotonic rise in cytosolic Ca^{2+} transitioning to a faster at more substantial Ca^{2+} release. These results were similar to those observed with Tg (see Figure 8) further suggesting that although CPA and Tg may differentially interact with SERCA1, both were more potent at eliciting Ca^{2+} releases under conditions where SERCA1 enzyme states had become influenced by threshold luminal Ca^{2+}.

Tg and CPA clearly affected the ability of the SERCA1 pump to maintain Ca^{2+} gradients across HSR membranes. The SERCA1 inhibitors appeared to shift the balance of HSR Ca^{2+} handling, from normal maintenance of high outward Ca^{2+} gradients, to favoring luminal Ca^{2+} efflux. Although not unexpected, these results importantly identified a role for luminal Ca^{2+} and active SERCA1 pumps in the Ca^{2+} release process. The inhibition of SERCA1 pumps by Tg and CPA were subsequently examined under conditions where SERCA1 catalytic activity was uncoupled from the influences of

luminal Ca^{2+} and states of the RyR1. In these experiments, HSR membranes were permeabilized with ionomycin creating high Ca^{2+} leaks and maximal rates of SERCA1 activity (Figure 13). In Panel A, NADH consumption was compared between ionomycin treated and ionomycin untreated HSR vesicles (250 $\mu g.ml^{-1}$) undergoing Mg.ATP-dependent Ca^{2+} transport. In the (-) condition, basal rates of SERCA1 activity were observed (440 nmol NADH/mg HSR/min) upon attainment of cytosolic Ca^{2+} sequestration and maintenance of the low, outwardly directed, luminal Ca^{2+} gradient (CG2 trace, data not shown). When membranes were treated with ionomycin (+), Ca^{2+} sequestration was entirely interrupted (not shown), and the uncoupled SERCA1 activity became maximally stimulated to rates 27 fold higher than in the absence of ionomycin (11895 nmol NADH/mg HSR/min). HSR membranes were subsequently pretreated with CPA (Panel B) or Tg (Panel C) under conditions where HSR membranes had been permeabilized with ionomycin. Panel B demonstrates that NADH consumption with 5 or 10 μM CPA was biphasically reduced when compared to ionomycin controls, even though cytosolic Ca^{2+} remained elevated and unchanged throughout the experiment (CG2 trace, not shown). Pre-treatment with 5 μM CPA resulted in a >2 fold difference between partial inactivation (2878 nmol NADH/ mg HSR/min) and the subsequent and more complete inactivation (1183 nmol NADH/mg HSR/min) of SERCA1 catalysis. When CPA concentrations were increased to 10 μM, the inactivation differences were also >2 fold (1680 compared with 753 nmol NADH/mg HSR/min, respectively) but more complete inactivation of SERCA1 pumps occurred comparably much sooner. These biphasic reductions in maximal SERCA1 activity were absent from the Tg pretreatment experiments (Panel C). Indeed, rates of NADH consumption were reduced to 210 (1 μM

Tg condition) and 172 (5 μM Tg condition) nmol NADH/mg HSR/min. When maximal rates of SERCA1 inhibition between 100 μM CPA (Panel B) and 5 μM Tg (Panel C) are compared, Tg concentrations approximately 20 fold lower were found to inhibit NADH consumption rates with ~1.5 times higher potency. This further indicated that Tg was more potent than CPA in the inhibition of SERCA pumps.

Assumptions pertaining to the observed Tg and CPA-induced Ca^{2+} leak states indicated that Ca^{2+} leaks were probably governed by RyR1 openings. The results demonstrating activation of SERCA1 activity in the face of Tg-ICR also indicated activated RyR1 channels (Figure 10). To examine the effects of Tg and CPA further, ryanodine was used to initially activate, then inhibit the Ca^{2+} release channel as originally demonstrated in Figure 9. In these experiments (Figure 14), HSR membranes (500 $\mu g.ml^{-1}$) were incrementally loaded with Ca^{2+} to threshold (~ 180 nmol Ca^{2+}/mg HSR) and 0, 1, 10, 100, or 500 μM ryanodine was added to activate RyR1's and induce Ca^{2+} release. Following Ca^{2+} re-sequestration, RyR1's were expected to be inhibited (as previously demonstrated), and single boluses of either 10 μM Tg (Panel A) or 100 μM CPA (Panel B) were added to elicit Ca^{2+} release. Only the point of Tg or CPA addition of the converted CG2 traces are shown. In the absence of ryanodine, Tg-, or CPA-induced Ca^{2+} release was robust and rapid, reaching maximum cytosolic Ca^{2+} transients of about 50 and 45 nmol Ca^{2+} released/mg HSR, respectively. Inhibition of the RyR1 with treatment by 1 μM ryanodine resulted in a 50 % reduction in Ca^{2+} release to the cytosol. Under these conditions, the profile of Tg-ICR was sigmoidal in shape and reached a maximum cytosolic Ca^{2+} concentrations of 4.0 μM with-in 50 seconds. Conversely, CPA-ICR resulted in a monotonic increase in cytosolic Ca^{2+}, only reaching a

maximum of 3.6 μM during the elapsed time of the experiment (200 seconds). The Tg- and CPA-induced Ca^{2+} transients following 10 μM ryanodine-induced RyR1 inhibition were only 20 % of maximal recorded in the absence of ryanodine. RyR1 inhibition by 100 and 500 μM ryanodine resulted in complete blockage of Tg and CPA-induced Ca^{2+} release. These results further verified the importance of continuous SERCA1 activity in the maintenance of HSR vesicle outward Ca^{2+} gradients and that the inhibition of SERCA1 resulted in outward Ca^{2+} fluxes controlled by opening of the RyR1.

D. Luminal Ca^{2+} transients: identification of two luminal Ca^{2+} pools.

Results presented thus far have implicated luminal Ca^{2+} for the dual regulation of both RyR1's and SERCA1 pumps. Importantly, increased luminal Ca^{2+} loads had an obvious influence upon ryanodine-sensitive states of the RyR1 and thapsigargin-sensitive states of the SERCA1 (Figure 8). Also, RyR1-mediated Ca^{2+} release was intimately dependent upon the filling (Figure 5), as well as the rate of filling (Figure 7), of a luminal Ca^{2+} pool(s). Furthermore, sub-stoichiometric Tg concentrations, and to a lesser extent CPA concentrations, resulted in RyR1-mediated Ca^{2+} efflux from HSR membranes accompanied by activation of SERCA1 catalytic turnover. If luminal Ca^{2+} does ultimately coordinate the complex cycling between Ca^{2+} release and Ca^{2+} sequestration then recording changes in luminal Ca^{2+} during HSR membrane Ca^{2+} transport may reveal mechanisms by which this occurs. To satisfy these objectives, two fluorescence indicators that may report upon luminal Ca^{2+} were employed. Both Mag-Fura-2 and chlortetracycline were shown to report on luminal Ca^{2+} and the following results will

demonstrate that the differences in fluorescence signals likely reflect Ca^{2+} changes in different luminal Ca^{2+} compartments.

The acetoxymethyl (AM) ester of Mag-Fura-2 (MF2) was loaded into HSR membranes as described in "Experimental Procedures". The luminal origin of the fluorescence ratio is verified in Figure 15. In Panel A, the MF2 fluorescence responses to sequential Ca^{2+} pulse loading are shown at low (trace 1, 0 exogenous) and high (trace 2, 30 μM exogenous) Ca^{2+} loads. Trace 1 shows that addition of Mg.ATP resulted in a sharp fluorescence increase followed by a slower fluorescence decrease whose pattern was repeated for the first five-5 μM Ca^{2+} additions. At the sixth-5 μM Ca^{2+} pulse, after attainment of luminal Ca^{2+} loads of 150 nmol Ca^{2+}/mg HSR and thus the expected point of CICR, a much larger and more sustained MF2 fluorescence transient was observed. In a pattern similar to those observed with cytosolic Ca^{2+} indicators (see Figure 5), (1) each successive Ca^{2+} addition resulted in a larger, upward Ca^{2+} fluorescence transient, (2) a minimum luminal Ca^{2+} load was required before CICR was realized (150 nmol Ca^{2+}/mg HSR) and (3) CICR was accompanied by a much larger increase in fluorescence that subsequently decreased to prior levels of fluorescence. Prior to Mg.ATP addition (curved arrow) in trace 2, the addition of 30 μM Ca^{2+} (at time = 27.5 seconds) resulted in immediate fluorescence increases that stabilized quickly to steady state. The response of MF2 fluorescence signals in the absence of ATP indicated that cytosolic Ca^{2+} could be partially and passively loaded into HSR membranes with an equilibration of added Ca^{2+} across the membrane. This in turn may reflect the free and shallow nature of the MF2 fluorescence signal (see later). The addition of Mg.ATP in trace 2, resulted in a much larger fluorescence increase when compared to trace 1 and subsequent fluorescence

decreases were considerably slower ($k = 0.0106s^{-1}$ compared with $0.0450s^{-1}$ for trace 1). The luminal origin of the MF2 fluorescence signals were initially verified by these large Mg.ATP-dependent fluorescence increases that were in direct contrast to fluorescence decreases observed with cytosolic Ca^{2+} indicators. Furthermore, while cytosolic Ca^{2+} transients comparable with CICR remained elevated for approximately 1 minute, luminal MF2 fluorescence increases were sustained for periods > 3 minutes.

In a manner similar to Figure 6, larger boluses of Ca^{2+} were added to MF2-loaded HSR membranes (low luminal Ca^{2+} load) following Mg.ATP dependent sequestration of endogenous Ca^{2+}. In Figure 15, Panel B, a single pulse of 35 μM Ca^{2+} was added, resulting in large MF2 fluorescence ratio increases comparable with the CICR-like events noted in Panel A. Under these conditions, the fluorescence increases remained elevated for >3 minutes and fluorescence levels never declined back to original fluorescence values. In this panel, the coinciding CG2 trace has been overlaid to compare the cytosolic and luminal Ca^{2+} changes. These traces demonstrated that high cytosolic Ca^{2+} transients were accompanied by increased luminal MF2 fluorescence. Under these conditions, luminal Ca^{2+} decreases preceded the removal of Ca^{2+} from the cytosol but remained elevated during the time course of the experiment. The elevated MF2 signal may represent Ca^{2+} overload conditions as threshold luminal Ca^{2+} levels would be surpassed with the sequestration of 35 μM Ca^{2+}.

Figure 15, Panel C demonstrated that arresting SERCA1-mediated Ca^{2+} sequestration also blocked the Ca^{2+}-dependent MF2 fluorescence increases resulting from Mg.ATP and Ca^{2+} additions. In this experiment, HSR membranes were pretreated with 10 μM Tg to inhibit all SERCA1-mediated Ca^{2+} loading. The lack of fluorescence

change, even with several 5 μM Ca^{2+} pulses added cytosolically, indicated that increases in MF2 signal (Panel A) were governed by SERCA1 pumps and luminal in origin. This was further indicated by the substantial fluorescence decrease upon addition of ionomycin.The reported Kd of MF2:Ca^{2+} is 25 μM. The specific pH (7.0) and conditions for HSR Ca^{2+} transport used in this study may affect these reported values. In order to calibrate the fluorescence values obtained with MF2, HSR membranes loaded with the luminal dye were initially permeabilized with ionomycin and treated with 10 μM thapsigargin which ensured no SERCA1 pump contribution to fluorescence readings. These calibrations were run in the presence of 1 mM Tris.ATP for consistency with Ca^{2+} transport assays. Finally, the membranes were subjected to known concentrations of cytosolic Ca^{2+} (0 - 1250 μM) expected to equilibrate across the membrane. The fluorescence ratio values obtained with increased Ca^{2+} concentrations were fit to a single site hyperbola shown in Figure 16, Panel A. The experimentally determined Kd from this curve was slightly higher than reported and approximated to 33 μM. Converting MF2 fluorescence ratios to Ca^{2+} concentration required the Kd and Equation 3. The trace shown in Figure 16, Panel B is the control Ca^{2+} loading experiment from Panel A in Figure 15 (trace 1).

Equation 3:

$$[Ca^{2+}] = Kd * ((R - R_{MIN})(R_{MAX} - R)) * (F_{380}MAX / F_{380}MIN)$$

where:Kd = 33 μM

R = MF2 fluorescence ratio (including daily ratio MIN and MAX)

F = fluorescence MIN and MAX at 380 nm

As seen in Panel B, the starting luminal Ca^{2+} concentration before Mg.ATP addition is approximately 10 μM, while initiation of Ca^{2+} transport resulted in rapid increases in luminal Ca^{2+} to >20 μM. This value correlated well with the determined amounts of contaminating Ca^{2+} as determined with absorption spectroscopy. Relatively small luminal Ca^{2+} increases were observed for the initial four-5 μM Ca^{2+} pulses. However, the fifth and sixth Ca^{2+} pulses, expected to activate RyR1 channels with concomitant activation of SERCA1 pumps, resulted in comparably larger increases in luminal Ca^{2+}. Indeed, sustained luminal Ca^{2+} increases, reaching approximately 50 μM, were observed at CICR when SERCA1 pumps were near-maximally activated.

Uniquely different fluorescence responses were seen when CTC was employed to track luminal Ca^{2+} changes. CTC has been reported to penetrate the SR membrane but the movement of CTC (cytosolic to luminal) was slower than transported Ca^{2+} and thus a significant amount of co-transport occurred between CTC and SERCA-mediated Ca^{2+} sequestration (69, 181). Indeed, the rate of change of CTC fluorescence with Mg.ATP or Ca^{2+} addition was considerably slower than changes observed with CG2 or luminal MF2. In CTC experiments, HSR membranes were preincubated with 40 μM CTC for >5 minutes prior to initiation of Ca^{2+} transport (see "Experimental Procedures"). In Figure 17, Panel A, Mg.ATP addition and initial Ca^{2+} sequestration of endogenous Ca^{2+} resulted in a fairly rapid increase in CTC fluorescence which leveled at a stable fluorescence after ~ 1 minute. Sequential Ca^{2+} pulse loading of CTC membranes (Panel A, trace 1) yielded expected fluorescence increases with each of the initial four- 5 μM Ca^{2+} pulses. Interestingly, at the fifth-5 μM Ca^{2+} addition, a small fluorescence decrease was observed

which was transiently followed by larger fluorescence increases to maximum CTC fluorescence values obtained in these experiments. The fifth-5 μM Ca^{2+} pulse coincided with increased MF2 fluorescence (Figure 16) and burst SERCA1 activation (Figure 5) resulting from Ca^{2+} leak state formation. The observed CTC fluorescence responses at the sixth-5 μM Ca^{2+} pulse were large fluorescence decreases that persisted for >5 minutes before fluorescence returned to original levels. These CTC observable CICR's occurred at expected threshold luminal Ca^{2+} loads (five-5 μM Ca^{2+} additions = luminal Ca^{2+} of 150 nmol Ca^{2+}/mg HSR) corresponding to CICR as elucidated with CG2 (Figure 5). Trace 2, in Panel A, demonstrated that at the nadir of CTC fluorescence decreases associated with CICR, further 5 μM Ca^{2+} additions simply resulted in slowed fluorescence increases. The luminal origin of the CTC fluorescence signal was initially verified by ionomycin additions (Figure 17, Panel A and C) which caused immediate and complete losses of Ca^{2+}-dependent fluorescence.

In Figure 17, Panel B, HSR membranes pre-incubated with CTC were subjected to increased Ca^{2+} preloads (trace 1 - 20 μM exogenous, trace 2 - 30 μM exogenous). In contrast to the passive Ca^{2+} responses seen with luminal MF2 in Figure 15, no CTC fluorescence increases were observed prior to Mg.ATP addition and therefore were dependent upon active Ca^{2+} sequestration. Under these high Ca^{2+} conditions, Ca^{2+}-dependent CTC fluorescence increases reached steady state levels in >300 seconds. In comparison, similar Ca^{2+} preloads were sequestered in approximately 100 seconds when examined with CG2. At sub-threshold Ca^{2+} loads (trace 1, 120 nmol Ca^{2+}/mg HSR), further Ca^{2+} loading of one 5 μM Ca^{2+} pulse was required before CTC fluorescence increases reached maximum and decreases associated with CICR were observed with

subsequent Ca^{2+} additions. However, when Ca^{2+} loads were increased to just beyond threshold (180 nmol Ca^{2+}/mg HSR) (trace 2), a single addition of 5 μM Ca^{2+} resulted in CICR. Panel A and B both show that CTC faithfully tracked the luminal Ca^{2+} dependency of CICR as first examined with CG2 (Figure 5). In a similar manner to Figure 6, (Figure 17) Panel C, trace 1 demonstrated that at near-threshold loading (120 nmol Ca^{2+}/mg HSR) of HSR membranes, a bolus addition of 20 μM Ca^{2+} elicited expected CTC fluorescence decreases associated with CICR. In trace 2, the bolus addition of 20 μM Ca^{2+} at low, endogenous, luminal Ca^{2+} loads resulted in a relatively slow increase in CTC fluorescence to maximum fluorescence values which occurred in the absence of observable fluorescence decreases/CICR. The similar experiment with CG2 and NADH (Figure 6, Panel C) demonstrated that SERCA1 activation was delayed with large bolus additions of Ca^{2+} to HSR membranes under conditions of low luminal Ca^{2+} load. Thus RyR1 activation is probably delayed under these conditions and maximal increases in CTC fluorescence may not occur until RyR1 inactivation. The results from Figure 15, Panel B, indicated that MF2 fluorescence increases due to a large bolus addition of Ca^{2+} began declining after ~ 2.5 minutes. This time point coincided with the attainment of near-maximal CTC fluorescence observed in trace 2, Panel C. Overall, comparison of Figure 17 and Figure 15 preliminarily suggested that two distinct luminal Ca^{2+} compartments were being reported by CTC and MF2 fluorescence.

The rates of fluorescence change between active and passive Ca^{2+} loading with MF2 were compared in Figure 18, Panel A. For this analysis, maximum values obtained with MF2 fluorescence ratio were normalized for each experimental loading protocol. The increases in fluorescence were complete within 10 to 15 secs for Mg.ATP-dependent

active loading of endogenous or 50 μM Ca^{2+} preloads. The rate of MF2 fluorescence increase with passive loading of 50 μM Ca^{2+} were >2 fold slower possibly indicating an equilibration of Ca^{2+} between the accessible MF2 luminal Ca^{2+} compartment and the cytosolic space to which the Ca^{2+} was added. The site of cytosolic to luminal passive Ca^{2+} movement was quite possibly the RyR1 which was shown to be in an open state during the incubation period before Mg.ATP addition. Therefore, MF2 was assumed to report on a free but shallow luminal Ca^{2+} compartment. Rates of MF2 fluorescence increases during active loading of endogenous and 50 μM Ca^{2+} were 1.53 and 0.54 s^{-1}, respectively. Rates for passive loading of 50 μM Ca^{2+} into the MF2-visible Ca^{2+} compartment were ~5 fold slower with k equal to 0.16 s^{-1}

By contrast, no passive Ca^{2+} loading/fluorescence increases were observed with CTC. Furthermore, the rates of change of CTC fluorescence increases during initial, active Ca^{2+} sequestration were magnitudes slower than observed with MF2. In Panel B, the normalized CTC fluorescence change for active loading of endogenous and 30 μM Ca^{2+} are shown. The elapsed time for attainment of steady state CTC fluorescence during initial Ca^{2+} sequestration by HSR membranes occurred over a period of 1 minute and 5 minutes for low and high Ca^{2+} loads, respectively. The calculated rates of CTC fluorescence increases were 0.059 and 0.005 for active loading of endogenous and 30 μM Ca^{2+}, respectively. These reduced rates of fluorescence increase likely reflect the slow CTC permeation rates that are coupled to active Ca^{2+} transport. Therefore, detection of fast luminal Ca^{2+} changes during the initial Ca^{2+} sequestration are limited by fluorophore incorporation into HSR membranes. On the other hand, rates of Ca^{2+} release from CTC-visible Ca^{2+} compartments were in agreement with previous CG2 recorded values which

suggested that the dissociation of Ca^{2+} from CTC is not limiting for the detection of fast Ca^{2+} release.

CTC is known to exhibit membrane-enhanced fluorescence changes due to the association of the CTC moiety with the hydrophobic domains of biological membranes (33, 34). The difficulties in assessing the distinctly different luminal responses of CTC and MF2 during Ca^{2+} pulse loading experiments was that, if CTC-visible Ca^{2+} fluorescence was reporting on near-membrane Ca^{2+}, how could this Ca^{2+} be maintained differentially separated from the bulk free luminal Ca^{2+}? In other words, what would delimit a near-membrane CTC responses from the overall free luminal Ca^{2+} changes possibly recognized by MF2 fluorescence responses? HSR preparations contain an abundance of the luminal Ca^{2+} binding protein, CSQ, which is hydrophobic in nature. This led to the proposal that CTC fluorescence signals may be originating from an interaction of the fluorophore with CSQ. To test this hypothesis, CTC fluorescence responses in the presence of isolated CSQ were examined. Figure 19 demonstrates that CTC incubated in TB responded to 1 (trace 1), 5 (trace 2), or 10 (trace 3) mM added Ca^{2+} with increased fluorescence but that these responses were enhanced up to 2.5 times by the subsequent addition of 75 μg/ml isolated CSQ. In trace 4, the addition of CSQ alone to CTC containing buffers had little effect upon CTC fluorescence. However, the addition of 1 mM Ca^{2+} under these conditions increased CTC fluorescence 3.5 fold. These findings strongly suggested that CTC fluorescence responses in Ca^{2+} transport experiments may arise from the interaction of CTC with CSQ. Given the documented interactions of CSQ with membranous environments, a second possibility may be that CTC is reporting on near-membrane, near-CSQ Ca^{2+} changes within the SR lumen.

Despite the different possibilties of the origin of the overall CTC fluorescence signals, the data from Figure 19 clearly indicate that CTC may be reporting changes in the Ca^{2+} binding states of the luminal Ca^{2+} binding protein, CSQ, during Ca^{2+} pulse loading.

MF2 responded to passive influx of Ca^{2+} into HSR membranes suggested that this Ca^{2+} indicator may be reporting on a shallow, free pool of luminal Ca^{2+}. To further examine this possibility, MF2-loaded HSR membranes (500 $\mu g.ml^{-1}$) were either pre-treated with the ionophore, ionomycin, or given repeated additions of ionomycin during active Ca^{2+} transport (Figure 20). Ionomycin concentrations of 17.5 μM were selected since complete Ca^{2+} efflux from luminal stores were observed using CG2 under these conditions. In Panel A, ionomycin addition prior to Mg.ATP-dependent Ca^{2+} sequestration at low (endogenous) Ca^{2+} loads (trace 1) produced no net increase in MF2 fluorescence. Upon Mg.ATP addition, activated SERCA1 pumps resulted in increased fluorescence not unlike control traces. Trace 2 demonstrated that the addition of ionomycin subsequent to a 30 μM Ca^{2+} addition during HSR membrane pre-incubation resulted in further MF2 fluorescence increases although Mg.ATP addition and stimulation of SERCA1 activity did not effectively increase fluorescence beyond low Ca^{2+} load conditions (trace 1). The resultant MF2 fluorescence increases were due to SERCA1 activation as the addition of a large bolus of Tg (20 μM) resulted in diminished fluorescence signals to original fluorescence values. Interestingly, Tg caused more substantial loss of MF2 fluorescence in the low Ca^{2+} load condition (trace 1) compared to the high Ca^{2+} load condition (trace 2).

Similar low (trace 1) and high (trace 2) Ca^{2+} pre-loads were utilized in Figure 20, Panel B, where repeated additions of ionomycin were performed following Mg.ATP-

stimulated Ca^{2+} sequestration. With low luminal Ca^{2+} loads, four additions of 17.5 μM ionomycin resulted in relatively small decreases in MF2 fluorescence. At high luminal Ca^{2+} loads (180 nmol Ca^{2+}/mg HSR), each addition of ionomycin caused more substantial decreases in MF2 luminal signals but a persistent level of MF2 fluorescence remained even after three ionomycin additions. As in Panel A, addition of 20 μM Tg resulted in loss of luminal Ca^{2+} fluorescence that was more complete for low Ca^{2+} loads when compared to high Ca^{2+} loads. These results demonstrated that MF2 fluorescence probably reported on a shallow, free luminal Ca^{2+} pool that was relatively ionomycin insensitive. Under these conditions, maintained fluorescence enhancement of MF2 was directly associated with activated SERCA1 pumps. The relative insensitivity of MF2 luminal Ca^{2+} signals to ionomycin treatment was in direct contrast to complete fluorescence losses observed with luminal CTC (Figure 17) and the large fluorescence increases seen with cytosolic CG2 (Figure 10) upon similar ionomycin treatment of HSR membranes.

To further elucidate the role of SERCA1 pumps upon luminal Ca^{2+} changes, Tg was utilized in both CTC (Figure 21) and MF2 (Figure 22) loaded HSR membranes. The increased sensitivity of SERCA1 pumps to Tg treatment with increased luminal Ca^{2+} loads as well as the increased sensitivity of HSR membranes to CICR with sub-stoichiometric concentrations of Tg as observed with CG2 and NADH were further examined with the luminal Ca^{2+} probes. In Figure 21, Panel A, CTC loaded HSR membranes were subjected to Tg pre-treatment at concentrations similar to those examined in Figure 11. Trace 1 in Panel A is a control Ca^{2+} loading trace which consistently showed that 500 $\mu g.ml^{-1}$ HSR membranes required a luminal Ca^{2+} load of

150 nmol Ca^{2+}/mg HSR before the subsequent addition of a 5 μM Ca^{2+} pulse resulted in CICR. Upon Ca^{2+} re-accumulation following CICR, as indicated by the attainment of maximal CTC fluorescence, HSR membranes were treated with a single bolus of 1 μM Tg. Under these conditions of high luminal Ca^{2+} load, Tg addition resulted in a biphasic reduction in CTC fluorescence. A rapid phase of luminal Ca^{2+} depletion was followed by a slower, monotonic decrease in CTC fluorescence. Ionomycin addition caused a complete loss of luminal CTC fluorescence signals.

By comparison, trace 2 demonstrated the effects of 0.5 μM Tg pre-treatment upon Mg.ATP-dependent Ca^{2+} pulse loading of HSR membranes. Similar to the 0.67 μM condition in Figure 11, 0.5 μM Tg would be expected to decrease the rate of Ca^{2+} sequestration while concomitantly activating SERCA1 catalytic activity as recorded with CG2 and NADH fluorescence. CTC fluorescence changes showed that 0.5 μM Tg slightly decreased the steady state, resting fluorescence following Mg.ATP addition. Furthermore, the initial two-5 μM Ca^{2+} pulses resulted in decreased rates of fluorescence increase when compared to control and appeared to sufficiently load the membranes as the third-5 μM Ca^{2+} pulses gave fluorescence decreases expected at CICR. The CTC fluorescence increases following CICR were also greatly reduced especially after the fourth-5 μM Ca^{2+} addition. Therefore, the luminal Ca^{2+} requirement for CICR was reduced to between 60 and 90 nmol Ca^{2+}/mg HSR. Since decreases in CTC fluorescence associated with CICR are a consequence of RyR1 activation, trace 2 demonstrated that decreasing the rate of Ca^{2+} removal from the cytosol with sub-stoichiometric Tg concentrations resulted in increased sensitivity of the Ca^{2+} release channel to activation by sub-threshold luminal Ca^{2+} loads and/or cytosolic trigger pulses of Ca^{2+}. When HSR

membranes were pre-treated with 0.75 or 1 μM Tg, CTC fluorescence increases were markedly slower and of reduced magnitude (Panel A, trace 3 and 4). With >2 μM Tg, all Ca^{2+}-dependent CTC fluorescence increases were abolished. Additions of 5 μM Ca^{2+} were made to traces 3, 4, and 5 in a similar manner to that shown for trace 2. Under these conditions, Ca^{2+} did not alter the fluorescence pattern of luminal CTC signals.

In Panel B, Tg additions following Mg.ATP-dependent initial endogenous Ca^{2+} sequestration were examined. In CG2 experiments, treatment of HSR membranes in low Ca^{2+} load conditions with 0.75 μM Tg resulted in elevated cytosolic steady state Ca^{2+} levels and decreased Ca^{2+} load requirements of CICR (Figure 10). Trace 1 in Panel B demonstrated that 0.75 μM Tg caused a reduction in CTC luminal fluorescence that was delayed ~98 seconds from the point of addition. The delay between the point of Tg addition and CTC fluorescence decreases was reduced with increased luminal Ca^{2+} loads (data not shown). With luminal Ca^{2+} loads of 60 and 120 nmol Ca^{2+}/mg HSR, Tg-ICR was delayed 32 and 7 seconds, respectively. In Panel B, the observed CICR-like fluorescence decrease was transiently followed by a persistent, monotonic CTC fluorescence increase to values beyond steady state. This fluorescence increase occurred in the absence of added Ca^{2+} which suggested that under these conditions Ca^{2+} was recruited into the CTC-visible Ca^{2+} pool. When 10 μM Tg was added (trace 2) to HSR membranes undergoing active Ca^{2+} transport, CTC fluorescence was seen to transiently increase and subsequently decrease sharply to fluorescence levels close to those observed following ionomycin treatment in trace 1. This Tg concentration resulted in immediate increases in cytosolic Ca^{2+} transients as recorded with CG2.

Using identical protocols, Tg pre-treatment and Tg addition following Ca^{2+} sequestration were examined with MF2-loaded HSR membranes in Figure 22. In Panel A, vesicles (500 $\mu g.ml^{-1}$) were pre-treated with 0.5 μM Tg and Ca^{2+} sequestration was subsequently initiated with the addition of Mg.ATP. In a similar manner to CTC, the Ca^{2+} load requirement of CICR was reduced from that of controls with large MF2 fluorescence increases occurring with the fourth-5 μM Ca^{2+} addition. It can also be seen from Panel A that each successive MF2 Ca^{2+} transient was increased over those observed with control pulse loading (see Figure 15, Panel A). The effects were more prominent when Tg pre-treatment was increased to 1 μM and large MF2 increases were seen following only two-5 μM Ca^{2+} pulses. These findings were in comparison different from 1 μM Tg pre-treatments with CTC-loaded HSR membranes where fluorescence increases were nearly abolished. Thus, reducing the rate at which Ca^{2+} is sequestered to the lumen of HSR membranes potentiated increases in Ca^{2+} signals in the MF2-visible Ca^{2+} pool while greatly inhibited Ca^{2+} influx into the CTC-visible luminal Ca^{2+} pool.

Figure 22, Panel C, demonstrates the effects of Tg addition following sequestration of endogenous Ca^{2+}. In this Figure, the cytosolic Ca^{2+} transient recorded with CG2 (trace 1a) is directly overlaid with the luminal Ca^{2+} transient as recorded with MF2 (trace 1b). Under these low Ca^{2+} load conditions, addition of 2 μM Tg resulted in Ca^{2+} release from HSR membranes following a delay of ~1 minute (trace 1a). This delay between Tg addition and Ca^{2+} release was similar to results obtained with CTC. The MF2 luminal Ca^{2+} transient mirrored these cytosolic Ca^{2+} changes. The addition of Tg resulted in a similar delay before MF2 fluorescence signals increased from about 12 μM to 20 μM, concomitantly with those of CG2. Steady state CG2 fluorescence peaked and

remained at ~1.5 μM while MF2 fluorescence monotonically decreased following attainment of maximal fluorescence. Addition of ionomycin increased cytosolic Ca^{2+} to 2.5 μM while decreasing luminal Ca^{2+} to approximately the same value.

The addition of 10 μM Tg to endogenously-loaded HSR membranes (Figure 22, Panel C, trace 2), which is expected to result in a more rapid Ca^{2+} release as seen with CG2, caused a transient increase to 4 μM luminal Ca^{2+} followed by decreases in MF2-visible Ca^{2+} to levels close to minimum fluorescence observed with ionomycin addition. The similarly delayed responses of CTC, CG2, and MF2 fluorescence signals to Tg treatment at low Ca^{2+} loads indicated that the three Ca^{2+} indicators were differentially recording the same event. As CG2 fluorescence increased along with MF2 to maximal levels, CTC fluorescence transiently decreased. Following attainment of maximal fluorescence, MF2 exhibited a slow loss of fluorescence while CTC signals were slowly increasing, and CG2 fluorescence remained at peak values. This provided evidence that MF2 and CTC may undergo Ca^{2+} exchange from one luminal Ca^{2+} pool to the other. Under these conditions, when the RyR1 had been activated, CTC fluorescence decreased while MF2 fluorescence increased. Subsequent attainment of perhaps a partially inactivated RyR1 state resulted in slow CTC fluorescence increases with a comparably slow MF2 fluorescence decrease.

The profound influence of Tg upon Ca^{2+} loading into the CTC and MF2 luminal pools further indicated the importance of rates of SERCA1 turnover upon RyR1 channel activation and Ca^{2+} release. This dynamic and apparently coordinated nature of SERCA1 Ca^{2+} sequestration and RyR1-mediated Ca^{2+} release in isolated HSR membranes led to further examination of RyR1 channel activation and inhibition in lew of luminal Ca^{2+}

transients. Experiments manipulating states of the RyR1 were performed using ryanodine as both activator and inhibitor of Ca^{2+} release channel function. In Figure 23, Panel A, HSR membranes were pre-treated with increasing ryanodine concentrations and active Ca^{2+} transport was initiated by Mg.ATP addition. In this panel, trace 1 represents control Ca^{2+} loading while trace 2 and 3 were 10 μM and 500 μM ryanodine pre-treatments, respectively. As shown with the CG2 experiments in Figure 4, a pre-treatment with either 5 or 50 μM ryanodine resulted in slowed cytosolic Ca^{2+} removal and either brief activation (5 μM) or near-maximal activation (50 μM) of SERCA1 catalysis. These results were indicative of RyR1 activation during initial Ca^{2+} sequestration. Under these conditions, both 10 and 500 μM ryanodine pre-treatment resulted in increased CTC fluorescence during initial sequestration of low load, endogenous Ca^{2+}. Given that endogenous Ca^{2+} changed little from experiment to experiment, ryanodine appeared to potentiate the movement of Ca^{2+} into the CTC-visible luminal Ca^{2+} pool. Cytosolic MF2 Ca^{2+} loading traces demonstrated that 10 μM ryanodine pre-treatment reduced the luminal Ca^{2+} load required for CICR from 150 nmol Ca^{2+}/mg HSR to 90 nmol Ca^{2+}/mg HSR (data not shown). On the other hand, 500 μM ryanodine pretreatment decreased the rate of removal of cytosolic Ca^{2+} (as recorded with cytosolic MF2), inhibited CICR, and markedly slowed the removal of each 5 μM Ca^{2+} loading pulse. In Panel A, Ca^{2+} loading of the 10 μM ryanodine pre-treatment condition (see top Ca^{2+} arrows) showed further increases in CTC fluorescence with each Ca^{2+} addition, but, aside from a very small fluorescence decrease at the fifth-5 μM Ca^{2+} pulse, CICR was never realized. This inhibition of CTC-visible CICR was more evident with the 500 μM ryanodine condition where demarcation of fluorescence increases from each

Ca^{2+} addition was lost following the second Ca^{2+} pulse. Interestingly, maximum CTC fluorescence following Ca^{2+} pulse additions was similar in all three cases. Thus it appeared that ryanodine-induced activation of RyR1's during initial Ca^{2+} sequestration facilitated the influx of Ca^{2+} into the CTC luminal Ca^{2+} pool. This result was in contrast to CTC fluorescence losses observed with RyR1 activation during control Ca^{2+} loading procedures. Clearly, the subsequent ryanodine-induced RyR1 inactivation abolished all Ca^{2+}-dependent CTC fluorescence decreases associated with CICR.

Similar to procedures employed in Figure 8 with CG2, ryanodine additions (500 μM) were made to HSR membranes under conditions of high (30 μM exogenous, trace 1) and low (endogenous, trace 2) luminal Ca^{2+} loads. Like the results shown in Figure 8, ryanodine addition at low luminal Ca^{2+} loads had only subtle effects upon CTC fluorescence. A small CTC fluorescence decrease was followed by a monotonic and sustained CTC fluorescence increase. The apparent Ca^{2+} movement into the CTC-visible Ca^{2+} pool was similar in magnitude to fluorescence increases observed with ryanodine pre-treatment in Panel A. At high Ca^{2+} loads ryanodine resulted in rapid and maximal Ca^{2+} release as seen by CTC fluorescence decreases. Ca^{2+} re-sequestration into the CTC-visible Ca^{2+} pool following Ca^{2+} release did not attain maximal CTC fluorescence levels as observed prior to ryanodine addition. Differing from the ryanodine pre-treatment results, under conditions where luminal Ca^{2+} loading is high and Ca^{2+} release channels are most sensitive to activation, ryanodine-induced activation resulted in expected CTC fluorescence decreases.

By comparison, ryanodine pre-treatment of MF2-loaded HSR membranes also resulted in increased MF2 fluorescence signals (Figure 24, Panel A and B). Ryanodine

pre-treatment (10 μM) in Panel A resulted in similar decreases in the luminal Ca^{2+} requirement for luminal MF2-visible CICR as previously mentioned for CTC and CG2 data. Large MF2 fluorescence increases were observed following luminal Ca^{2+} loads of 60 nmol Ca^{2+}/mg HSR while control Ca^{2+} loading experiments required luminal Ca^{2+} loads of 150 nmol Ca^{2+}/mg HSR (see Figure 15, Panel A). The time course (~3.5 minutes) for the rise in MF2 fluorescence and return to decreased fluorescence levels at CICR was similar for both control and 10 μM ryanodine pre-treatment conditions. But the two differed in the transient fluorescence decreases associated with completion of Ca^{2+} release. In control experiments, sustained increases in MF2 fluorescence were followed by a rapid then slow phase of MF2 fluorescence decrease. In Panel A, ryanodine pre-treatment appeared to diminish the sustained phase of fluorescence increase, and Ca^{2+} loss from the MF2-visible luminal pool went through a reversed slow then fast profile of MF2 fluorescence decrease. When ryanodine pre-treatments were increased to 500 μM, the magnitude of initial fast increases in MF2 fluorescence upon Mg.ATP addition were unchanged but the rate of subsequent fluorescence decreases was greatly diminished. Under these conditions each successive 5 μM Ca^{2+} pulse resulted in large MF2 fluorescence increases while the resulting subsequent rates of fluorescence decreases due to Ca^{2+} loss from the MF2-visible luminal Ca^{2+} pool were increased at each Ca^{2+} addition.

Ryanodine effects upon MF2 fluorescence were further examined under conditions of high luminal Ca^{2+} loads (180 nmol Ca^{2+}/mg HSR) where RyR1 channels were sensitized to activation. In Figure 24, Panel C, ryanodine addition following Ca^{2+} sequestration resulted in a multiphasic loss of MF2 fluorescence. Comparable to Figure

9, ryanodine treatment should result in RyR1 activation followed by channel inactivation as recorded with CG2. The multiphasic MF2 fluorescence decrease seen in Panel C may represent both RyR1 activation and inactivation. However, MF2 fluorescence would be expected to increase during Ca^{2+} release channel activation as observed during control Ca^{2+} loading protocols. At these Ca^{2+} loads, ryanodine-induced activation of the RyR1 appeared to result in maximal Ca^{2+} release both from the CTC-visible and MF2-visible luminal Ca^{2+} pools. When Ca^{2+} was the trigger for CICR, RyR1 activation may be brief or conformationally different from ryanodine-induced activations. Thus during CICR, SERCA1 activity would maintain MF2-visible Ca^{2+} in elevated levels. The observed transition from the first MF2 fluorescence decrease to the second decrease occurred over a time course of >6 minutes while ryanodine-induced Ca^{2+} release and subsequent RyR1 inhibition was complete in ~3 minutes. The second MF2 fluorescence decrease may therefore indicate increased affinity of Ca^{2+} binding by CSQ during RyR1 inactivation.

The order of addition of ionomycin and Tg following RyR1 inactivation/MF2 fluorescence decreases resulted in differential changes to the luminal MF2 fluorescence signal (Panel C). In trace 1, 20 μM Tg resulted in a small MF2 fluorescence increase that was diminished by the subsequent addition of ionomycin. Given that Tg-induced Ca^{2+} release was inhibited by ryanodine-induced RyR1 inactivation (see Figure 14) this result was not unexpected. But in trace 2, the initial addition of ionomycin resulted in large fluorescence increases which were abolished by the subsequent addition of 20 μM Tg. The sensitivity of the CTC-visible Ca^{2+} pool to ionomycin, together with inhibited RyR1 channels, appeared to facilitate Ca^{2+} movement to the MF2 luminal Ca^{2+} pool in a SERCA1-dependent manner.

FIGURE 1. Characterization of SR membranes isolated for Ca^{2+} transport assays. Rabbit skeletal muscle SR membranes were isolated then fractionated by sucrose density centrifugation as described in 'Experimental procedures' yielding ISR and HSR fractions. In Panel A, 100 μg HSR (lanes 1 and 3) and ISR (lanes 2 and 4) membranes were resolved by staining 3-13 % SDS-PAGE gradient gels with either Coomassie-R250 (lanes 1 and 2) or Stains-all (lanes 3 and 4). Location of the RyR1 (565 kDa), SERCA1 (100 kDa) and CSQ (43 kDa) are indicated. Panel B shows immunoreactive staining for RyR1 (lane 1) or triadin (lane 2) in HSR membranes. Panel C similarly shows the immunoreactive staining for the presence of SERCA1 (lane 1) or SERCA2 (lane 2) in HSR membranes. Panel D is an electron micrograph of HSR vesicles at 60000x magnification. The arrows indicate regions where 'feet' structures appear aligned in neighboring vesicles. The inset box isolates one of these regions where vesicles are connected with one another.

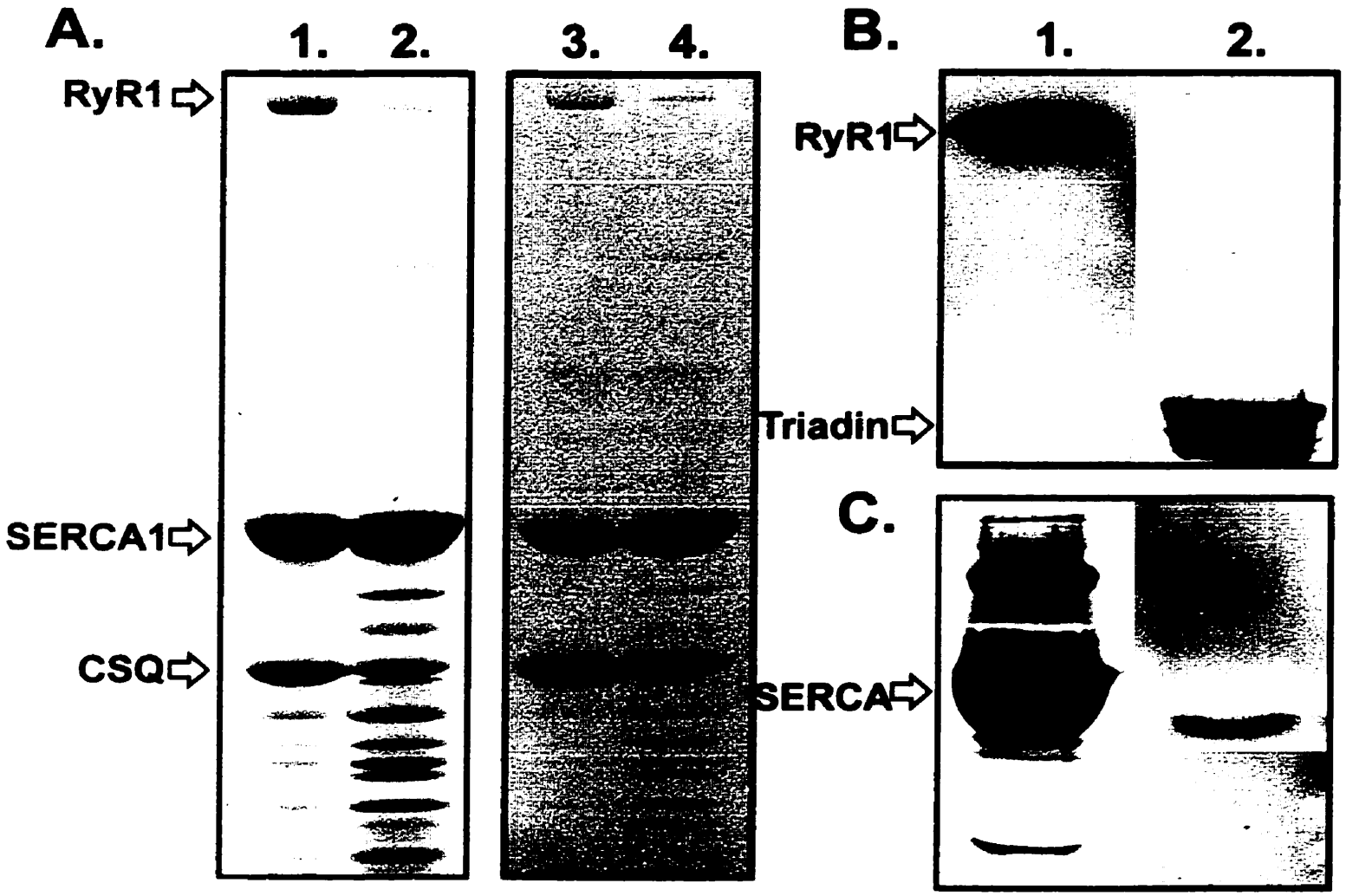

D.

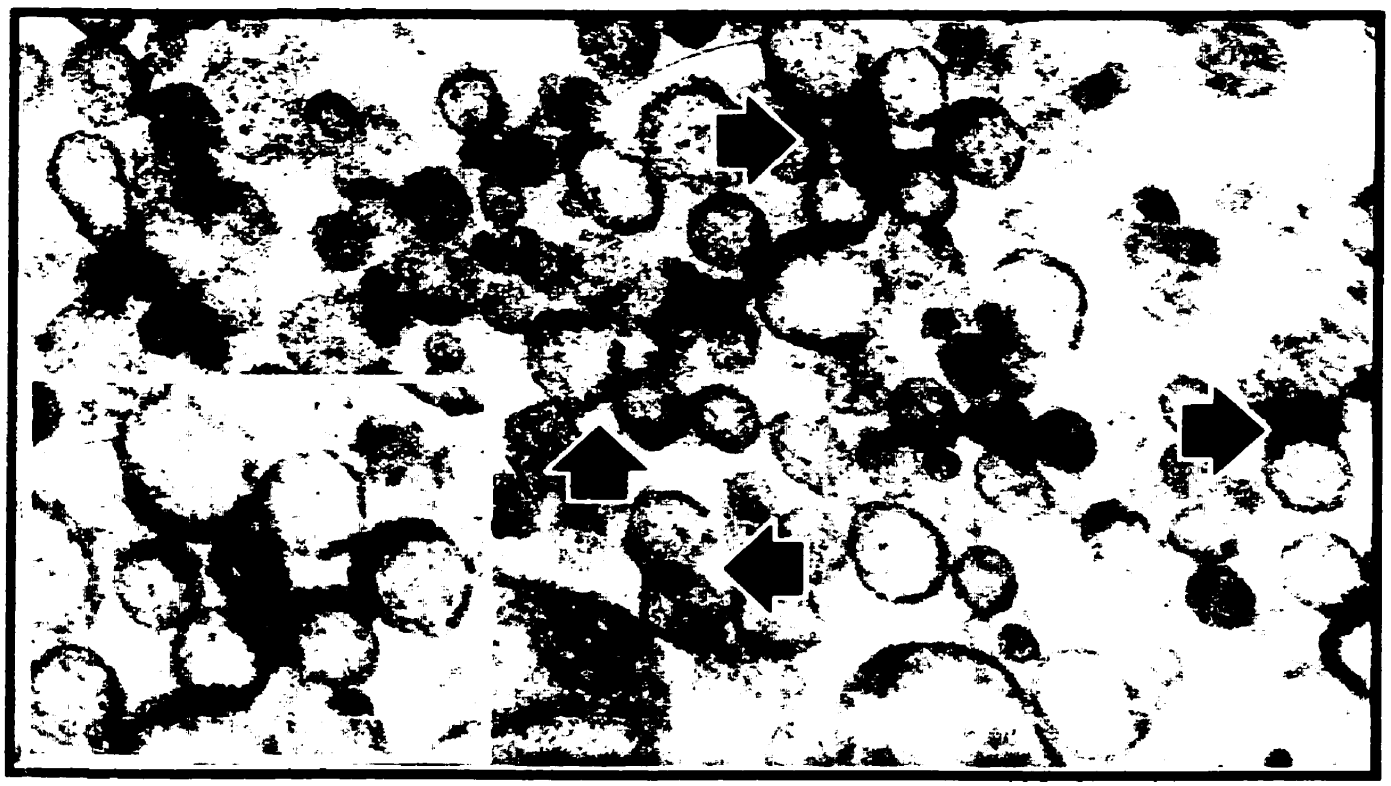

FIGURE 2. Calibration of NADH and Calcium Green-2 responses for conversion to NADH and Ca^{2+} concentrations. Emission scans (400 to 480 nm) were performed on increasing NADH concentrations, from 0 to 400 μM in 25 μM steps, in transport buffer. NADH fluorescence maximums (Em 451 nm) were plotted against NADH concentration and was well-described by a second order polynomial. The plot is shown in Panel A. In Panel B, Calcium Green-2 (0.8 μM) was calibrated in transport buffer in the presence (open symbols) and absence (closed symbols) of HSR membranes (250 $\mu g.ml^{-1}$). Free Ca^{2+} concentrations (0 to 1 mM) were controlled with the combined additions of Ca^{2+} and 2 mM EGTA. Fluorescence maximums and minimums were obtained and used to acquire the Hill Plot shown.

A.

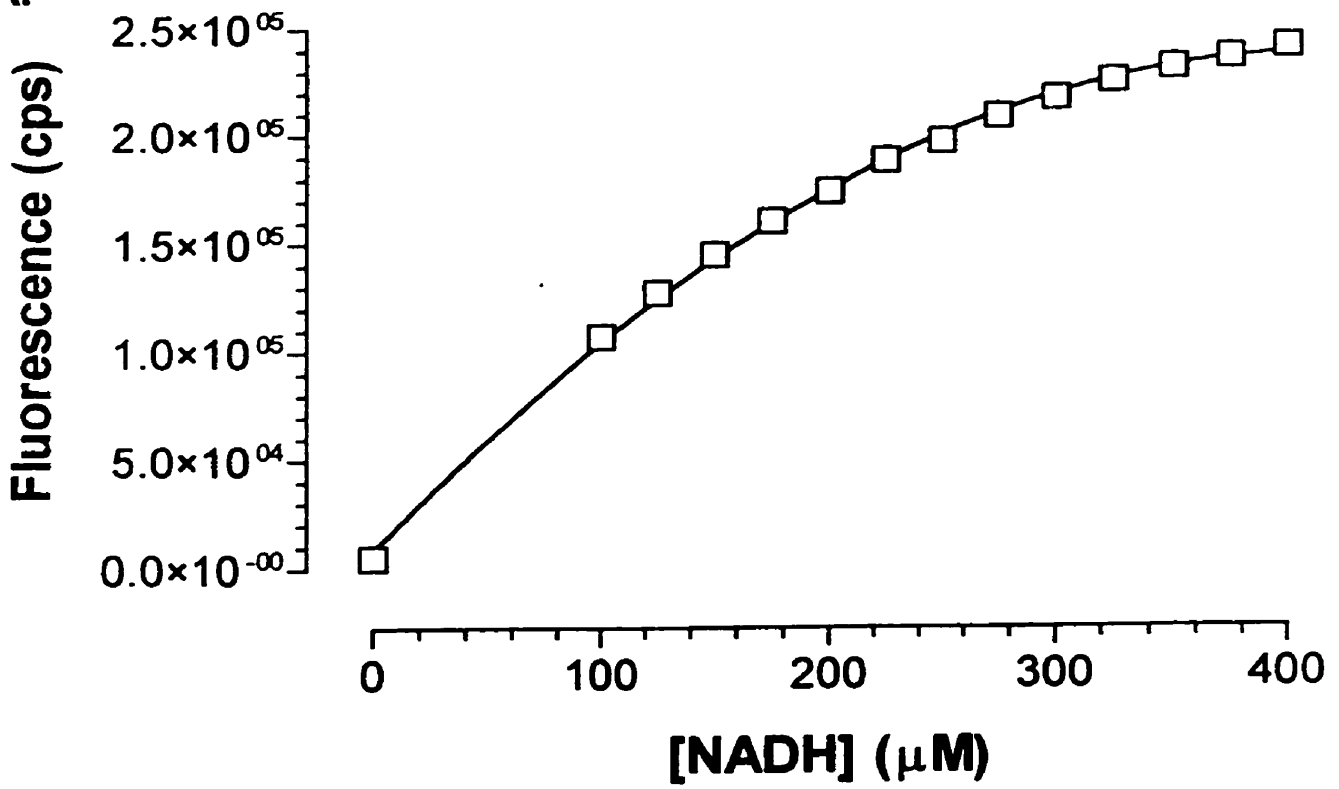
Fluorescence (cps)
2.5×10^05
2.0×10^05
1.5×10^05
1.0×10^05
5.0×10^04
0.0×10^-00
0
100
200
300
400
[NADH] (μM)

B.

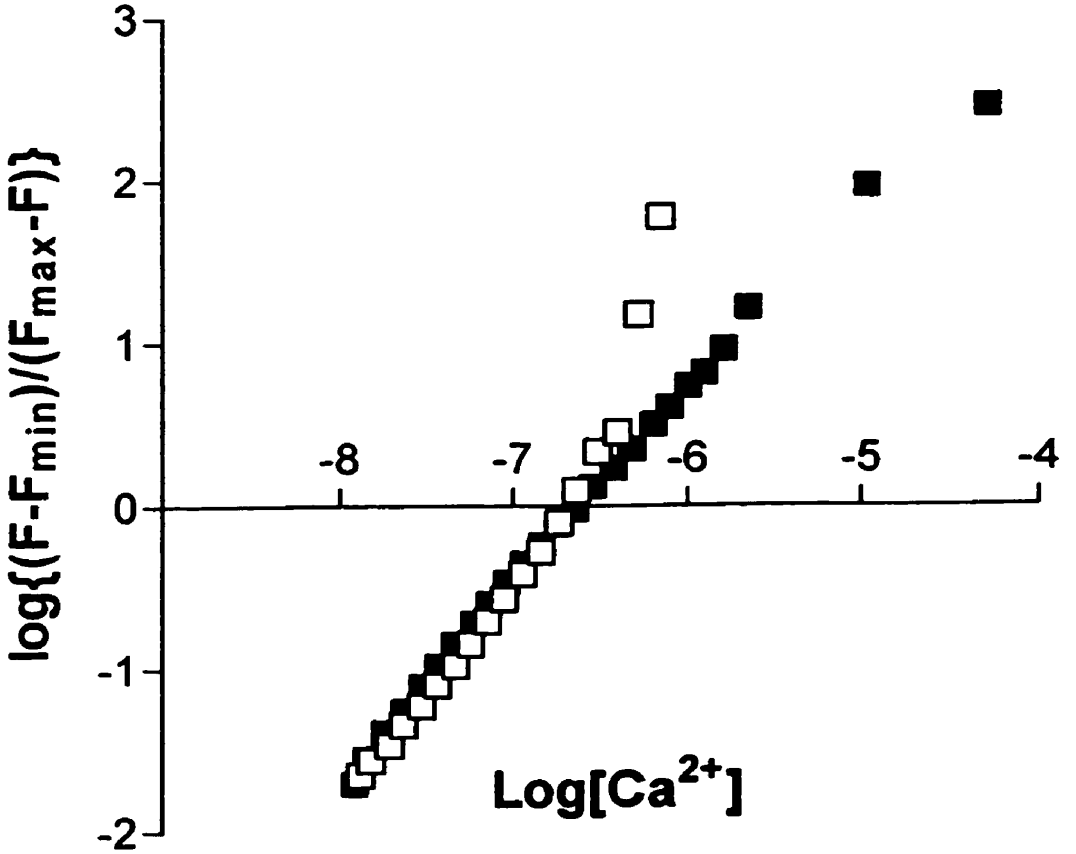
log{(F-F_min)/(F_max-F)}
3
2
1
0
-1
-2
-8
-7
-6
-5
-4
Log[Ca2+]

FIGURE 3. SERCA1 catalytic activity as determined from NADH fluorescence traces. HSR membranes (100 $\mu g.ml^{-1}$) were pre-incubated in transport buffer with 17.5 units/ml PK and LDH, 400 μM NADH and 250 μM EGTA:Ca^{2+}. The cytosolic Ca^{2+} concentrations were adjusted to values of 10, 100, 200, 300, 400, 500, and 750 nM to 1 or 5 μM with EGTA. Ca^{2+} transport/SERCA1 pumping was initiated by the combined addition of 10 mM PEP/1mM MgATP as with most experiments. Replicates (n=3) of each Ca^{2+} condition were performed in the presence of ryanodine (50 μM, closed triangles), in the presence of ionomycin (17.5 μM, open squares), or in the absence of either compound (closed squares). Free Ca^{2+} concentrations were converted to log values (abscissa) while NADH fluorescence traces were converted to NADH consumed by the SERCA1 pump (nmols) per mg HSR protein per minute (ordinate).

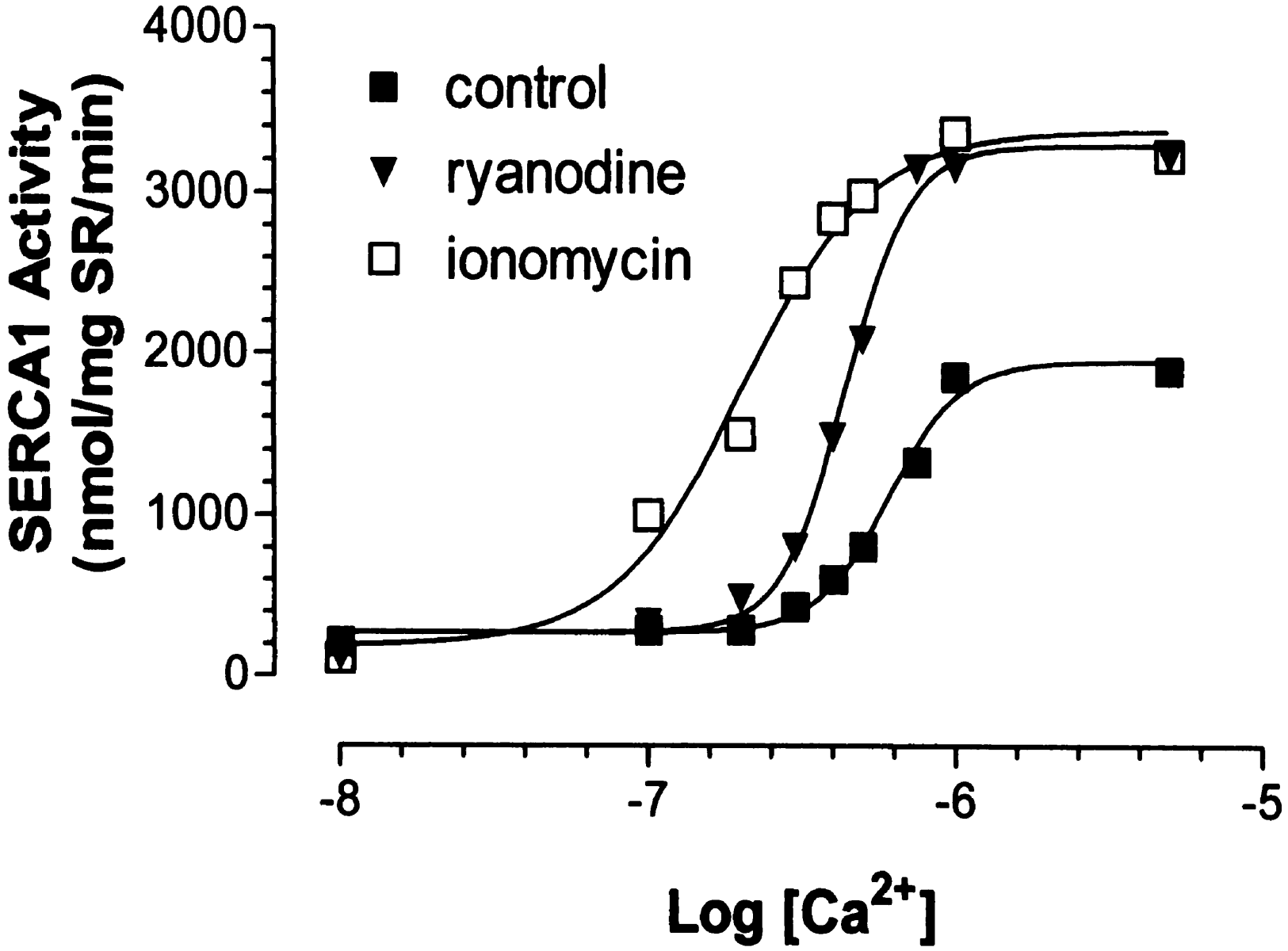
SERCA1 Activity
(nmol/mg SR/min)
4000
3000
2000
1000
0
control
ryanodine
ionomycin
-8
-7
-6
-5
Log [Ca2+]

FIGURE 4. SERCA1 catalytic responses to Ca^{2+} and ryanodine pre-treatments. HSR membranes (500 $\mu g.ml^{-1}$; Panel A and B)(250 $\mu g.ml^{-1}$ Panel C and D) were incubated for >5 minutes in transport buffer containing 17.5 units/ml PK and LDH, and 400 μM NADH, as well as increasing exogenous Ca^{2+} concentrations (0, 15, 17.5 μM; Panel A and B) or concentrations of ryanodine (0, 5, 50 μM; Panel C and D). In all cases, Ca^{2+} transport was initiated with 10 mM PEP/1 mM MgATP at time 0 and the Calcium Green-2 (Panels A and C) and NADH (Panels B and D) fluorescence responses were recorded. All curves were converted to Ca^{2+} or NADH concentration as described (see 'Results').

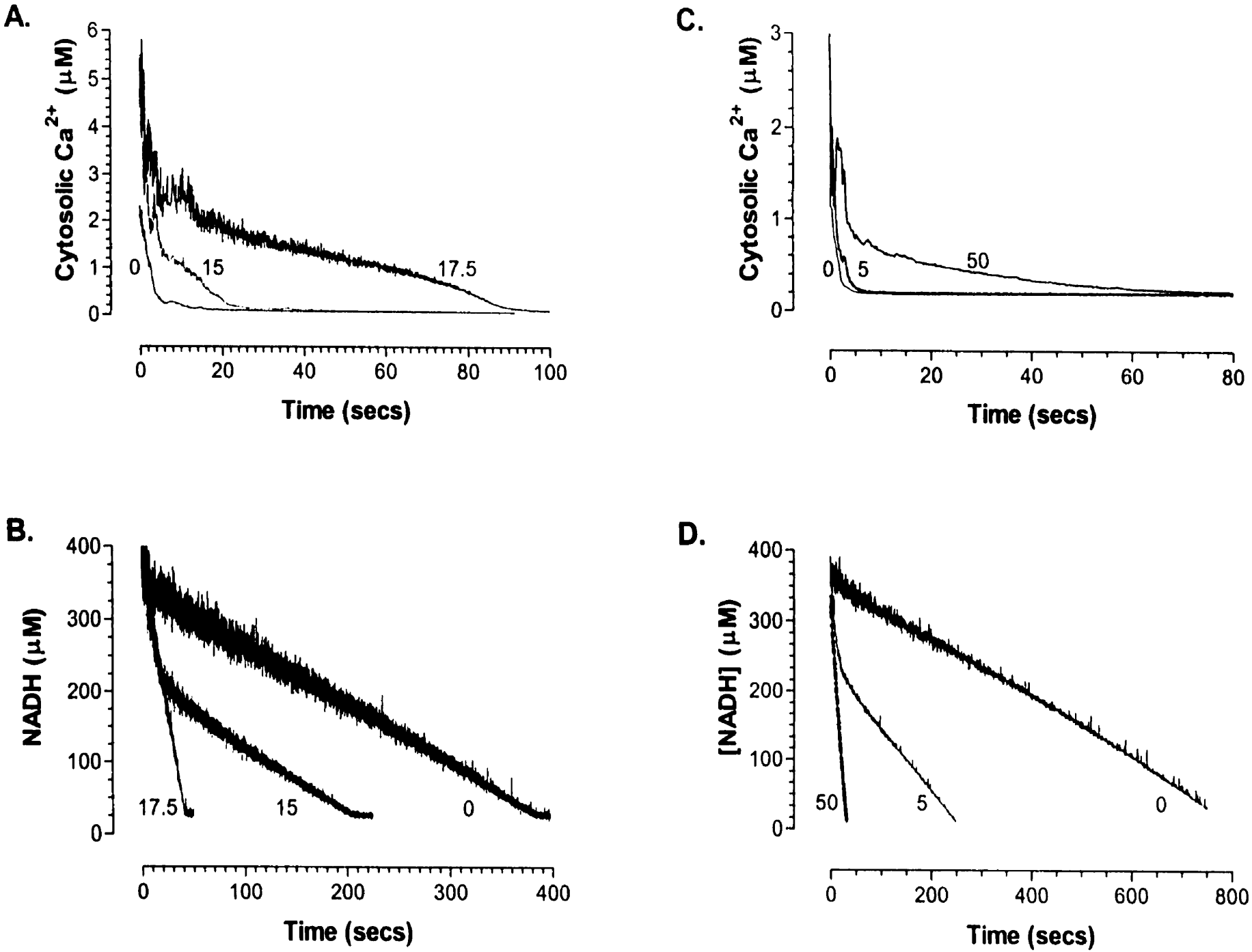
A.
Cytosolic Ca2+ (μM)
0
15
17.5
Time (secs)
B.
NADH (μM)
17.5
15
0
Time (secs)
C.
Cytosolic Ca2+ (μM)
0
5
50
Time (secs)
D.
[NADH] (μM)
50
5
0
Time (secs)

FIGURE 5. Ca^{2+} pulse loading , Ca^{2+}-induced Ca^{2+} release and verification of RyR1 channel activation as revealed with Calcium Green-2 and Mag-Fura 2 fluorescence responses. HSR membranes were incubated for > 5 minutes in transport buffer (pH 7.0, 25°C) containing 17.5 units/ml PK and LDH, and 400 μM NADH, before stimulation of MgATP-dependent Ca^{2+} sequestration (curved arrow). In Panel A and B, HSR membranes (500 $\mu g.ml^{-1}$) were subsequently loaded with repeated pulses (small black arrows) of 5 μM Ca^{2+} while continuously monitored with either 0.8 μM Calcium Green-2 (Panel A) or Mag-Fura 2 (Panel B). In Panel C, 250 $\mu g.ml^{-1}$ HSR membranes were incrementally pulse loaded with two additions of 5 μM Ca^{2+} (small black arrows) and CICR was evoked on the third addition. During the large cytosolic Ca^{2+} transient recorded with Calcium Green-2, 250 μM ryanodine was added timely during different points (trace 1, 2 or 3) of the Ca^{2+} re-sequestration phase of CICR. The final Ca^{2+} addition is referable to trace 3.

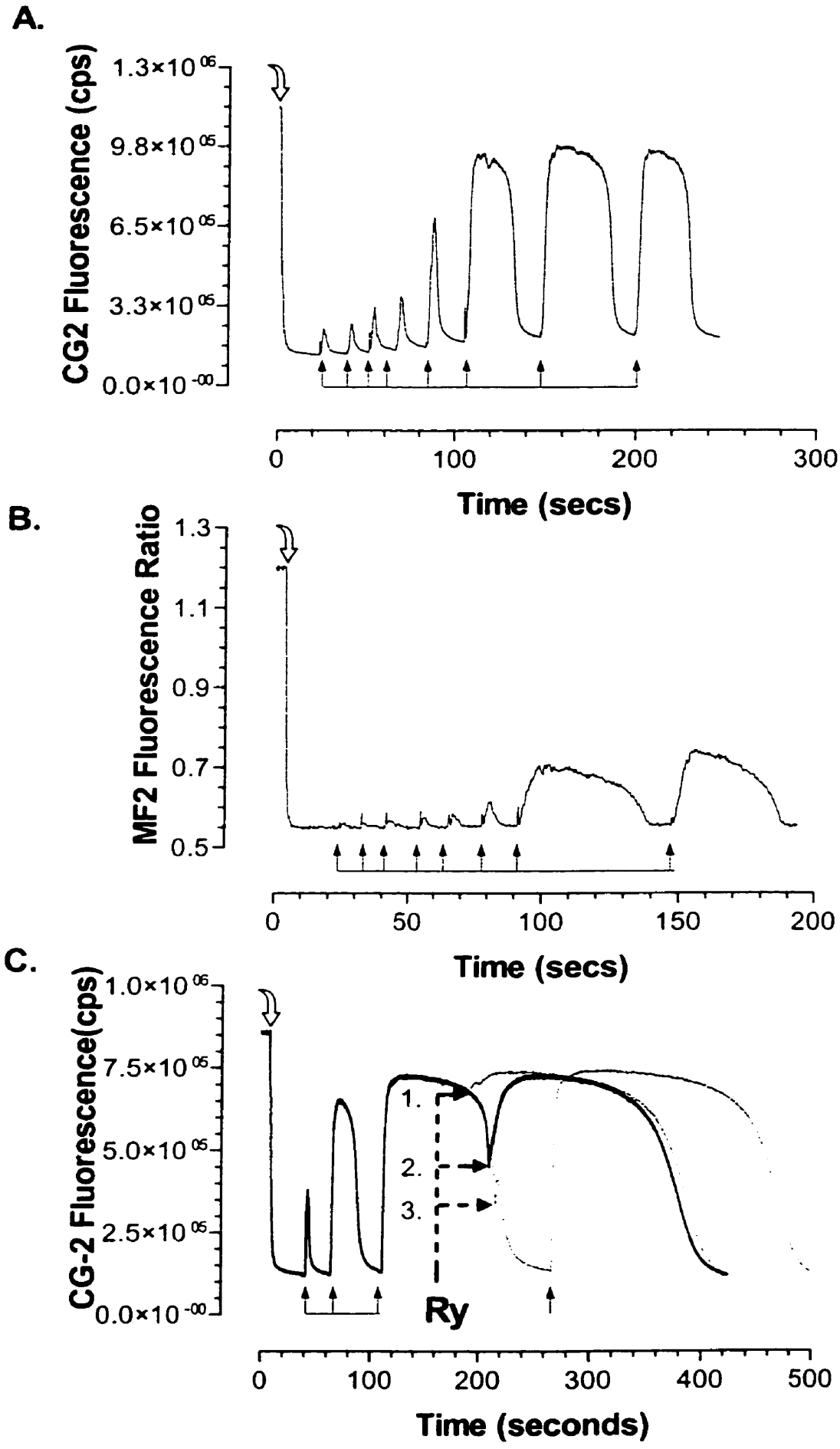
A.
CG2 Fluorescence (cps)
1.3×10 06
9.8×10 05
6.5×10 05
3.3×10 05
0.0×10 -00
0
100
200
300
Time (secs)
B.
MF2 Fluorescence Ratio
1.3
1.1
0.9
0.7
0.5
0
50
100
150
200
Time (secs)
C.
CG-2 Fluorescence(cps)
1.0×10 06
7.5×10 05
5.0×10 05
2.5×10 05
0.0×10 -00
1.
2.
3.
Ry
0
100
200
300
400
500
Time (seconds)

FIGURE 6. The relationship between luminal Ca^{2+} load and activation of RyR1 channels/SERCA1 pumps at varying cytosolic Ca^{2+} concentrations. HSR membranes (500 $\mu g.ml^{-1}$) were incubated in transport buffer (pH 7.0, 25°C) containing 17.5 units/ml PK and LDH, and 400 μM NADH prior to initiation of Ca^{2+} transport with the combined addition of 10mM PEP/1 mM MgATP at the zero timepoint. Subsequent Ca^{2+} additions (small arrows) were made with a repeater pipette as either 2.5 μM (Panel A), 5 μM (Panel B), or 10 μM (Panel C) Ca^{2+} pulses. Consumption of NADH for each loading condition are the grey traces in each panel. Luminal Ca^{2+} load and cytosolic Ca^{2+} for each RyR1 open event inferred by SERCA1 burst activation were calculated and plotted for the complete series of increasing Ca^{2+} pulse loading curves (Panel D, see also 'Results').

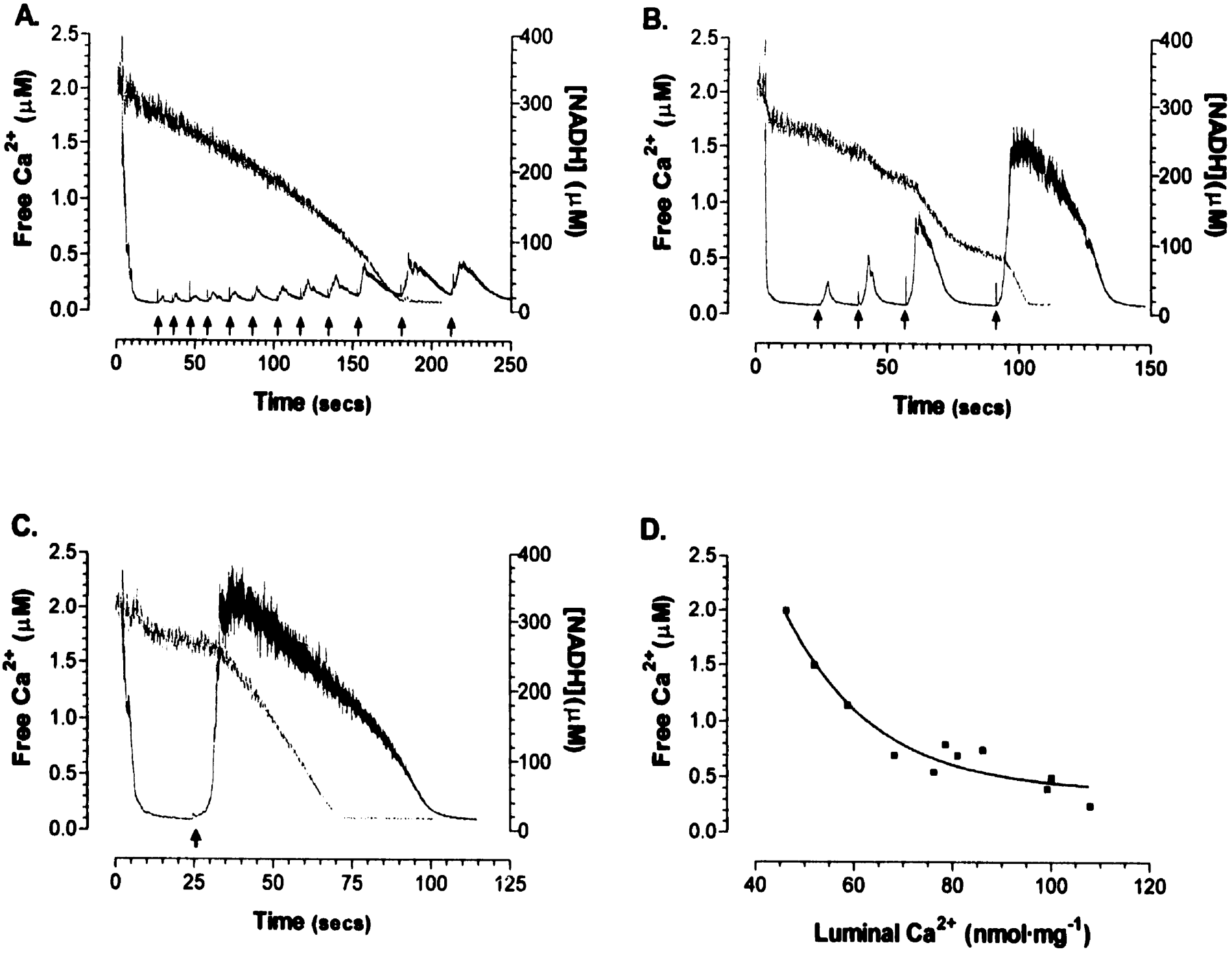
A.
Free Ca2+ (μM)
[NADH] (μM)
Time (secs)
B.
Free Ca2+ (μM)
[NADH](μM)
Time (secs)
C.
Free Ca2+ (μM)
[NADH](μM)
Time (secs)
D.
Free Ca2+ (μM)
Luminal Ca2+ (nmol·mg-1)

FIGURE 7. **The relationship between rate of presentation of Ca^{2+} pulses and Ca^{2+}-induced Ca^{2+} release in HSR membranes.** HSR vesicles (1000 $\mu g.ml^{-1}$) were incubated in transport buffer (pH 7.0, 25°C) containing 17.5 units/ml CPK prior to the stimulation of SERCA1-mediated Ca^{2+} sequestration by the combined addition of 10 mM CP/1 mM MgATP (time = 0). In Panel A, HSR vesicles were pulse loaded with relatively rapid consecutive 5 μM Ca^{2+} additions and CICR was realized following the fourteenth Ca^{2+} pulse. In Panel B, consecutive 5 μM Ca^{2+} pulse additions were presented at a much slower rate (section A, ~1 pulse every 48 secs), followed by an increased rate of frequency (section B, ~1 pulse every 16 secs). The rates of Ca^{2+} sequestration following the first (closed squares) and thirteenth (open squares) Ca^{2+} additions from Panel A were calculated by a one phase exponential decay and are shown in Panel C.

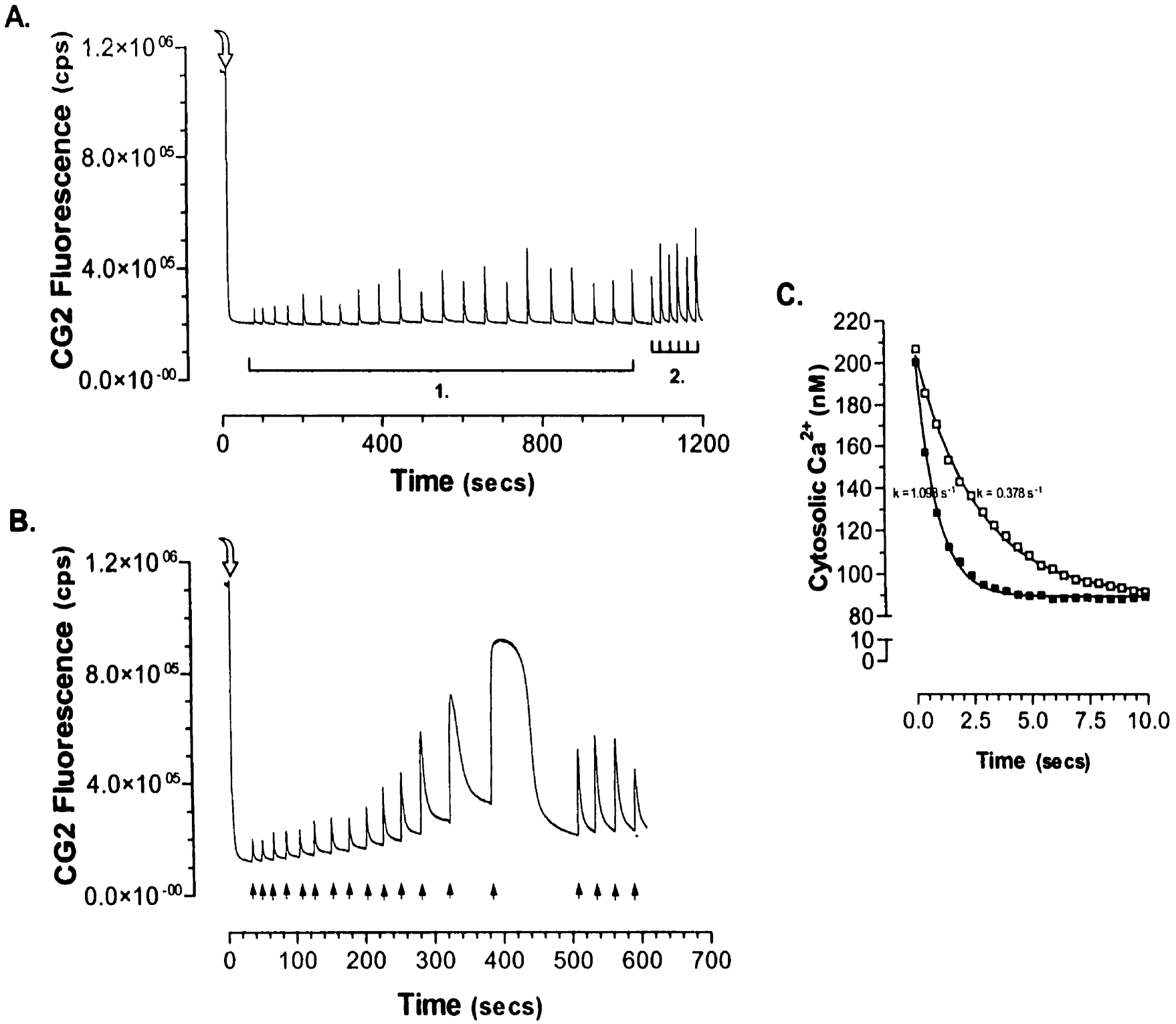
A.
CG2 Fluorescence (cps)
1.2×10 06
8.0×10 05
4.0×10 05
0.0×10 -00
1.
2.
0
400
800
1200
Time (secs)
B.
CG2 Fluorescence (cps)
1.2×10 06
8.0×10 05
4.0×10 05
0.0×10 -00
0
100
200
300
400
500
600
700
Time (secs)
C.
Cytosolic Ca 2+ (nM)
220
200
180
160
140
120
100
80
10
0
k = 1.093 s-1
k = 0.378 s-1
0.0
2.5
5.0
7.5
10.0
Time (secs)

FIGURE 8. Threshold luminal Ca^{2+} loading sensitized the RyR1 and SERCA1. HSR membranes (500 $\mu g.ml^{-1}$) were treated with either 500 μM ryanodine (Panel A and B) or 500 nM thapsigargin (Panel C and D) following initiation of MgATP-dependent Ca^{2+} transport. Panels A and C represent drug treatments under low Ca^{2+} load conditions (0 exogenous Ca^{2+}). Panels B and D were drug treatments under high Ca^{2+} loads of 25 μM added exogenous luminal Ca^{2+}.

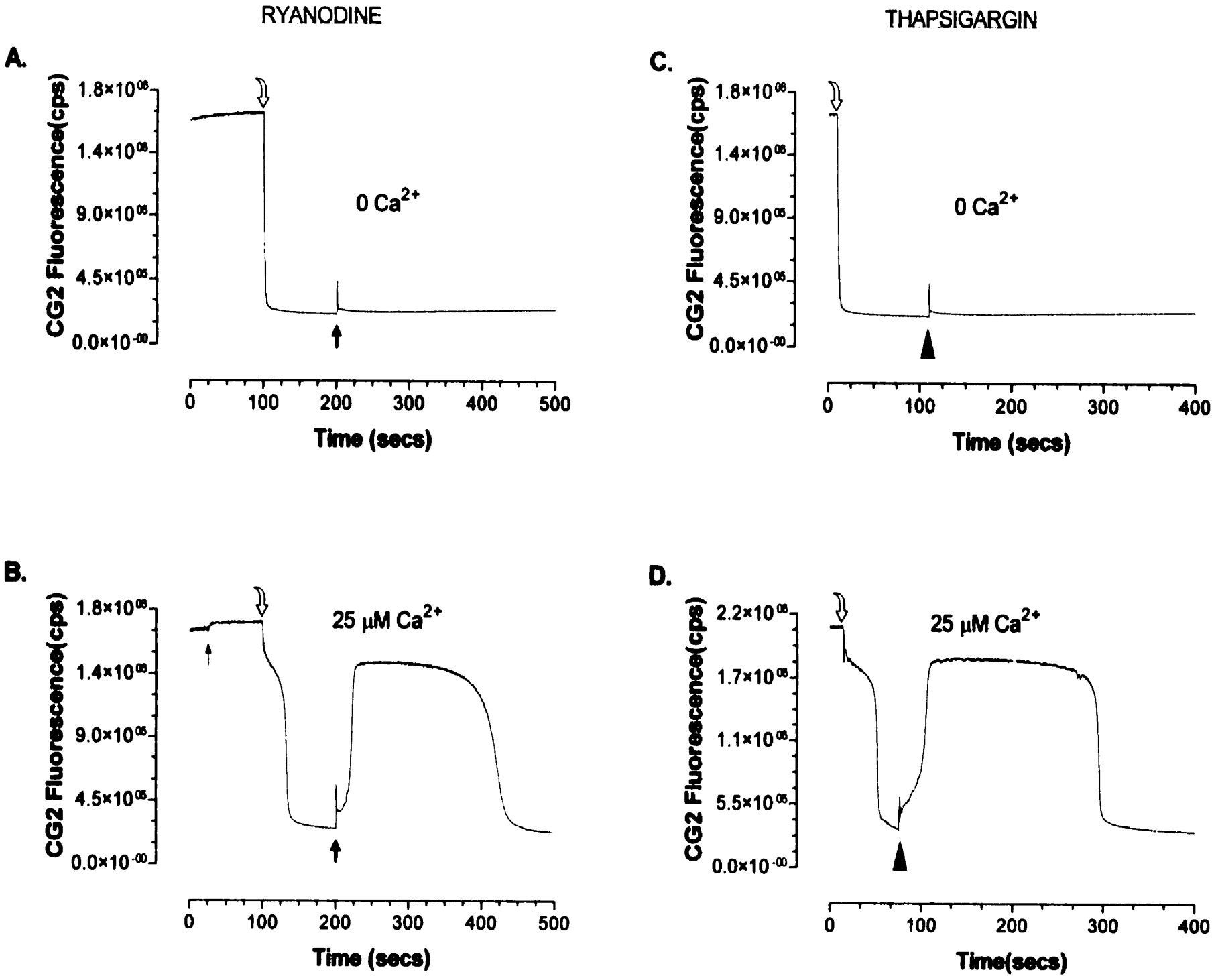
RYANODINE
THAPSIGARGIN
A.
B.
C.
D.
CG2 Fluorescence(cps)
1.8×10⁰⁶
1.4×10⁰⁶
9.0×10⁰⁵
4.5×10⁰⁵
0.0×10⁻⁰⁰
2.2×10⁰⁶
1.7×10⁰⁶
1.1×10⁰⁶
5.5×10⁰⁵
0 Ca2+
25 µM Ca2+
0
100
200
300
400
500
Time (secs)
Time(secs)

FIGURE 9. **Ryanodine activation of RyR1-mediated Ca^{2+} release was accompanied by apparent reversal of the SERCA1 pump.** HSR membranes (250 $\mu g.ml^{-1}$) were incubated in transport buffer (pH 7.0, 25°C) containing 17.5 units/ml PK and LDH, and 400 μM NADH. Following initiation of Ca^{2+} transport by the combined addition of 10 mM PEP/1 mM MgATP (Panel A), membranes were incrementally pulse loaded with six additions of 2.5 μM Ca^{2+} (small black arrows). Membranes were subsequently treated with 250 μM ryanodine (large black arrow) and Calcium Green-2 and NADH responses were monitored. A final 2.5 μM Ca^{2+} pulse is shown not to stimulate further Ca^{2+} release. In Panel B, the point of ryanodine addition has been expanded from Panel A. Both Calcium Green-2 and NADH fluorescence have been converted to Ca^{2+} (hatched trace) and NADH (solid trace) concentrations, respectively (see 'Experimental Procedures').

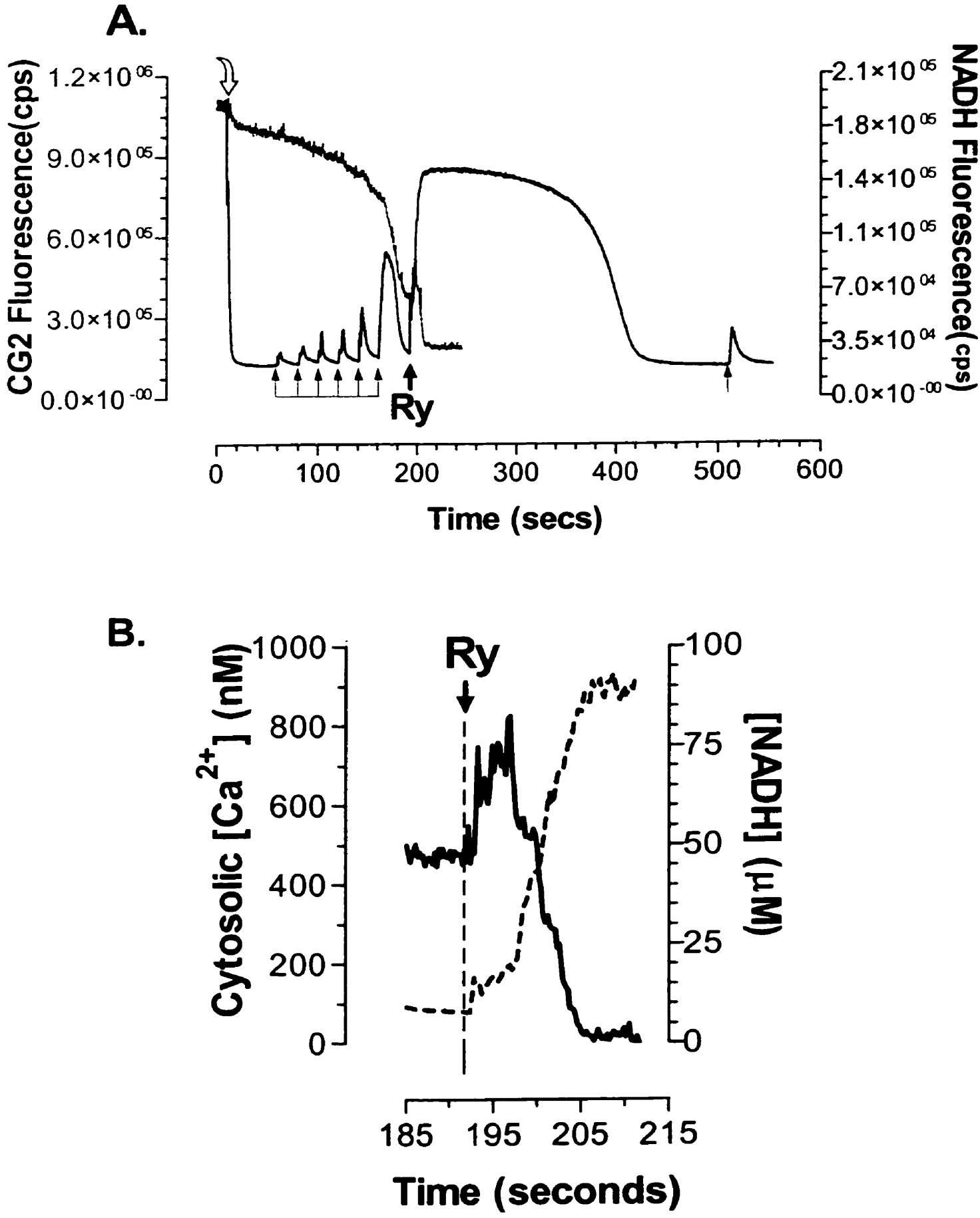
A.
CG2 Fluorescence(cps)
1.2×10 06
9.0×10 05
6.0×10 05
3.0×10 05
0.0×10 -00
NADH Fluorescence(cps)
2.1×10 05
1.8×10 05
1.4×10 05
1.1×10 05
7.0×10 04
3.5×10 04
0.0×10 -00
Ry
0
100
200
300
400
500
600
Time (secs)
B.
Cytosolic [Ca2+] (nM)
1000
800
600
400
200
0
Ry
100
75
50
25
0
[NADH] (μM)
185
195
205
215
Time (seconds)

FIGURE 10. Thapsigargin treatment of HSR membranes at various points during active Ca^{2+} transport. HSR membranes (500 $\mu g.ml^{-1}$) were incubated in transport buffer (pH 7.0, 25°C) containing 17.5 units/ml PK and LDH, and 400 μM NADH and Ca^{2+} transport was subsequently initiated by the combined addition of 10 mM PEP/1 mM MgATP (curved arrow). In Panel A, thapsigargin (750 nM, large black arrowhead) treatment was performed immediately following initial Ca^{2+} sequestration. At approximately 1200 seconds, three pulses of 5 μM Ca^{2+} were added (small black arrows) followed by a single addition of 17.5 μM ionomycin (large black arrow). In Panel B, three pulses of 5 μM Ca^{2+} (small black arrows) preceded treatment with 750 nM thapsigargin (large black arrowhead). Panel C shows the addition of four-5 μM Ca^{2+} pulses (small black arrows) prior to thapsigargin treatment (large black arrowhead).

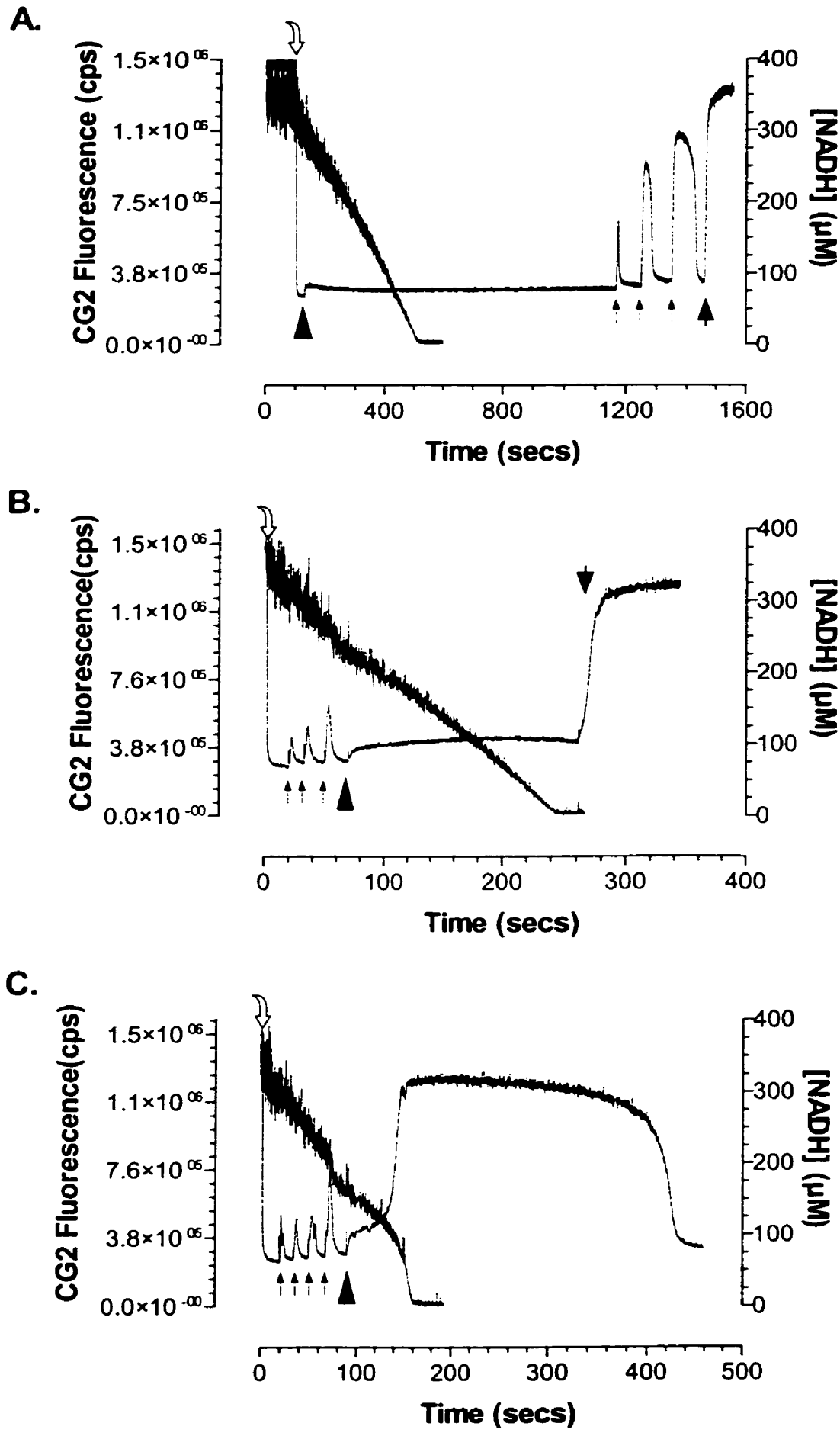
A.
CG2 Fluorescence (cps)
1.5×10 06
1.1×10 06
7.5×10 05
3.8×10 05
0.0×10 -00
[NADH] (µM)
400
300
200
100
0
0
400
800
1200
1600
Time (secs)
B.
CG2 Fluorescence(cps)
1.5×10 06
1.1×10 06
7.6×10 05
3.8×10 05
0.0×10 -00
[NADH] (µM)
400
300
200
100
0
0
100
200
300
400
Time (secs)
C.
CG2 Fluorescence(cps)
1.5×10 06
1.1×10 06
7.6×10 05
3.8×10 05
0.0×10 -00
[NADH] (µM)
400
300
200
100
0
0
100
200
300
400
500
Time (secs)

FIGURE 11. Thapsigargin pretreatment of HSR membranes at low and high exogenous Ca^{2+}. HSR membranes (500 $\mu g.ml^{-1}$) were incubated in transport buffer containing 17.5 units/ml PK, LDH, 400 μM NADH and increasing concentrations of thapsigargin (0 - 5 μM as designated) under conditions of low (0 exogenous; Panel A) and high (17.5 μM exogenous; Panel C) Ca^{2+} pre-loads. The corresponding NADH consumption traces are shown in Panels B and D, respectively. Stimulation of SERCA1-mediated Ca^{2+} transport occurred with the combined addition of 10 mM PEP/1 mM MgATP (curved arrow). Conversion of NADH fluorescence values to NADH concentration were performed as described (see 'Results').

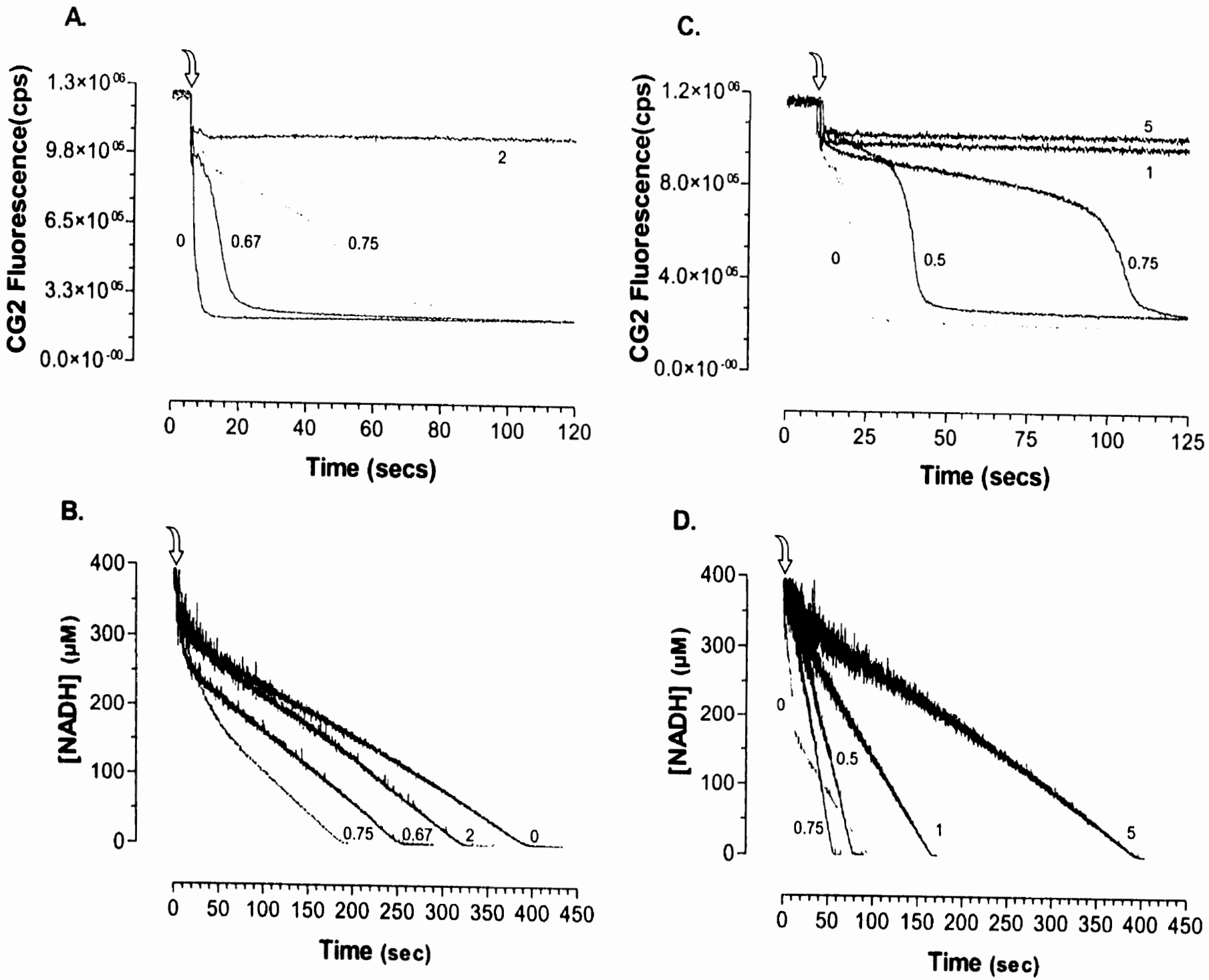
A.
CG2 Fluorescence(cps)
1.3×10^06
9.8×10^05
6.5×10^05
3.3×10^05
0.0×10^-00
0
0.67
0.75
2
0 20 40 60 80 100 120
Time (secs)
C.
CG2 Fluorescence(cps)
1.2×10^06
8.0×10^05
4.0×10^05
0.0×10^-00
0
0.5
0.75
1
5
0 25 50 75 100 125
Time (secs)
B.
[NADH] (μM)
400
300
200
100
0
0.75
0.67
2
0
0 50 100 150 200 250 300 350 400 450
Time (sec)
D.
[NADH] (μM)
400
300
200
100
0
0
0.5
0.75
1
5
0 50 100 150 200 250 300 350 400 450
Time (sec)

FIGURE 12. Cyclopiazonic acid pretreatment and inhibition of SERCA1 pumps in HSR membranes undergoing active Ca^{2+} transport. In all Panels, HSR membranes were incubated in transport buffer (pH 7.0, 25°C) containing 17.5 units/ml PK and LDH, and 400 μM NADH and Ca^{2+} transport was subsequently initiated by the combined addition of 10 mM PEP/1 mM MgATP (curved arrow). In Panel A, HSR vesicles (250 $\mu g.ml^{-1}$) were additionally incubated with 0, 5, 10 or 100 μM cyclopiazonic acid and the corresponding NADH fluorescence traces are shown in Panel B. Direct comparison of thapsigargin- and cyclopiazonic acid-induced Ca^{2+} efflux in low Ca^{2+} load HSR membranes (500 $\mu g.ml^{-1}$) is shown in Panel C. Addition of either 20 μM thapsigargin (large arrowhead; trace 1) or cyclopiazonic acid (large arrowhead; trace 2) preceded ionomycin treatment (large black arrow). In Panel D, the efficacy of cyclopiazonic acid treatment (large arrowheads) at low (0 exogenous) and high (25 μM exogenous) Ca^{2+} pre-loads was examined with 500 $\mu g.ml^{-1}$ HSR membranes.

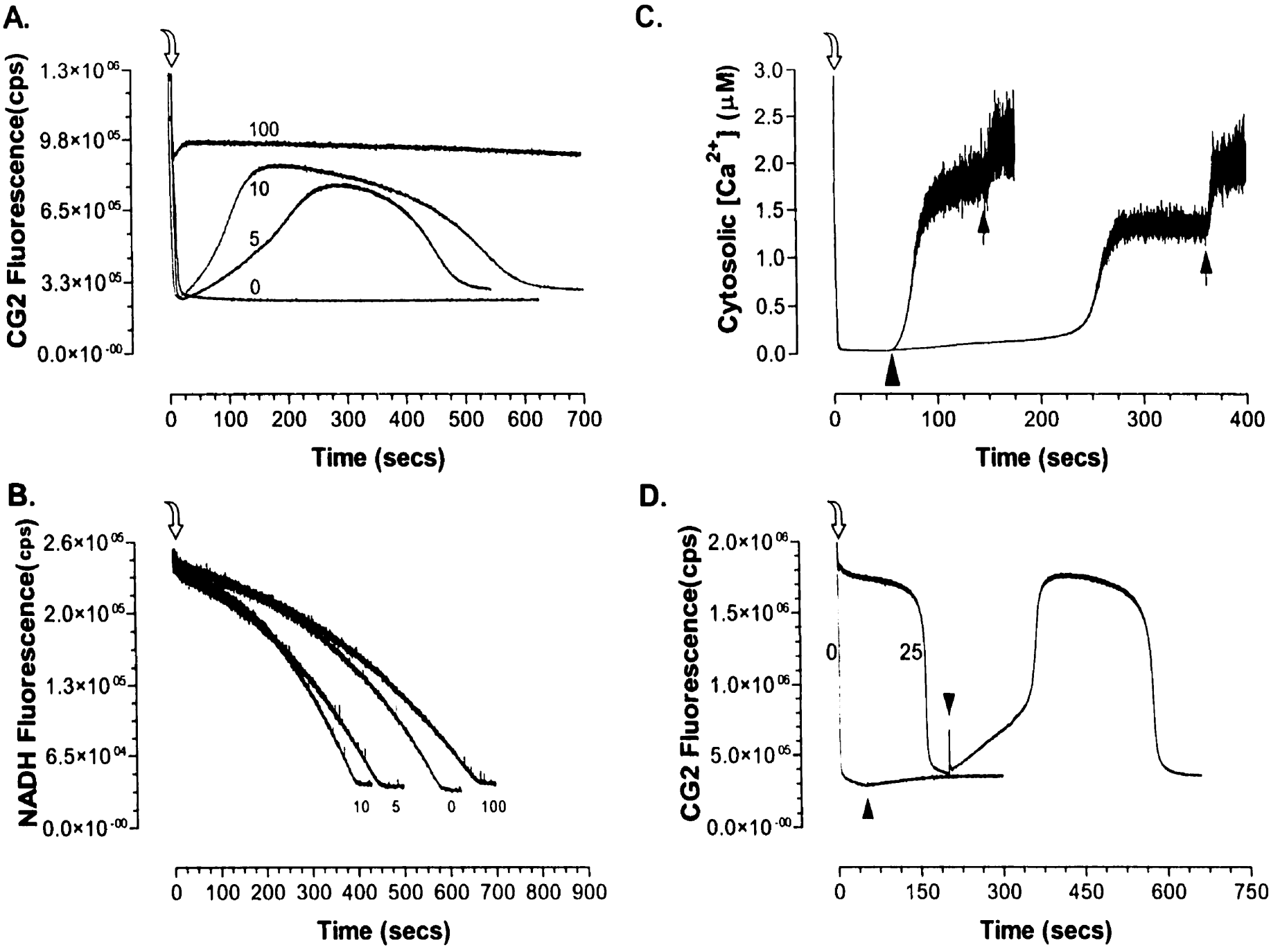
A.
CG2 Fluorescence(cps)
1.3×10^06
9.8×10^05
6.5×10^05
3.3×10^05
0.0×10^-00
100
10
5
0
0 100 200 300 400 500 600 700
Time (secs)
C.
Cytosolic [Ca2+] (μM)
3.0
2.5
2.0
1.5
1.0
0.5
0.0
0 100 200 300 400
Time (secs)
B.
NADH Fluorescence(cps)
2.6×10^05
2.0×10^05
1.3×10^05
6.5×10^04
0.0×10^-00
10 5 0 100
0 100 200 300 400 500 600 700 800 900
Time (secs)
D.
CG2 Fluorescence(cps)
2.0×10^06
1.5×10^06
1.0×10^06
5.0×10^05
0.0×10^-00
0
25
0 150 300 450 600 750
Time (secs)

FIGURE 13. Thapsigargin and cyclopiazonic acid inhibition of SERCA1 in HSR membranes treated with ionomycin. HSR membranes (250 $\mu g.ml^{-1}$) were incubated in transport buffer (pH 7.0, 25°C) containing 17.5 units/ml PK and LDH, and 400 μM NADH. In Panel A, NADH consumption traces in the absence (-iono) and presence (+iono) of ionomycin were compared following initiation of MgATP-dependent SERCA1 activation (curved arrow). In the presence of ionomycin, membranes were pretreated with 0, 5, 10 or 100 μM cyclopiazonic acid (Panel B) or with 0, 1, or 5 μM thapsigargin (Panel B) and NADH consumption was recorded following the addition of 10 mM PEP/1 mM MgATP (curved arrow). NADH fluorescence was converted to NADH concentration as described (see 'Results').

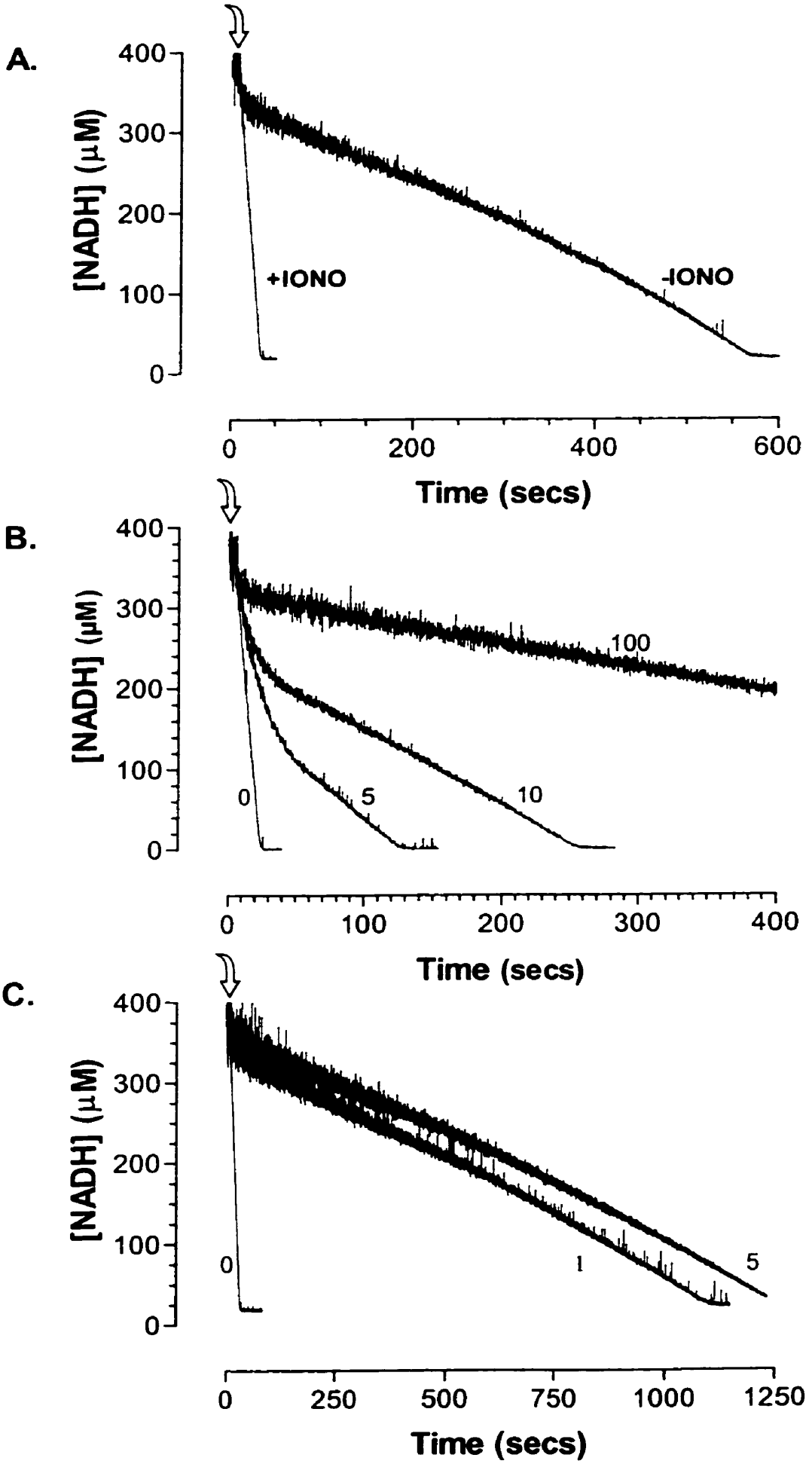
A.
[NADH] (μM)
400
300
200
100
0
+IONO
-IONO
0
200
400
600
Time (secs)
B.
[NADH] (μM)
400
300
200
100
0
100
0
5
10
0
100
200
300
400
Time (secs)
C.
[NADH] (μM)
400
300
200
100
0
0
1
5
0
250
500
750
1000
1250
Time (secs)

FIGURE 14. **Ryanodine-mediated inhibition of thapsigargin- and cyclopiazonic acid-induced Ca^{2+} efflux from HSR membranes.** HSR membranes (500 $\mu g.ml^{-1}$) were incubated in transport buffer (pH 7.0, 25°C) containing 17.5 units/ml CPK. Ca^{2+} transport was initiated with 10 mM CP/1 mM MgATP and the vesicles were incrementally loaded to threshold with 5 μM additions of Ca^{2+}. Ryanodine (0, 1, 10, 100, or 500 μM as labeled at right of traces) was subsequently added to initially activate, then inhibit the RyR1. During RyR1-inactivation, membranes were treated with either 10 μM thapsigargin (Panel A) or 100 μM cyclopiazonic acid (Panel B) to evoke Ca^{2+} efflux. Only the sections of the original Calcium Green-2 traces pertaining to thapsigargin and cyclopiazonic acid additions are shown. Ionomycin addition (17.5 μM) is indicated by the large arrow (Panel B). Calcium Green-2 fluorescence was converted to Ca^{2+} concentration as indicated in 'Results'.

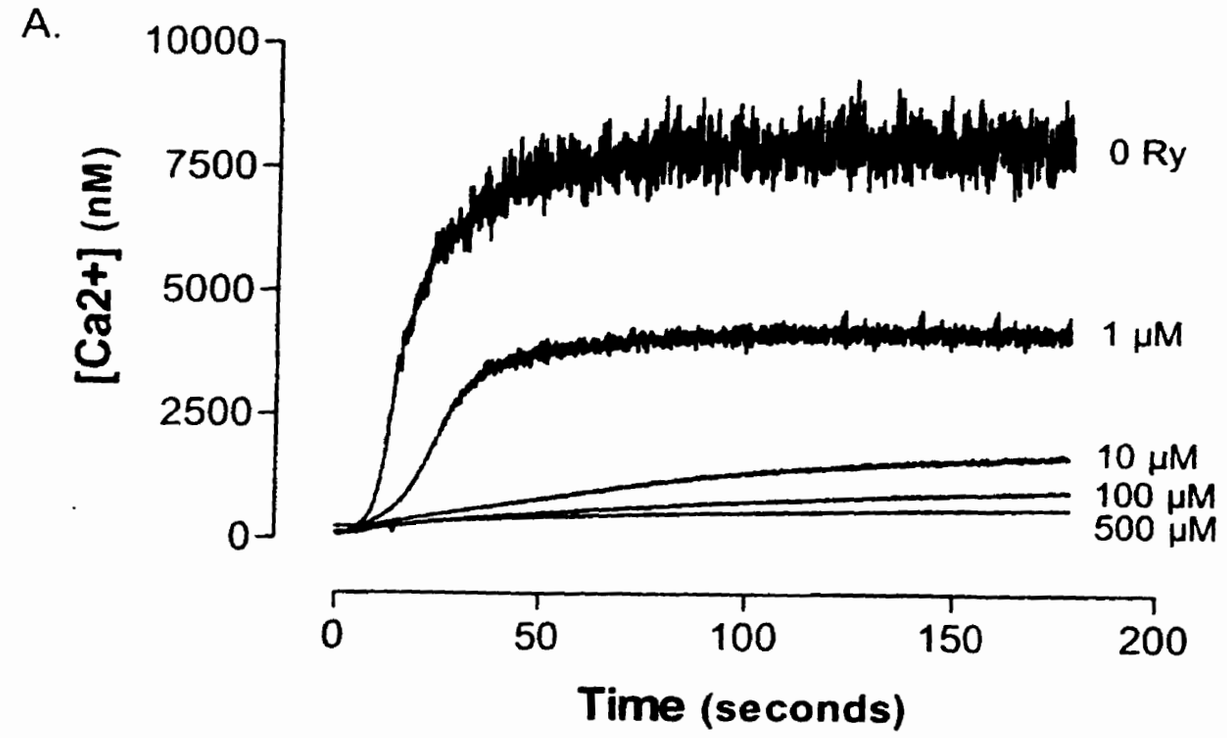
A.
10000
7500
5000
2500
0
[Ca2+] (nM)
0 Ry
1 μM
10 μM
100 μM
500 μM
0
50
100
150
200
Time (seconds)

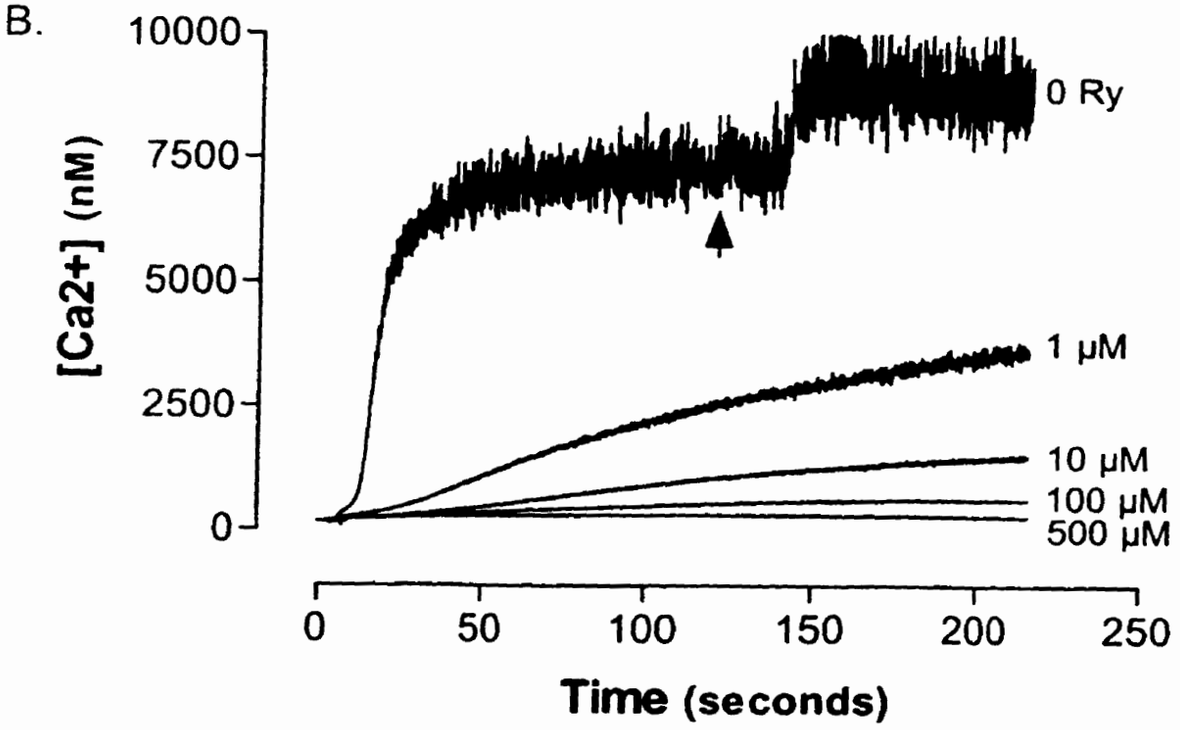
B.
10000
7500
5000
2500
0
[Ca2+] (nM)
0 Ry
1 μM
10 μM
100 μM
500 μM
0
50
100
150
200
250
Time (seconds)

FIGURE 15. Mag-Fura 2 (AM) fluorescence signals were Ca^{2+}-dependent and luminal in origin. HSR membranes (500 $\mu g.ml^{-1}$) previously loaded with cell-permeant Mag-Fura 2 (see 'Experimental Procedures') were initially incubated in transport buffer (pH 7.0, 25°C) containing 17.5 units/ml CPK. In Panel A, MgATP-dependent Ca^{2+} uptake (curved arrow) was initiated at low (0 exogenous; trace 1) and high (30 μM exogenous; trace 2) Ca^{2+} loads. Trace 1 shows the incremental pulse loading with six-5 μM Ca^{2+} additions (small black arrows) while a single 5 μM Ca^{2+} pulse was added in trace 2. Panel B compares the addition of a single bolus of 35 μM Ca^{2+} (small black arrow) following initial Ca^{2+} sequestration with both cytosolic Calcium Green-2 (trace 1) and luminal Mag-Fura 2 (trace 2). In Panel C, membranes were treated with 10 μM thapsigargin prior to stimulation of Ca^{2+} transport (curved arrow). Following steady state fluorescence, six-5 μM Ca^{2+} pulses were added (small black arrows) followed by 17.5 μM ionomycin (large black arrow).

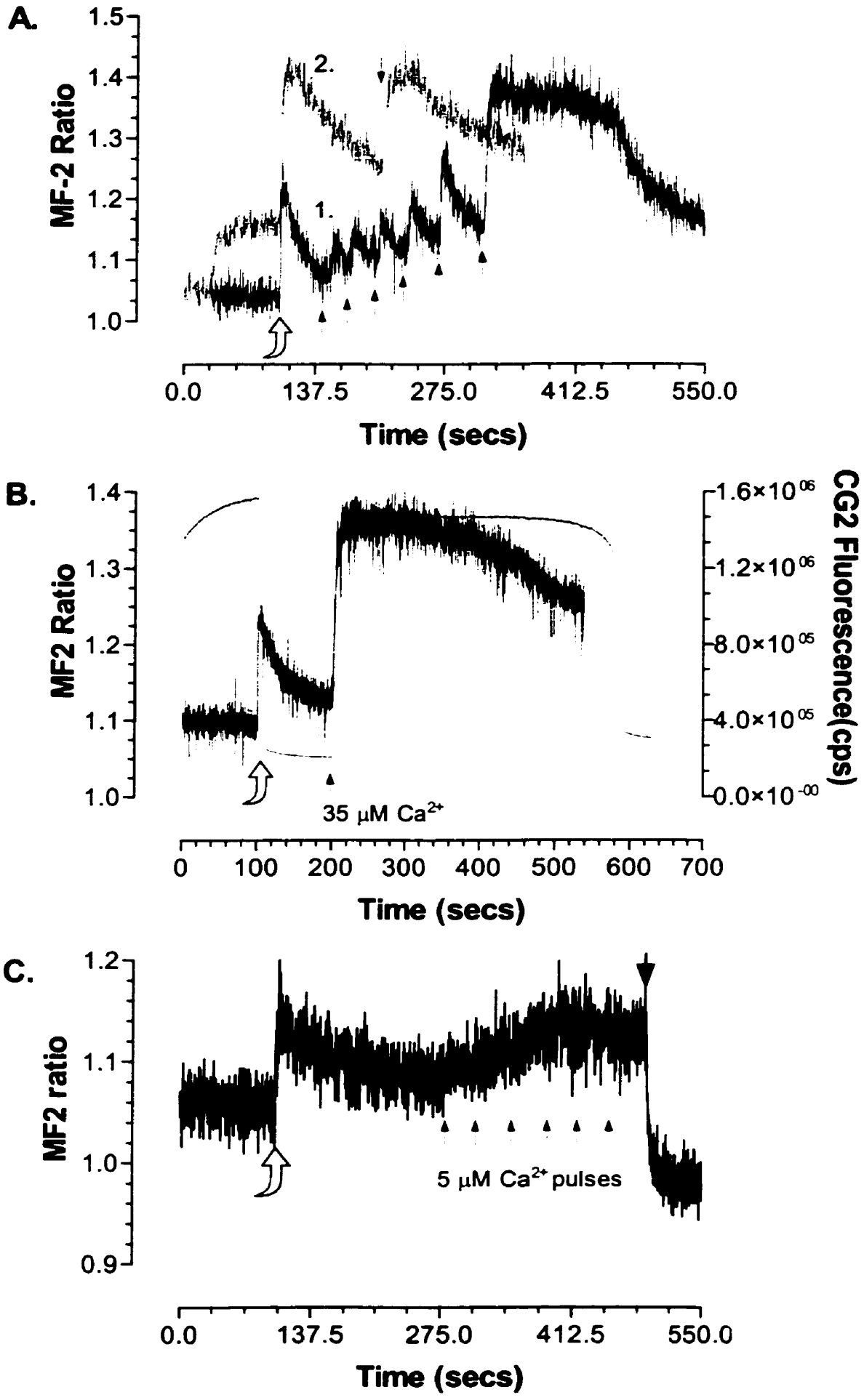
A.
MF-2 Ratio
1.5
1.4
1.3
1.2
1.1
1.0
2.
1.
0.0
137.5
275.0
412.5
550.0
Time (secs)
B.
MF2 Ratio
1.4
1.3
1.2
1.1
1.0
1.6×10^06
1.2×10^06
8.0×10^05
4.0×10^05
0.0×10^-00
CG2 Fluorescence(cps)
35 μM Ca2+
0
100
200
300
400
500
600
700
Time (secs)
C.
MF2 ratio
1.2
1.1
1.0
0.9
5 μM Ca2+ pulses
0.0
137.5
275.0
412.5
550.0
Time (secs)

FIGURE 16. Calibration of the luminal Mag-Fura 2 fluorescence signal and conversion to luminal Ca^{2+} concentration. In Panel A, Mag-Fura 2-loaded HSR membranes (500 $\mu g.ml^{-1}$) were incubated in transport buffer (pH 7.0, 25°C) containing 17.5 units/ml CPK, 10 mM CP, 17.5 μM ionomycin, 10 μM thapsigargin and 1 mM TrisATP. Ca^{2+} concentrations ranging from 0 to 1250 μM were added and the Mag-Fura 2 responses recorded. The values obtained were fit to a single site binding hyperbola curve to obtain a kD for Mag-Fura 2 of 33 μM. The Mag-Fura 2 fluorescence ratio values from FIGURE 15, Panel A (trace 1) were then converted to Ca^{2+} concentration as outlined in 'Results' and the converted trace is shown in Panel B. The curved arrow represents 10 mM CP/1 mM MgATP addition and the small black arrows are additions of 5 μM Ca^{2+}.

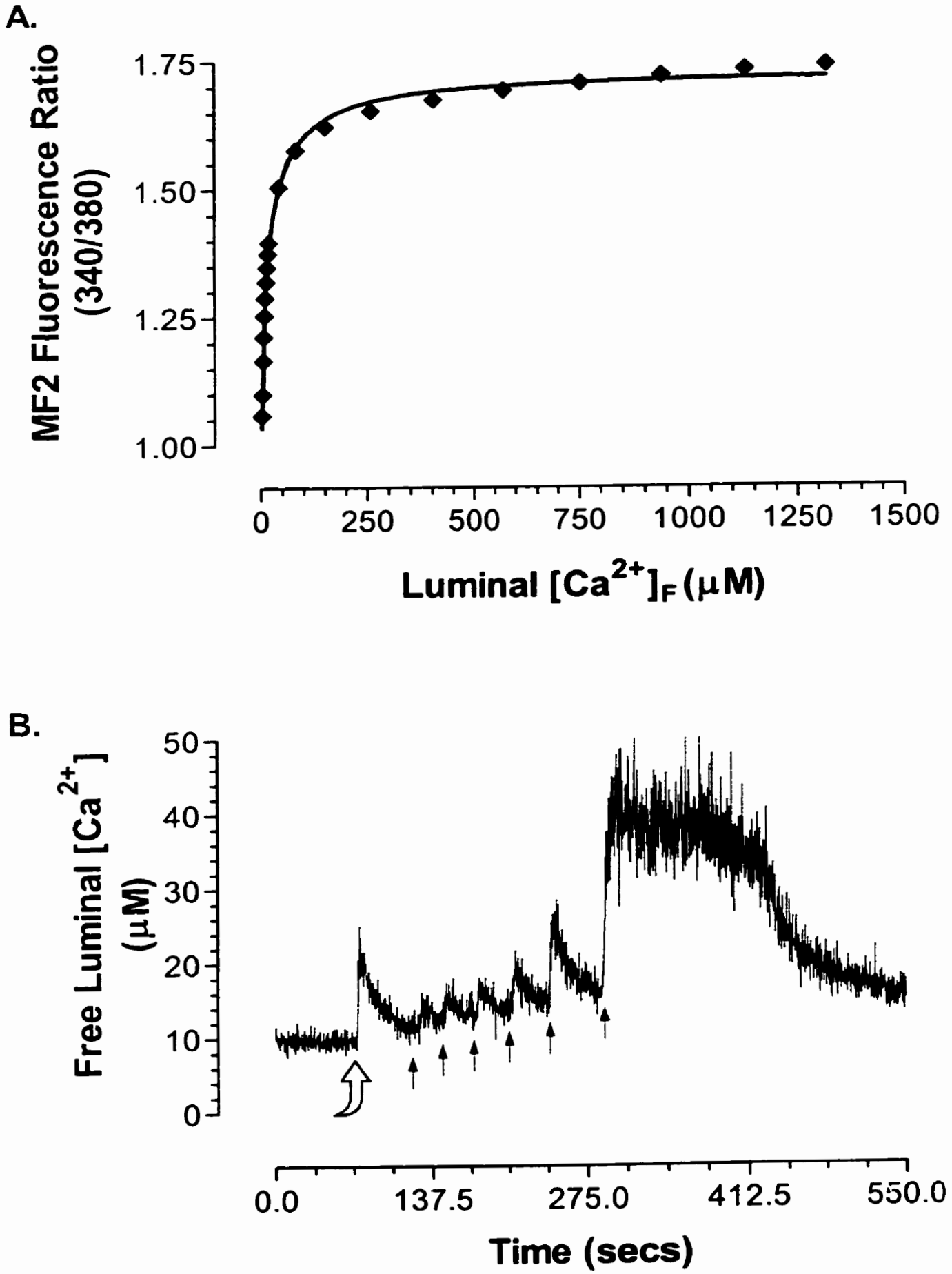
A.
MF2 Fluorescence Ratio (340/380)
1.75
1.50
1.25
1.00
0
250
500
750
1000
1250
1500
Luminal [Ca2+]F (μM)
B.
Free Luminal [Ca2+] (μM)
50
40
30
20
10
0
0.0
137.5
275.0
412.5
550.0
Time (secs)

FIGURE 17. Chlortetracycline fluorescence faithfully tracks the luminal Ca^{2+} dependence of Ca^{2+}-induced Ca^{2+} release in HSR membranes. For all Panels, HSR membranes (500 $\mu g.ml^{-1}$) were incubated in transport buffer (pH 7.0, 25°C) containing 17.5 units/ml CPK and 40 μM chlortetracycline as described in 'Experimental Procedures'. Ca^{2+} transport was initiated with the combined addition of 10 mM CP/1 mM MgATP (curved arrow). In Panel A, membranes under low Ca^{2+} load (0 exogenous) were incrementally loaded with additions of 5 μM Ca^{2+} (small arrows). Trace 2 differs from trace 1 in that 5 μM Ca^{2+} additions were made at the nadir of chlortetracycline fluorescence decreases and a final addition of 17.5 μM ionomycin (large black arrow) was made. In Panel B, exogenous Ca^{2+} loads of 20 μM (trace 1) or 30 μM (trace 2) preceded MgATP-dependent Ca^{2+} sequestration. The small black arrows represent 5 μM Ca^{2+} additions. Panel C compares the conditions in which a 20 μM exogenous Ca^{2+} preload is followed by a single bolus of 20 μM Ca^{2+} (trace 1) with a low Ca^{2+} load (0 exogenous) in which a single addition of 20 μM Ca^{2+} was made (trace 2). The large black arrows represent final ionomycin additions (17.5 μM).

A.

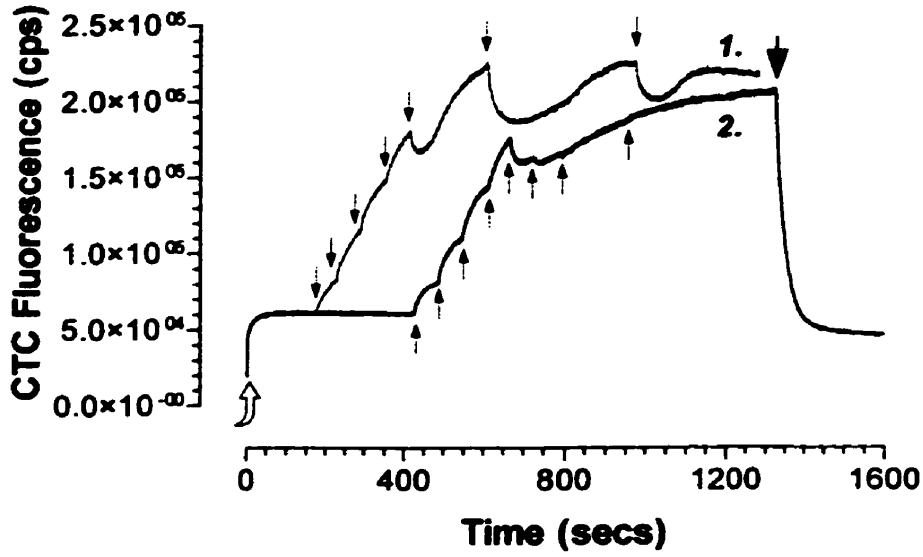
CTC Fluorescence (cps)
2.5×10^05
2.0×10^05
1.5×10^05
1.0×10^05
5.0×10^04
0.0×10^-00
1.
2.
0
400
800
1200
1600
Time (secs)

B.

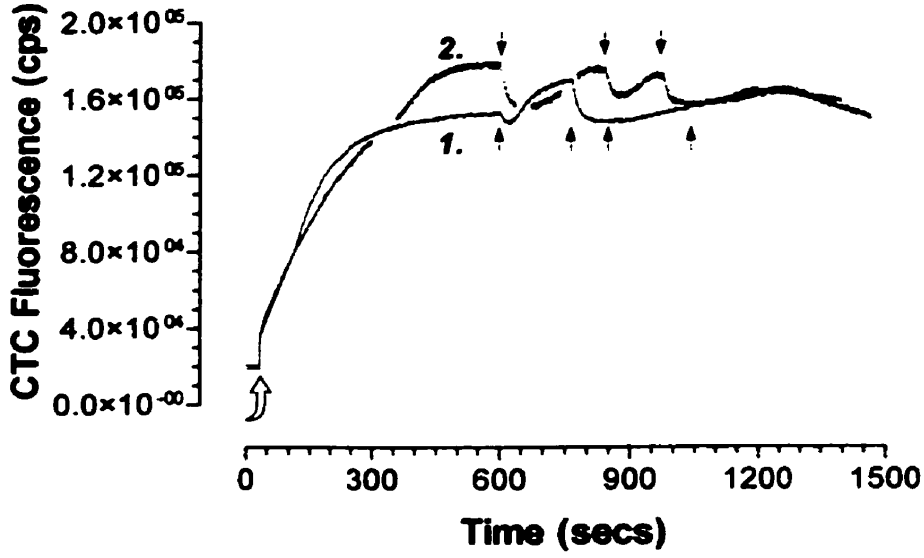
CTC Fluorescence (cps)
2.0×10^05
1.6×10^05
1.2×10^05
8.0×10^04
4.0×10^04
0.0×10^-00
2.
1.
0
300
600
900
1200
1500
Time (secs)

C.

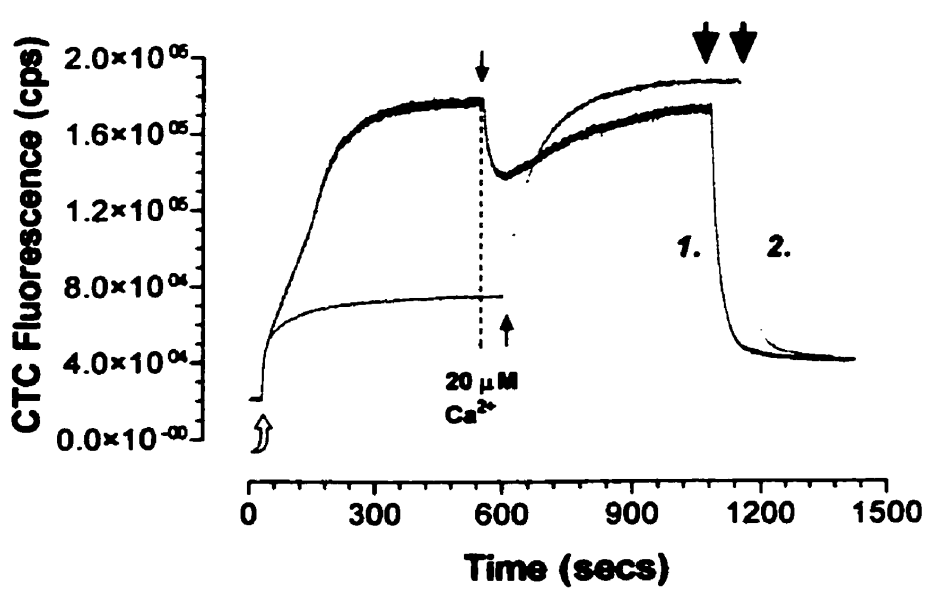
CTC Fluorescence (cps)
2.0×10^05
1.6×10^05
1.2×10^05
8.0×10^04
4.0×10^04
0.0×10^-00
1.
2.
20 µM
Ca2+
0
300
600
900
1200
1500
Time (secs)

FIGURE 18. Comparison of initial Ca^{2+} uptakes as realized by Mag-Fura 2 and chlortetracycline luminal fluorescence. In Panel A, initial fluorescence increases with Mag-Fura 2 upon addition of 50 μM Ca^{2+} (passive loading; closed squares) or stimulation of active Ca^{2+} sequestration by the addition of MgATP (active loading endogenous Ca^{2+}; open diamonds)(active loading exogenous 50 μM Ca^{2+}; open squares) were compared. Maximum Mag-Fura 2 fluorescence ratio increases were normalized to 1.0 for comparative purposes. In Panel B, initial chlortetracycline fluorescence increases for MgATP-dependent active Ca^{2+} sequestration are compared for low (0 exogenous; trace 1) and high (20 μM exogenous; trace 2) Ca^{2+} loads. Again, maximum chlortetracycline fluorescence was normalized to 1. All traces were further analyzed by curve fit to one phase exponential association for rate determination (see 'Results').

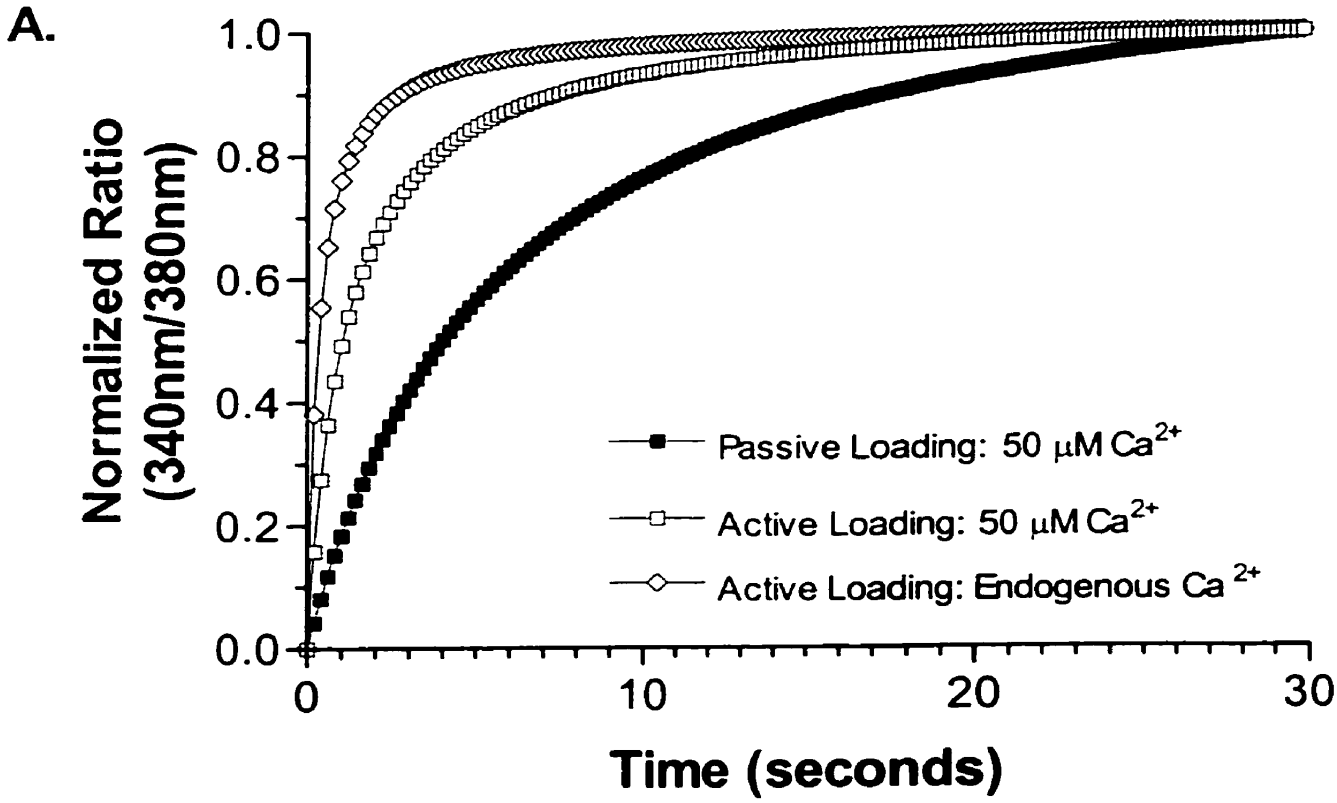
A.
Normalized Ratio (340nm/380nm)
1.0
0.8
0.6
0.4
0.2
0.0
0
10
20
30
Time (seconds)
Passive Loading: 50 μM Ca2+
Active Loading: 50 μM Ca2+
Active Loading: Endogenous Ca 2+

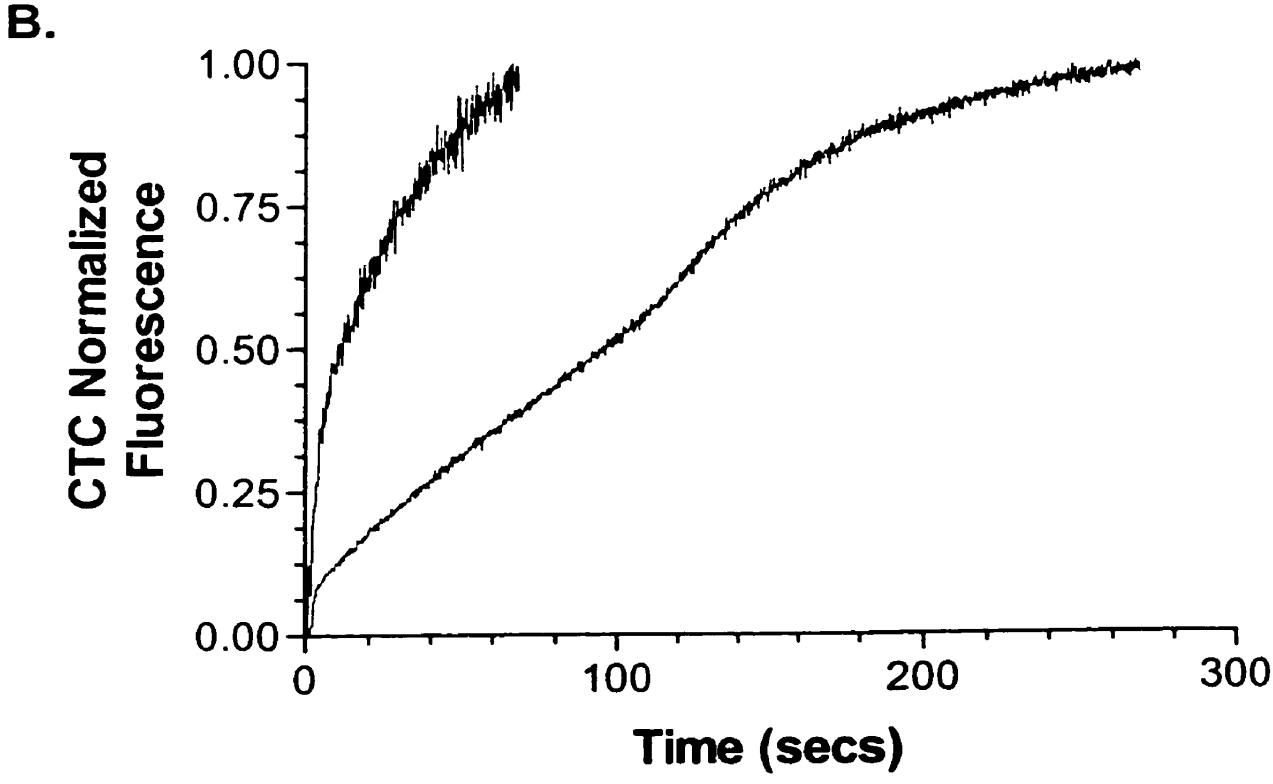
B.
CTC Normalized Fluorescence
1.00
0.75
0.50
0.25
0.00
0
100
200
300
Time (secs)

FIGURE 19. Chlortetracycline fluorescence was enhanced by the presence of isolated calsequestrin. Chlortetracycline was incubated for 5 minutes in transport buffer (pH 7.0, 25°C) and baseline fluorescence was established. Subsequent addition of 1 mM (trace 1), 5 mM (trace 2), or 10 mM (trace 3) Ca^{2+}, marked by the small downward arrow, preceded the addition of 75 $\mu g.ml^{-1}$ calsequestrin (large downward arrow). Trace 4 differs in that 75 $\mu g.ml^{-1}$ calsequestrin (large upward arrow) addition was made prior to the addition of 1 mM Ca^{2+} (small upward arrow). Calsequestrin was isolated as per 'Experimental Procedures'.

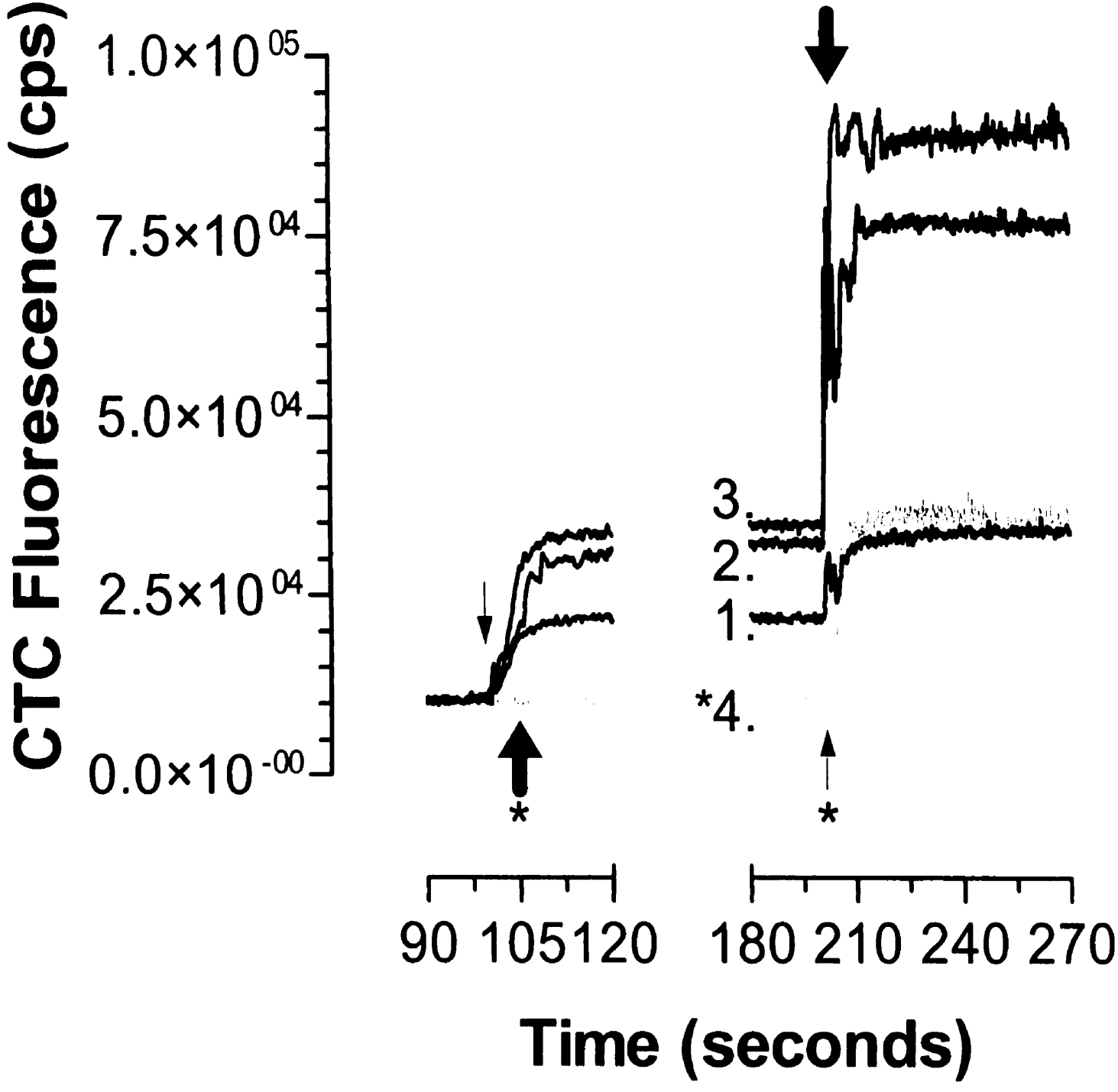
CTC Fluorescence (cps)
1.0×10 05
7.5×10 04
5.0×10 04
2.5×10 04
0.0×10 -00
3.
2.
1.
*4.
*
*
90 105120
180 210 240 270
Time (seconds)

FIGURE 20. **Mag-Fura 2 luminal Ca^{2+} fluorescence signals were unresponsive to ionomycin treatment but responsive to thapsigargin treatment in HSR membranes undergoing active Ca^{2+} transport.** Mag-Fura 2-loaded HSR membranes (500 $\mu g.ml^{-1}$) were incubated in transport buffer (pH 7.0, 25°C) containing 17.5 units/ml CPK. In both panels, Ca^{2+} sequestration was stimulated by the addition of 10 mM CP/1 mM MgATP (curved arrow). In Panel A, membranes were further incubated with 17.5 μM ionomycin (large arrow) (trace 1) or 17.5 μM ionomycin (large arrow) and 30 μM exogenous Ca^{2+} (trace 2) prior to MgATP addition. Final additions of 20 μM thapsigargin were made (large arrowhead). In Panel B, membranes were again examined at low (0 exogenous; trace 1) or high (30 μM exogenous; trace 2) Ca^{2+} loads. Subsequent to MgATP addition, a train of either three (trace 2) or four (trace 1) additions of 17.5 μM ionomycin (large arrows) were made. The large arrowhead represents the final thapsigargin addition (20 μM).

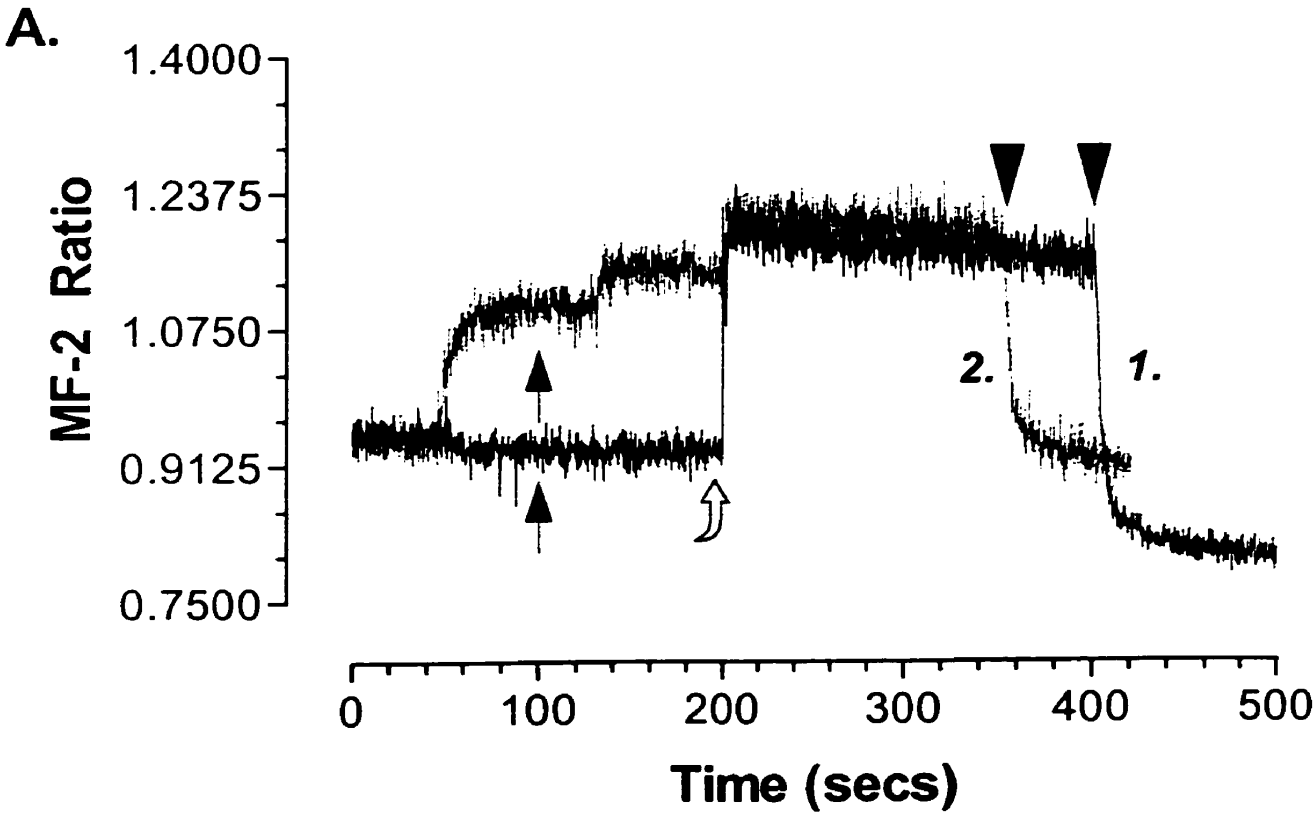
A.
1.4000
1.2375
1.0750
0.9125
0.7500
MF-2 Ratio
2.
1.
0
100
200
300
400
500
Time (secs)

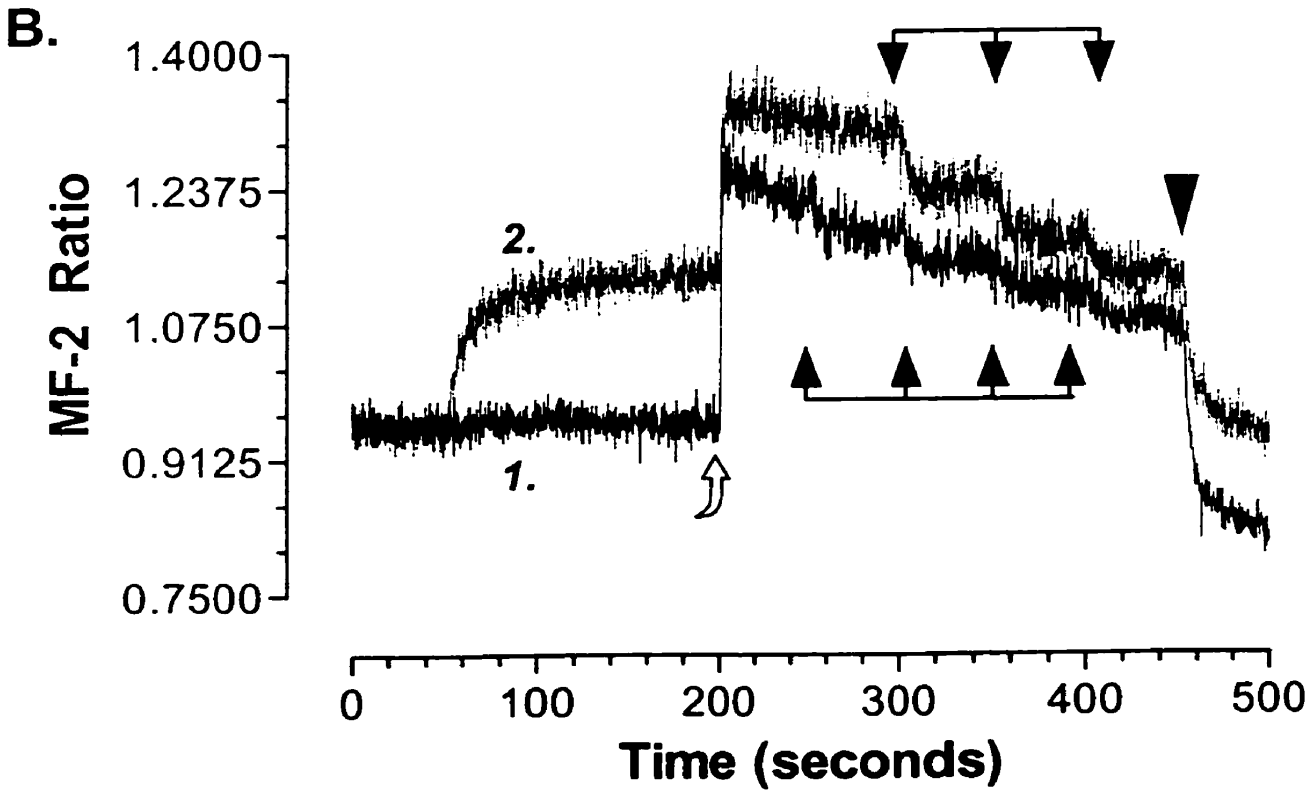
B.
1.4000
1.2375
1.0750
0.9125
0.7500
MF-2 Ratio
2.
1.
0
100
200
300
400
500
Time (seconds)

FIGURE 21. Chlortetracycline fluorescence was sensitive to thapsigargin treatment in HSR membranes. In both panels, HSR membranes (500 $\mu g.ml^{-1}$) were incubated in transport buffer (pH 7.0, 25°C) containing 40 μM chlortetracycline and 17.5 units/ml CPK. In Panel A, vesicles were additionally incubated with either 0 (trace 1), 0.5 μM (trace 2). 0.75 μM (trace 3), 1 μM (trace 4), or 2 to 10 μM (trace 5) thapsigargin prior to addition of 10 mM CP/1 mM MgATP (curved arrow) and stimulation of Ca^{2+} transport. Sequential pulse loading with 5 μM Ca^{2+} additions is shown (small arrows; trace 1 and 2). The Ca^{2+} additions in trace 2 represent Ca^{2+} additions made to traces 3, 4 and 5. In trace 1, 1 μM thapsigargin treatment (large arrowhead) preceded the addition of 17.5 μM ionomycin (large arrow, see also trace 2 and 5). In Panel B, membranes under low (0 exogenous) Ca^{2+} loads were treated with either 1 μM (large arrowhead; trace 1) or 10 μM (large arrowhead; trace 2) thapsigargin subsequent to stimulation of initial Ca^{2+} uptake (curved arrow). Final additions of 17.5 μM ionomycin (large arrows) are shown.

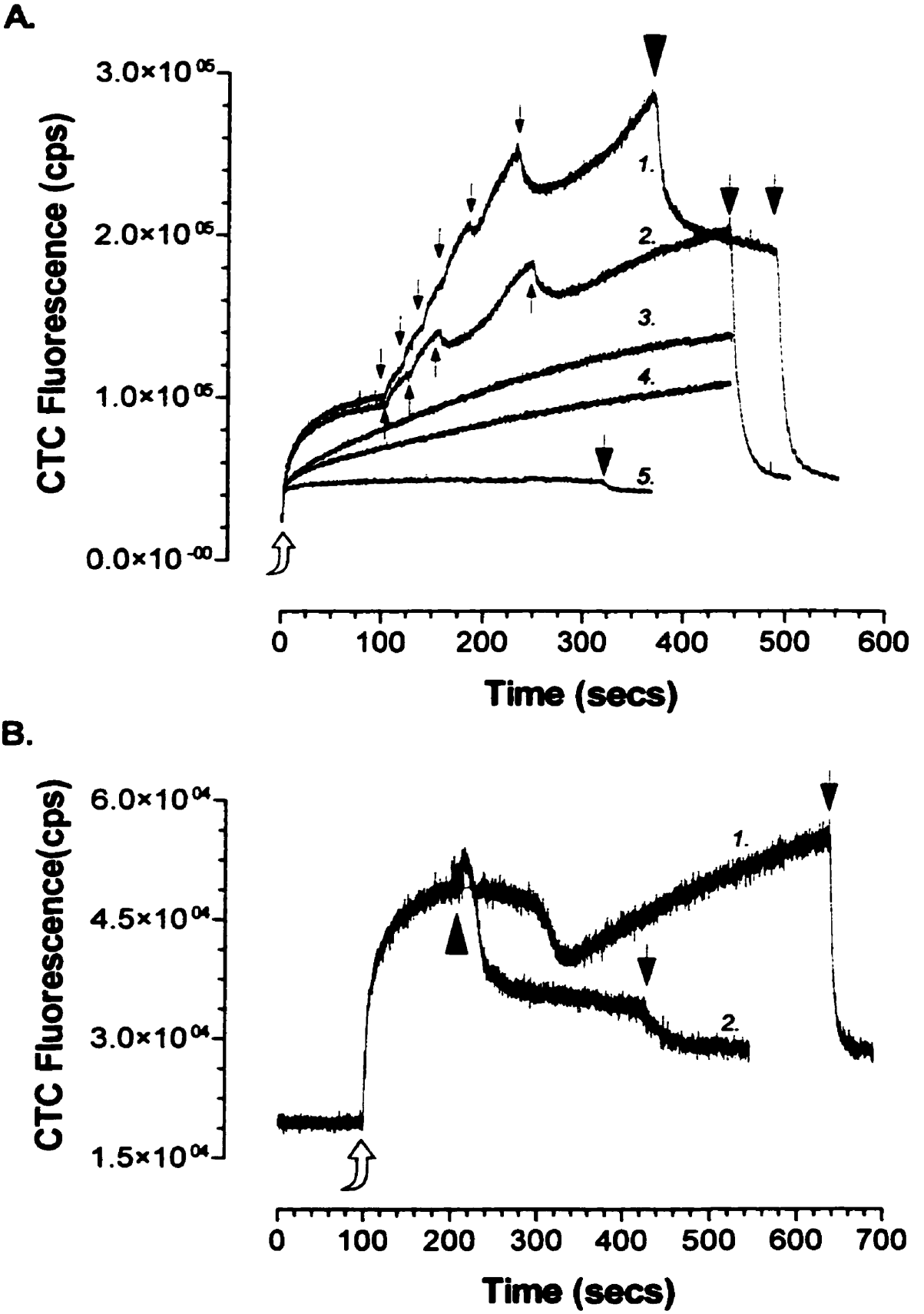
A.
3.0×10 05
2.0×10 05
1.0×10 05
0.0×10 -00
CTC Fluorescence (cps)
1.
2.
3.
4.
5.
0
100
200
300
400
500
600
Time (secs)
B.
6.0×10 04
4.5×10 04
3.0×10 04
1.5×10 04
CTC Fluorescence(cps)
1.
2.
0
100
200
300
400
500
600
700
Time (secs)

FIGURE 22. **Mag-Fura 2 luminal fluorescence was sensitive to thapsigargin treatment in HSR membranes.** Mag-Fura 2-loaded HSR membranes (500 $\mu g.ml^{-1}$) were incubated in transport buffer (pH 7.0, 25°C) containing 17.5 units/ml CPK. Membranes in Panels A and B were additionally incubated with either 0.5 μM or 1 μM thapsigargin, respectively. Following the addition of 10 mM CP/1 mM MgATP (curved arrow), the thapsigargin treated vesicles were incrementally loaded with four (Panel A) or two (Panel B) pulses of 5 μM Ca^{2+} (small arrows) and finally treated with 17.5 μM ionomycin (large arrows). In Panel C, HSR membranes were treated with 2 μM (trace 1b) or 10 μM (trace 2) thapsigargin (large arrowhead) following stimulation of Ca^{2+} uptake (curved arrow). Also shown is the cytosolic Ca^{2+} response (trace 1a) as recorded with Calcium Green-2 under identical conditions to trace 1b. Final ionomycin additions (17.5 μM) are indicated by the large arrows.

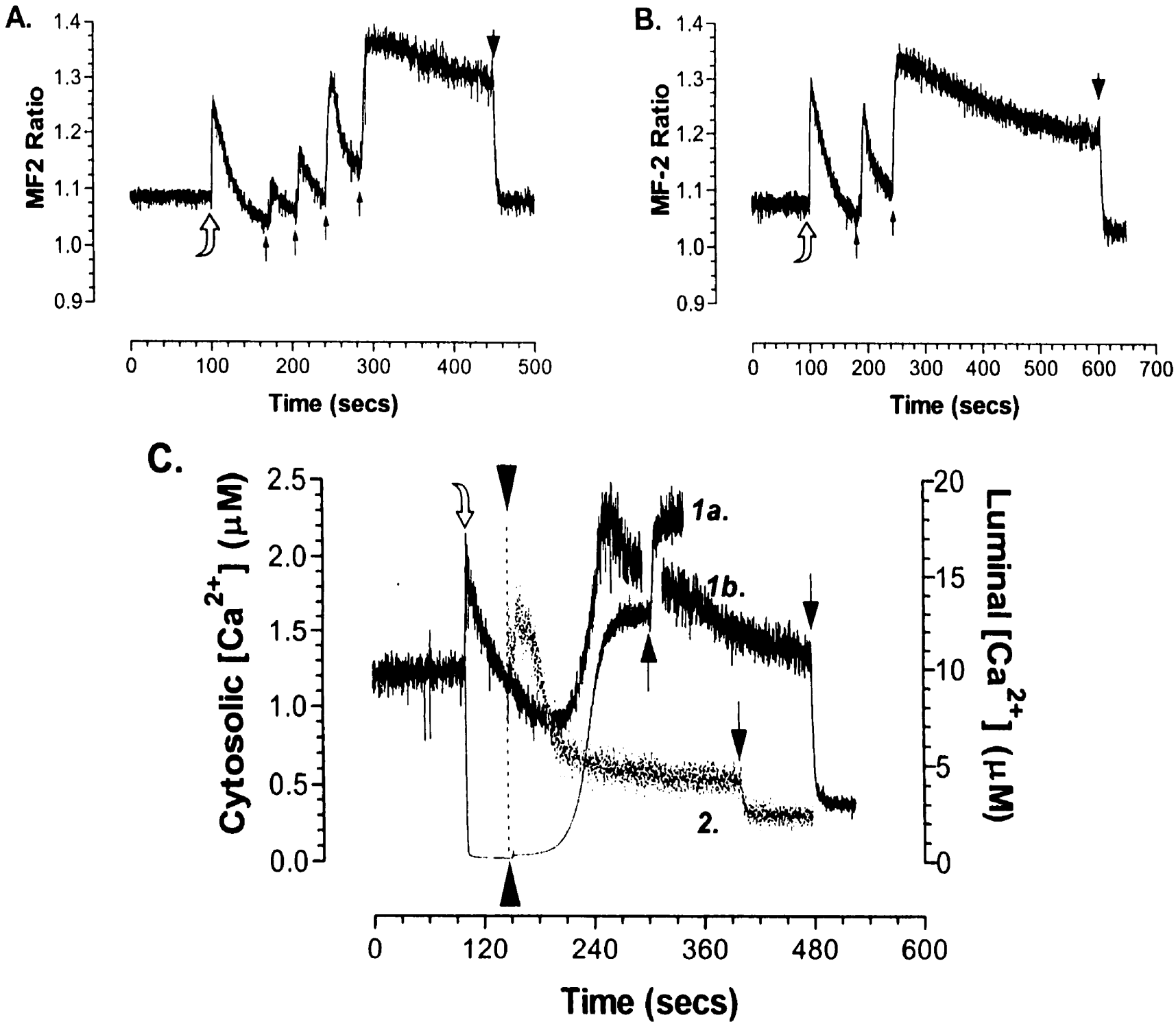
A.
MF2 Ratio
1.4
1.3
1.2
1.1
1.0
0.9
0
100
200
300
400
500
Time (secs)
B.
MF-2 Ratio
1.4
1.3
1.2
1.1
1.0
0.9
0
100
200
300
400
500
600
700
Time (secs)
C.
Cytosolic [Ca2+] (μM)
2.5
2.0
1.5
1.0
0.5
0.0
1a.
1b.
2.
Luminal [Ca2+] (μM)
20
15
10
5
0
0
120
240
360
480
600
Time (secs)

FIGURE 23. Chlortetracycline fluorescence was sensitive to ryanodine treatment in HSR membranes. HSR membranes (500 $\mu g.ml^{-1}$) were incubated in transport buffer (pH 7.0, 25°C) containing 40 μM chlortetracycline and 17.5 units/ml CPK. In Panel A, membranes were additionally incubated with either 0 (trace 1), 10 μM (trace 2), or 500 μM (trace 3) ryanodine prior to the initiation of Ca^{2+} sequestration by the addition of 10 mM CP/1 mM MgATP (curved arrow). Incremental loading of the membranes with pulses of 5 μM Ca^{2+} (small black arrows) was performed. The Ca^{2+} additions made to trace 3 also represent additions made to trace 2. In Panel B, membranes were treated with 500 μM ryanodine (black arrows) under condition of low (0 exogenous; trace 2) and high (30 μM exogenous; trace 1) MgATP-dependent Ca^{2+} loading. Final treatment with 17.5 μM ionomycin (large black arrows) is shown.

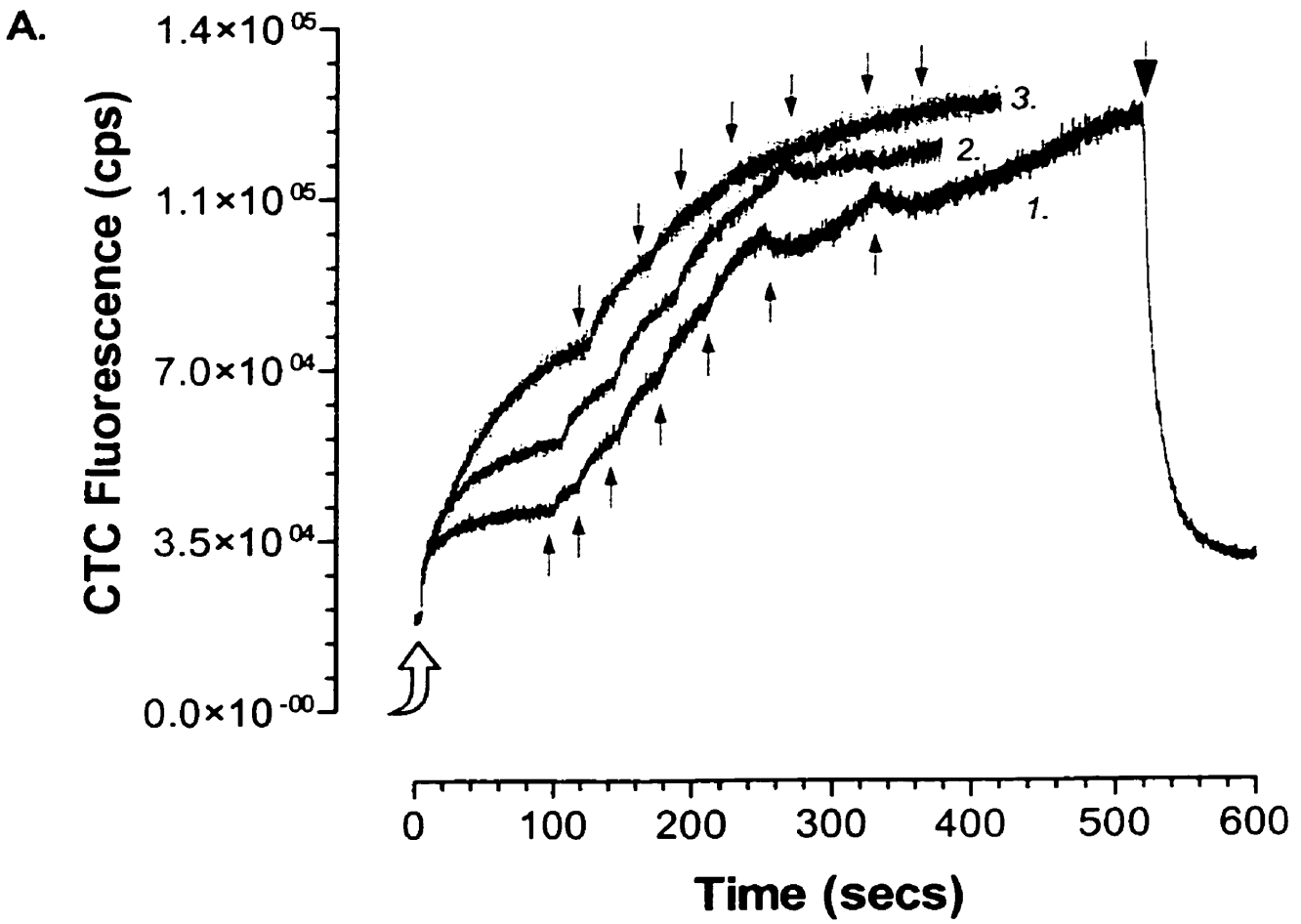
A.
1.4×10 05
1.1×10 05
7.0×10 04
3.5×10 04
0.0×10 -00
CTC Fluorescence (cps)
3.
2.
1.
0
100
200
300
400
500
600
Time (secs)

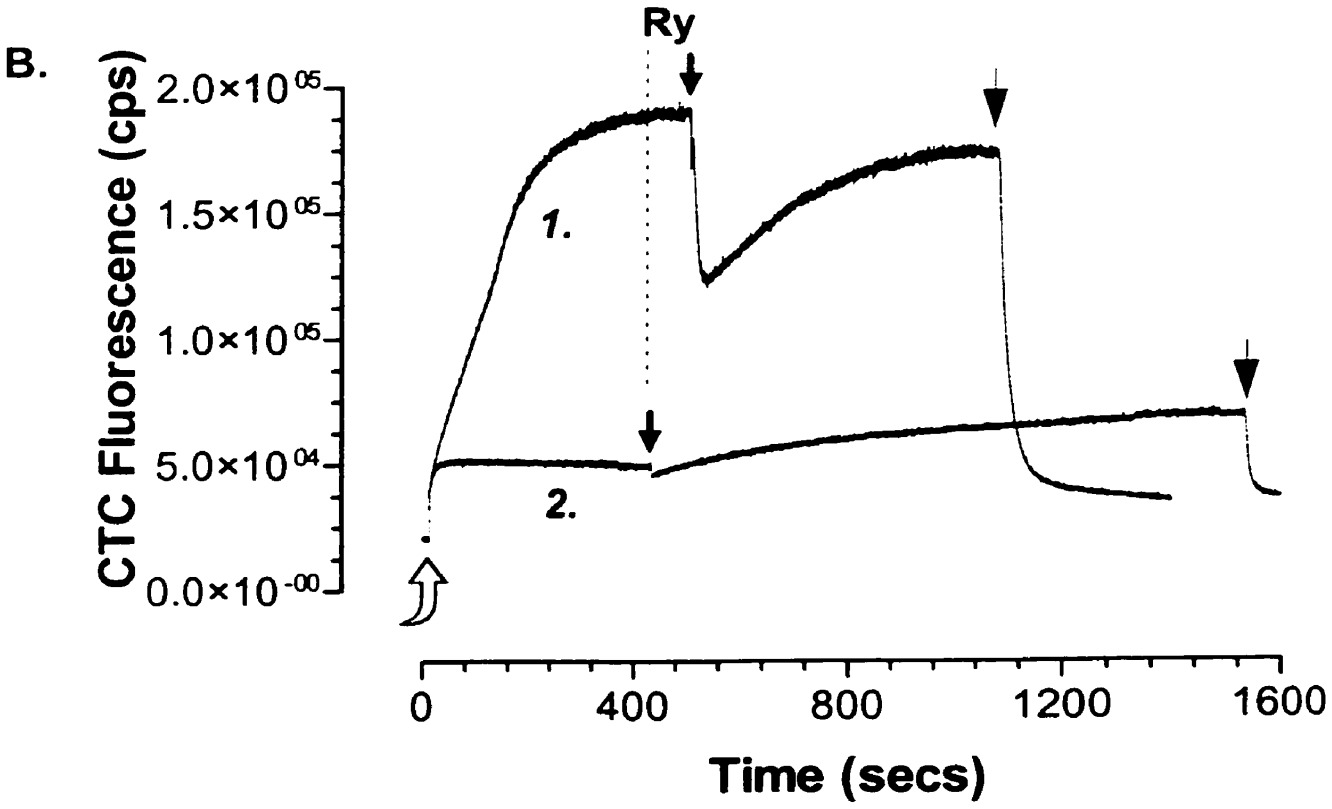
B.
2.0×10 05
1.5×10 05
1.0×10 05
5.0×10 04
0.0×10 -00
CTC Fluorescence (cps)
Ry
1.
2.
0
400
800
1200
1600
Time (secs)

FIGURE 24. Mag-Fura 2 luminal fluorescence was sensitive to ryanodine treatment in HSR membranes. Mag-Fura 2-loaded HSR membranes (500 $\mu g.ml^{-1}$) were incubated in transport buffer (pH 7.0, 25°C) containing 17.5 units/ml CPK. In Panels A and B, membranes were additionally incubated with either 10 μM or 500 μM ryanodine, respectively. Following the addition of 10 mM CP/1 mM MgATP (curved arrow) to stimulate active Ca^{2+} transport, membranes were sequentially loaded with four (Panel A) or two (Panel B) 5 μM Ca^{2+} pulses. In both cases, 17.5 μM ionomycin (large arrow) preceded 20 μM thapsigargin (large arrowhead) treatment. In Panel C, membranes were loaded with 30 μM Ca^{2+} before treatment with 500 μM ryanodine (black arrows). In trace 1, subsequent treatment with 20 μM thapsigargin (large arrowhead) preceded treatment with 17.5 μM ionomycin (black arrow). In trace 2, treatment with 17.5 μM ionomycin (black arrow) preceded treatment with 20 μM thapsigargin (black arrowhead).

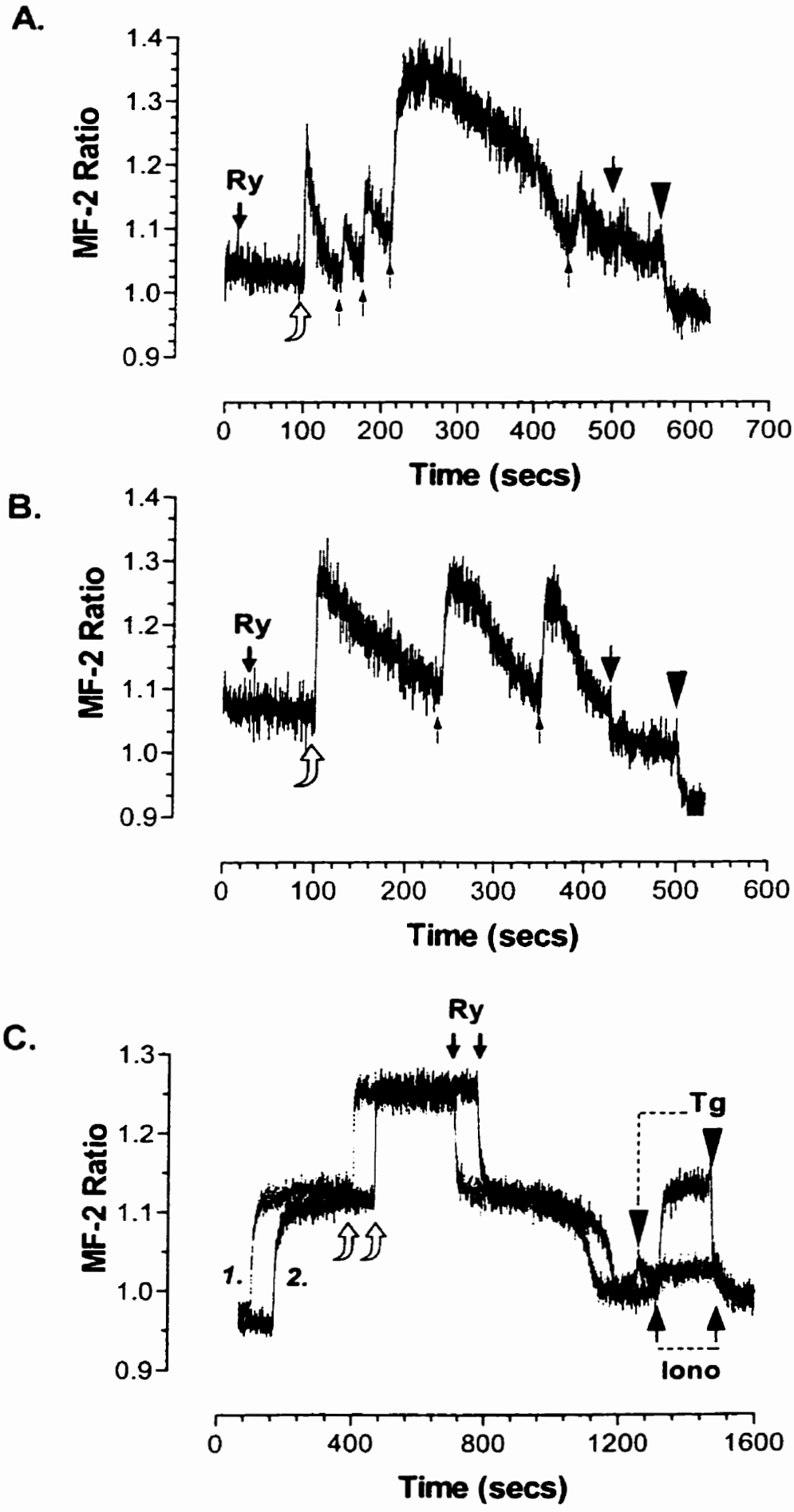
A.
MF-2 Ratio
1.4
1.3
1.2
1.1
1.0
0.9
Ry
0
100
200
300
400
500
600
700
Time (secs)
B.
MF-2 Ratio
1.4
1.3
1.2
1.1
1.0
0.9
Ry
0
100
200
300
400
500
600
Time (secs)
C.
MF-2 Ratio
1.3
1.2
1.1
1.0
0.9
Ry
Tg
1.
2.
Iono
0
400
800
1200
1600
Time (secs)

Discussion

Physiological Implications

Vesicle studies have been important for characterizing the protein components of fast-twitch skeletal muscle SR as well as for examining SR Ca^{2+} release and reuptake (40, 90, 176, 187, 270, 288). With the advent of isolation procedures for the RyR1 channel, many researchers began focusing upon characterization of the Ca^{2+} release process through single channel experiments (6, 112, 120, 126, 209). Although these data have been important for better understanding the gating mechanisms of the Ca^{2+} release channel, one of the noted problems with single channel studies is that interacting proteins, possibly important for modulating the Ca^{2+} release process (including FKBP12, calsequestrin, triadin, and calmodulin) are notably absent from isolated RyR1 preparations (111, 294). This in turn makes studies using isolated vesicles advantageous since these preparations have been shown to include many, if not all, of the proteins involved in SR Ca^{2+} uptake and Ca^{2+} release *in vivo* (see Figure 1, 91).

The current study differs from many reported vesicle studies in that Ca^{2+} release and sequestration by the isolated membranes has been monitored in real time, under quasi-physiological conditions, and not through passive Ca^{2+} loading or $^{45}Ca^{2+}$ or [^{3}H]-ryanodine binding which more or less provide end result data (79, 187, 256). To meet the objectives of the current study, assays were developed that allowed synchronous determinations of cytosolic and luminal Ca^{2+} with fluorescence indicators like Calcium Green-2, Mag-Fura 2, and chlortetracycline, accompanied by on and off cycles of the SERCA1 pump recorded with NADH oxidation in an enzyme reaction coupled to ATP hydrolysis.

The most significant finding to come out of these studies was that a luminally-mediated, Ca^{2+}-dependent, cross talk appears to balance the events of Ca^{2+} release with Ca^{2+} sequestration in isolated HSR membranes. This observation would have likely been unrecognizable were the assays not synchronous or not run in real time. However, HSR vesicles are capable of both Ca^{2+} sequestration and Ca^{2+} release, while, *in vivo*, the primary site of Ca^{2+} sequestration, the longitudinal SR , is spatially separated from the sites of Ca^{2+} release, the junctional triad. Nevertheless, corbular regions of the SR have been shown to contain both RyR1 channels and SERCA1 pumps that would presumably activate and inactivate while sensing identical cytosolic, and perhaps luminal, Ca^{2+} concentrations (133). In a similar manner to the specific events that lead to RyR1 activation and inactivation at the triadic junction, it is hard to imagine that these corbular pumps and channels, arranged in such close proximity, would operate in futile cycles in response to increased cytosolic Ca^{2+}. In this study, the well-balanced events of Ca^{2+} release and Ca^{2+} sequestration in HSR vesicles may be an experimental manifestation of how corbular pumps and channels are regulated. The corbular SR therefore provides an *in vivo* framework for the proposed luminal mediation of Ca^{2+} uptake and Ca^{2+} release in the current study.

The cycles of the SERCA1 pump

Importantly, observations with NADH and Calcium Green-2 identified that SERCA1 pumps in HSR membranes respond near-maximally under conditions where RyR1 leak states were imposed. Maximal catalytic activities of the SERCA1 pump, under conditions of active Ca^{2+} transport, observed in this study were 4200 nmol/mg/min

for Ca^{2+} activation of the RyR1, 4400 nmol/mg/min with ryanodine-induced RyR1 opening, and 11895 nmol/mg/min in the presence of ionomycin. The units for SERCA1 activity are in nmol NADH consumed per mg HSR membranes per minute where 1 nmol ATP consumed by the pump during Ca^{2+} transport would equate to 1 nmol NADH oxidized in the coupled enzymatic pathway. These values differed from values obtained under conditions where SERCA1 catalytic activity was monitored in the presence of EGTA-controlled concentrations of cytosolic Ca^{2+}. In Figure 3, maximal SERCA1 activities in the presence of EGTA and ryanodine or ionomycin were ~3000 nmol/mg/min, 2 fold higher than in the absence of either compound. Under conditions where cytosolic Ca^{2+} was kept constant by the presence of EGTA, ryanodine-induced activation of SERCA1 pumps approached catalytic activity observed in the presence of ionomycin. These differences in these results may reflect strictly cytosolic Ca^{2+} regulation of the SERCA1, as no meaningful Ca^{2+} gradient would be expected to form between the lumen and cytosol of HSR membranes with EGTA present. Furthermore, Ca.ATP complexes may be facilitated with EGTA-clamped cytosolic Ca^{2+} and these complexes have been shown to have an inhibiting effect upon SERCA1 pumps (290). However, during active Ca^{2+} transport experiments (in the absence of EGTA) , the collapse of the luminal to cytosolic Ca^{2+} gradients and the loss of luminal Ca^{2+} control upon the SERCA1 may be one explanation for the observed increases in maximal SERCA1 catalytic values and the apparent uncoupling of the SERCA1 with RyR1 Ca^{2+} leak states in the presence of ionomycin.

Increased luminal Ca^{2+} has been well documented as an inhibiting factor upon SERCA1 enzymes (54, 108, 114, 122). Only recently Saiki and Ikemoto (226) have

similarly suggested that SR Ca^{2+} release and Ca^{2+} sequestration were coordinated events. In their results, increased Ca^{2+} effluxes resulted in increased SERCA1 Ca^{2+} uptake rates that could not be described by increases in cytosolic Ca^{2+} alone. As they have suggested, one could improperly assume that SERCA1 pumps activate simply in response to elevations in cytosolic Ca^{2+}. In this report, the data in Figure 3 and Figure 6 clearly demonstrated that increased cytosolic Ca^{2+} alone was insufficient for near-maximal SERCA1 activation. It becomes evident from Figure 6, Panel B, that burst-like SERCA1 catalytic activations were well coordinated with RyR1 channel opening. The increases in cytosolic Ca^{2+} concentrations required for pump activation were distinctly 2-fold less in Panel B when compared to Panel C. The delayed onset of SERCA1 activation in Panel C, only upon attainment of maximal levels of cytosolic Ca^{2+}, indicated that RyR1 opening was similarly delayed. This would indicate that, initially, luminal Ca^{2+} was a predominant factor in back-inhibiting the SERCA1 pump. The RyR1 channel, in turn, was less sensitive to activation by cytosolic Ca^{2+} at these low luminal Ca^{2+} load conditions, yet was activated upon the realization of increased cytosolic Ca^{2+}. Therefore activation of the SERCA1 pump was delayed until such time as the luminally-mediated Ca^{2+} inhibition was removed. Although reaching similar conclusions, these results differed from those of Saiki and Ikemoto (226) in that these assays were done in real time with synchronous determinations of both cytosolic Ca^{2+} and SERCA1 activity. This afforded uninterrupted measurement of Ca^{2+} load, Ca^{2+} release and SERCA1 catalytic activation which then could be directly coordinated.

Energetically, SERCA1 ATP consumption becomes negligible in regard to HSR vesicle Ca^{2+} sequestration of presented Ca^{2+} pulses when in the absence of Ca^{2+} leak state

formations. Equally non-taxing on ATP supplies is SERCA1 maintenance of low luminal Ca^{2+} loads. Basal rates of SERCA1 catalytic activity 10-fold less (~300 to 400 nmol/mg/min) were invariably observed under conditions where RyR1 opening was unobserved. Only in the face of luminal Ca^{2+} effluxes through activated RyR1 channels (or membrane disruption by ionomycin) was ATP consumption by SERCA1 pumps unrelenting. Indeed, it appeared that some luminally-mediated Ca^{2+} inhibition of SERCA1 activity remained under RyR1 leak state formations as ionomycin resulted in catalytic rates close to 3-fold higher. The cyclical dependency of SERCA1 activation upon RyR1 opening, and SERCA1 inactivation upon RyR1 closure, suggests that the most important mechanism by which the on/off activity of SERCA1 pumps is controlled is through the maintenance or collapse of luminal, outwardly directed, Ca^{2+} gradients. The added problem with simplifying these results is that RyR1 channels, whose leak states influence SERCA1 activation, are similarly modulated by the same HSR membrane Ca^{2+} gradients.

The dual effects of outwardly-directed Ca^{2+} gradients.

Similarily to data showing that Ca^{2+} gradients modulate the Ca^{2+} release and Ca^{2+} sequestration events in HSR Ca^{2+} transport, these results have shown that the rate at which Ca^{2+} gradients were formed and maintained are equally significant in RyR1 and SERCA1 modulation. Figure 7 showed that initial Ca^{2+} pulses, during Ca^{2+} pulse loading experiments, were sequestered at a rate ~25-fold faster than Ca^{2+} pulses as threshold luminal Ca^{2+} loading for CICR was approached. This 'pumping up' of HSR vesicles was dependent upon the rate of presentation of Ca^{2+} pulses and was probably the result of

SERCA1 inhibition by luminal Ca^{2+}. With slowed Ca^{2+} pulse additions, luminal Ca^{2+} had an obvious lack of inhibition upon SERCA1. Along with the concomitant absence of Ca^{2+} release under these conditions, these results may indicate a time-dependent reorganization of luminal Ca^{2+} or perhaps Ca^{2+} precipitation by increased luminal phosphate concentrations (90). Nonetheless, this result further demonstrated a luminally-mediated Ca^{2+} modulation of both SERCA1-mediated Ca^{2+} sequestration and the advent of RyR1-mediated Ca^{2+} release in HSR membranes.

The rate dependence of Ca^{2+}-uptake upon HSR membrane Ca^{2+} release was further examined using sub-stoichiometric and stoichiometric concentrations of thapsigargin and cyclopiazonic acid. At these sub-stoichiometric concentrations, both SERCA1-specific inhibitors have been shown to decrease catalytic turnover and Ca^{2+} loading by the SERCA1 pump without formation of 'dead-end' complexes (137, 224). Stoichiometric concentrations result in dead-end inhibition of SERCA1 pumps and all Ca^{2+} sequestration becomes arrested. Initially, thapsigargin treatment (stoichiometric concentrations) were found to procure rapid and maximal Ca^{2+} release from HSR membranes under conditions of steady state low (or high) luminal Ca^{2+} loads during active Ca^{2+} transport. Using ryanodine to inactivate the Ca^{2+} release channel (demonstrated in Figure 9), thapsigargin- and cyclopiazonic acid-induced Ca^{2+} effluxes were shown to be RyR1-mediated. These early findings have been subsequently verified by the laboratory of Palade (54a). In their hands, SERCA1 specific inhibitors were shown to act like RyR1 activators, not only sensitizing the Ca^{2+} release channel to activation by caffeine, but at higher concentrations resulting in RyR1-mediated Ca^{2+} release that was effectively blocked by ruthenium red. Although the data was not shown

here, experiments done for this report further showed thapsigargin caused increased ryanodine binding to isolated HSR membranes, but not to isolated RyR1 receptors, confirming an indirect RyR1 Ca^{2+} release mechanism.

The stimulation of the release of Ca^{2+} by treatment of HSR membranes with high thapsigargin concentrations was an important demonstration that active SERCA1 pumps are necessary for maintenance of outwardly-directed Ca^{2+} gradients. In the presence of active SERCA1 pumps, luminal Ca^{2+} itself does not stimulate Ca^{2+} release (see Figure 6 and Figure 7). Yet, the rapid Ca^{2+} efflux from HSR membranes when pumps were inhibited with stoichiometric concentrations of thapsigargin or cyclopiazonic acid suggested that under these conditions luminal Ca^{2+} may indirectly promote Ca^{2+} release. Alternatively, active SERCA1 pumps may continually cycle small, specific Ca^{2+} effluxes from RyR1 receptors during steady state Ca^{2+} loads. Indeed, there are persistent basal rates of SERCA1 activity for maintenance of cytosolic Ca^{2+} concentrations of ~50 nM (see 0 conditions, Figure 11 and Figure 13). Furthermore, as Meissner originally suggested, luminal to cytosolic Ca^{2+} fluxes through the RyR1 may modulate the Ca^{2+} release channel (289). These Ca^{2+} fluxes were thought to have preferential access to Ca^{2+} inactivation sites located with-in the cytosolic portion of the channel. Thus the SERCA1 may be affiliated with actively regulating those fluxes by re-sequestering Ca^{2+} in this microenvironment, before it accumulates to higher concentrations, and thereby effectively modulating closed, steady state, RyR1 channels. A similar proposal, using HSR vesicles as a model, by Marie and Silva (170a) has suggested that a significant level of ATP consumption by SERCA1 pumps occurred in resting muscle due to Ca^{2+} cycling between small RyR1 leak states and SERCA1 pumps.

A novel finding in this study was that sub-stoichiometric concentrations of thapsigargin and cyclopiazonic acid, which were initially ineffective in collapsing the luminal to cytosolic Ca^{2+} gradient at low Ca^{2+} loads, became effective as Ca^{2+} loads reached near-threshold (see Figure 8 and Figure 12, Panel D). These results provided evidence of a direct mechanism of modulation of SERCA1 pumps by high luminal Ca^{2+} loading. Since thapsigargin is known to preferentially bind, and inhibit, the Ca^{2+} absent, low affinity state of the SERCA1 (284a), high luminal Ca^{2+} can be assumed to promote this conformation of the enzyme. This also correlates with the luminally Ca^{2+}-mediated back-inhibited form of the SERCA1 pump. However, the rapid nature of the Ca^{2+} efflux by sub-stoichiometric thapsigargin concentrations under these conditions further confirms the importance of basal catalytic rates of the SERCA1 pump for maintenance of high outwardly directed Ca^{2+} gradients and inactivated RyR1 channels.

From all indications, thapsigargin and cyclopiazonic acid treatment of HSR membranes under high luminal Ca^{2+} loads results in a two-step Ca^{2+} efflux process. Due to the complete inhibition of Ca^{2+} efflux by ryanodine inactivation of RyR1's, it can be assumed that thapsigargin treatment resulted in a slow RyR1 Ca^{2+} leak state that feeds forward to a regenerative CICR. These results support the idea that thapsigargin- and cyclopiazonic acid-induced collapse of outwardly directed Ca^{2+} gradients is initiated by the inability to reuptake Ca^{2+} fluxing through the RyR1. However, sub-stoichiometric concentrations of the SERCA1 inhibitors invariably resulted in the resequestration of released Ca^{2+}. Rate calculations from Figure 10 showed that CICR in the presence of thapsigargin resulted in Ca^{2+} reuptake rates that were 5-fold faster than Ca^{2+} reuptake following thapsigargin-induced Ca^{2+} efflux. Thapsigargin is thought to bind irreversibly

to the SERCA1 (182). If that is the case then these results indicate thapsigargin inhibition results in a reduced number of SERCA1 pumps actively resequestering the released Ca^{2+}. An alternate possibility is that thapsigargin behaves like cyclopiazonic acid, reversibly associating with the SERCA1 pump, slowing the overall rates of Ca^{2+} uptake.

Cyclopiazonic acid is thought to act as a competitive inhibitor of ATP binding to the SERCA1 pump but also, like thapsigargin, to interact with the Ca^{2+} free form of the enzyme (232). The data in figures 11 and 12 indicate that the mechanism of inhibition of SERCA1 by cyclopiazonic acid is different from that of thapsigargin. At stoichiometric concentrations both inhibitors effectively arrested Ca^{2+} sequestration. On the other hand, sub-stoichiometric concentrations of thapsigargin effectively decreased the rate at which Ca^{2+} is sequestered to the lumen of HSR vesicles while similar concentrations of cyclopiazonic acid appeared to require the attainment of steady state, low luminal Ca^{2+} loads before inhibition of the pump and collapse of the Ca^{2+} gradient. Whether the variance of thapsigargin and cyclopiazonic acid pretreatments stem from the differential actions of each compound upon different states of the SERCA1, or a differential requirement of cyclopiazonic acid for luminal Ca^{2+} loading, both inhibitors effectively increased the rate at which SERCA1 pumps were responding with treatment. Cyclopiazonic acid appeared to increase catalytic rates in a slow, nonlinear fashion, seemingly in response to the delayed collapse of the luminal Ca^{2+} gradient. Visibly absent from these traces were the burst-like transitions in SERCA1 activity seen with thapsigargin-induced delays in cytosolic Ca^{2+} removal and attainment of near-basal, steady state, luminal Ca^{2+} gradients.

When thapsigargin pretreatments were employed in the presence of added Ca^{2+} (Figure 11, Panel C and D) transitions from burst-like to near basal SERCA1 catalytic activity were not observed. It appeared that, although the exogenous Ca^{2+} had been sequestered to the lumen of the membranes (normally reducing the rate of SERCA1 activity), a persistent Ca^{2+} leak had slightly altered the resting, steady state, cytosolic Ca^{2+} levels (see 0.5 trace). This small Ca^{2+} leak resulted in sustained SERCA1 activation beyond the attainment of ~ 105 nmol/mg luminal Ca^{2+}. Thus the demonstration that luminal Ca^{2+} loading, in the presence of thapsigargin, had little effect upon near-maximal SERCA1 activation further indicated that small RyR1 leaks have large influences upon rates of pump activity.

Together these results suggest that steady state, outwardly directed, Ca^{2+} gradients are maintained both by (1) small Ca^{2+} fluxes through the inactivated RyR1 and (2) removal of these Ca^{2+} fluxes by basal rates of active SERCA1 pumps. These results have also indicated that these gradients not only sensitize the RyR1 to activation, but readily alter the conformation of the SERCA1 to a low Ca^{2+} affinity state (sensitive to thapsigargin and cyclopiazonic acid) which also appears necessary for Ca^{2+} release. Indeed, the observations where exogenous RyR1 modulators like ryanodine (see Figure 9) or ethanol resulted in apparent SERCA1 reversal at near-threshold luminal Ca^{2+} loads indicated a dual regulation by luminal Ca^{2+} upon these Ca^{2+} regulatory SR proteins.

Characterization of two distinct luminal Ca^{2+} pools.

The employment of two luminal Ca^{2+} indicators, Mag-Fura 2 (AM) and chlortetracycline, was important for defining how luminal Ca^{2+} may be regulating

SERCA1 pumps and RyR1 channels. The luminal origin of these fluorescence responses was verified by thapsigargin pretreatment and ionomycin treatment of Mag-Fura 2-loaded and CTC-incubated HSR membranes undergoing active Ca^{2+} transport. Lack of fluorescence increases with Ca^{2+} additions in the presence of stoichiometric concentrations of thapsigargin indicated that Mag-Fura 2 (Figure 15, Panel C) and chlortetracycline (Figure 21, Panel A) signals were indeed SERCA1-mediated and thus luminal. The large fluorescence decreases in the two signals upon ionomycin addition (the presence of thapsigargin was also necessary for Mag-Fura 2) was further evidence that luminal Ca^{2+} was causing the fluorescence increases observed with Mag-Fura 2 and chlortetracycline.

The luminal Ca^{2+} loading dependency of CICR in HSR membranes, initially characterized with Calcium Green-2, were consistent with both Mag-Fura 2 and chlortetracycline (compare Figure 5 with Figure 15, Panel A and Figure 17, Panel A). Loads of ~150 nmol Ca^{2+}/mg HSR were required before CICR-like events occurred with Calcium Green-2, Mag-Fura 2 or chlortetracycline. This value is consistent with other reported values (90, 226). However, the observed fluorescence responses of Mag-Fura 2 and chlortetracycline to Ca^{2+} loading were vectorally different.

Upon further examination of the Mag-Fura 2 fluorescence response, the importance of several findings became apparent. Firstly, Mag-Fura 2 responded immediately to passive Ca^{2+} loading (Figure 15, Panel A). This indicated that the luminal fluorescence signal was shallow. RyR1 channels have been shown to be in the open state during membrane preincubations (90) making the large membrane spanning pore of the RyR1 a likely Ca^{2+} influx pathway. Secondly, the rates of passive, as well as

Mg.ATP-dependent, active fluorescence increases with Mag-Fura 2 indicated that the signal was likely reporting on free luminal Ca^{2+} (Figure 18). Thirdly, the shallowness of the fluorescence signal was verified with the relative lack of responses to repeated ionomycin treatments (Figure 20). However, subsequent thapsigargin treatment potentially resulted in loss of Mag-Fura 2 fluorescence. The first and second observations suggested that the Mag-Fura 2 Ca^{2+} pool may be localized to the luminal mouth of the RyR1. However, the sensitivity of fluorescence to thapsigargin and not ionomycin along with the second observation indicated that the Mag-Fura 2 Ca^{2+} pool was equally likely to be in close association with SERCA1 pumps.

The fourth observation, calibration of the Mag-Fura 2 fluorescence signal, then indicated that the maximum capacity of this shallow and free pool of Ca^{2+} during active Ca^{2+} transport was ~50 μM free Ca^{2+}. This value is about 20 to 200- fold lower than other reported values that indicated free Ca^{2+} reached the low mM range (146). However, given the binding capacity of luminal calsequestrin, reportedly able to bind upward of 90 % of transported Ca^{2+} in HSR membranes (115), the predicted values of maximal free luminal Ca^{2+} may not be as high as previously thought.

Chlortetracycline fluorescence showed expected luminal increases with Ca^{2+} pulse loading and decreases upon attainment of threshold Ca^{2+} loading and CICR. The data collected in Figure 19 demonstrated that CTC fluorescence was greatly enhanced in the presence of both Ca^{2+} and isolated calsequestrin. This is supported by earlier observations that a fluorescence enhancement by chlortetracycline occurred upon its' interactions with biological membranes or strongly polar mediums (33). These results do not rule out a mixed chlortetracycline signal from near-membrane regions of the vesicle

lumen, however, it is hard to understand how these fluorescence responses would differ from the bulk free luminal responses reported by Mag-Fura 2. The distinctiveness of the chlortetracycline signal does indeed mirror the expected Ca^{2+} binding and Ca^{2+} release characteristics expected to occur with calsequestrin during active Ca^{2+} transport and Ca^{2+} release. Furthermore, calsequestrin reportedly interacts directly with the RyR1 or in an interaction mediated through junctin and triadin (294). Other reports have indicated that Ca^{2+} binding may regulate RyR1 activation and Ca^{2+} release, or that RyR1 activation may regulate Ca^{2+} binding to calsequestrin (90, 114). Therefore, chlortetracycline responses may in fact be direct luminal observations of calsequestrin-RyR1 mediated Ca^{2+} release.

The transitory nature of the Mag-Fura 2 signal during Ca^{2+} pulse loading may indicate the rapid entry and removal of Ca^{2+} into and from the free luminal Ca^{2+} pool (Figure 15, Panel A). It follows that Ca^{2+} would be sequestered by calsequestrin into the chlortetracycline, bound luminal Ca^{2+} pool (Figure 17, Panel A). Basal rates of SERCA1 activity are accompanied by minor fluorescence oscillations in Mag-Fura 2 and large fluorescence steppes in chlortetracycline signals. Upon activation of both RyR1 channels and SERCA1 catalysis, large increases in Mag-Fura 2 fluorescence accompany large decreases in chlortetracycline fluorescence. Therefore collapse of the Ca^{2+} gradient at CICR is attended by increased Ca^{2+} into the free Ca^{2+} pool. The modulation of both the RyR1 and SERCA1 by the attainment of high outwardly-directed Ca^{2+} gradients would then appear governed strictly by Ca^{2+} binding states of calsequestrin.

Thapsigargin and ryanodine provide further insight into the regulatory nature of luminal Ca^{2+} pools.

Calcium Green-2 and NADH traces had revealed that thapsigargin treatments (sub-stoichiometric concentrations) resulted in collapse of outwardly directed Ca^{2+} gradients by indirect activation of the RyR1. As discussed, these were accompanied by activations of SERCA1. Thapsigargin treatment, under these conditions, effectively reduced the luminal Ca^{2+} load required for CICR as recorded with Calcium Green-2 (Figure 10), chlortetracycline (Figure 21), and Mag-Fura 2 (Figure 22). Increased magnitude of Ca^{2+} transients in the free pool were accompanied by slowed and decreased fluorescence increases for the observed chlortetracycline nadirs. Thus it appears that activation of SERCA1 pumps in response to RyR1 leak states facilitated the entry of Ca^{2+} into the free, Mag-Fura 2, Ca^{2+} pool. The greatly reduced Mag-Fura 2 fluorescence decreases following Ca^{2+} additions (especially at CICR), indicated that the exchange from the free to bound luminal Ca^{2+} pools was in some way hampered by the slowing of Ca^{2+} removal from the cytosol and therefore the collapse of Ca^{2+} gradient formation.

In terms of the sequence of events leading to CICR, it remained unclear as to whether it was: the decreased removal of cytosolic Ca^{2+} which resulted in RyR1 activation; or the altered binding affinity of calsequestrin which resulted in increased free luminal Ca^{2+} and activation of the RyR1; or the facilitated movement of released Ca^{2+} back into the free pool, which altered the normal HSR membrane luminal organization of Ca^{2+}. Thapsigargin treatments that resulted in the biphasic, delayed release of Ca^{2+} from HSR membranes (Figures 8 and 10) caused complimentary delays in the decreases in chlortetracycline fluorescence and increases in Mag-Fura 2 fluorescence. Even these results could not clarify an exact mechanism for luminal Ca^{2+} reshuffling. These results did affirm that RyR1 channel opening and the accompanying SERCA1 activation lead to

loss of Ca^{2+} from the bound luminal compartment and entry into the free luminal compartment.

Further clarification came with ryanodine treatment of HSR membranes. Pretreatments that would facilitate the activation and subsequent inactivation of RyR1 channels resulted in increased luminal Mag-Fura 2 and chlortetracycline fluorescence signals. Under these conditions, Ca^{2+} was immediately moved to the bound Ca^{2+} pool, with a distinct absence of Ca^{2+} release. Ca^{2+} movement from the free to bound Ca^{2+} compartment was more rapid with each successive Ca^{2+} pulse (Figure 24, Panel B). Therefore, under ryanodine-induced inhibition of RyR1 channels, calsequestrin continually serves as a Ca^{2+} sink for the cytosolically added Ca^{2+} pulses which were initially but rapidly accumulated into the free Ca^{2+} pool.

Ryanodine-induced Ca^{2+} release was accompanied by apparent SERCA1 reversal prior to activation (Figure 9). Under high luminal Ca^{2+} loads, ryanodine treatment resulted in loss of Ca^{2+} from both the free and bound luminal Ca^{2+} pools. These rapid reductions in Mag-Fura 2 were only observed with ryanodine-induced Ca^{2+} effluxes. Indeed, losses of Ca^{2+} from the free luminal Ca^{2+} pool appeared otherwise dependent upon inactivated RyR1 channels and the increased binding affinity of calsequestrin. Therefore the rapid loss of Ca^{2+} from the SERCA1 mediated free pool may represent the efflux of Ca^{2+} through the SERCA1 pump. The conditions of high luminal Ca^{2+} load and stimulation of Ca^{2+} release by modulators of the RyR1 other than Ca^{2+} itself supported this possibility. One explanation for this phenomenon may be that ryanodine-induced Ca^{2+} releases initially uncouple the otherwise coordinated events of Ca^{2+} release and sequestration. The subsequent leveling of Mag-Fura 2 fluorescence followed by

complete fluorescence loss may indicate a readjusted SERCA1-RyR1-calsequestrin coordination.

Concluding Remarks

The evidence in this study for a luminally-mediated cross talk between SERCA1 pumps and RyR1 channels has been presented. Clearly the events modulating Ca^{2+} sequestration and CICR are complex and multifactorial. However, the assay systems developed in this report provide new insights into the possible luminal Ca^{2+} compartmentalization and the communication between free and bound Ca^{2+}. The free Ca^{2+} pool appears not to modulate SERCA1 activity but increases in response to it. The other factor that appeared to control this free Ca^{2+} pool was binding affinity states of calsequestrin. Decreasing the rate of Ca^{2+} gradient formation demonstrated that the filling of the calsequestrin-bound luminal pool was not a prerequisite to CICR. But inhibited RyR1 channels were shown to facilitate the movement of Ca^{2+} into this compartment. Therefore it appears that states of the RyR1 indeed govern the binding of Ca^{2+} to calsequestrin. Under conditions of normally regulated gradient formation, the filling of the bound Ca^{2+} pool was necessary for CICR. Therefore it appears that calsequestrin does indeed influence the sensitivity of the RyR1 to activation.

Ca^{2+} gradient formation, in turn, is dependent upon active SERCA1 pumps which rapidly remove added Ca^{2+} pulses and possibly Ca^{2+} fluxes from the RyR1. Maintenance of these Ca^{2+} gradients appears then to determine inactivated RyR1 channels and binding of Ca^{2+} to calsequestrin. The nature of luminal back-inhibition of the SERCA1 pump could not be fully resolved from this study. If anything, it appeared that the bound

luminal Ca^{2+} pool would be the exerting influence upon both the RyR1 and the SERCA1. Whether this influence is governed by calsequestrin reaching binding capacity, such that removal of accumulated Ca^{2+} from free to bound luminal compartments is decreased, or some direct (or accessory protein mediated) interaction remains to be determined.

Chlortetracycline as a luminal Ca^{2+} probe is limited to the formation of Ca^{2+} gradients across membranes in order for itself to pass to the HSR luminal environment. Therefore, one limitation of chlortetracycline would be unresolved luminal Ca^{2+} changes during the initial Ca^{2+} sequestration phase of Ca^{2+} transport by HSR membranes. Furthermore, the suggested origins of the luminal Ca^{2+} probes does not negate mixed luminal fluorescence signals from compartmentalization of both Mag-Fura 2 and chlortetracycline. Indeed, the exact origin of the MF2 and CTC signals could not be fully resolved in this study. The possibility that chlortetracycline and Mag-Fura 2 are reporting upon microenvironments within the HSR vesicle lumen is therefore a distinct possibility. The adoption of different AM ester dyes, with a variety of Kd's, into Ca^{2+} transport assay protocols may be an effective means of determining whether other luminal signals are possible or to verify the current report. This, in turn, may identify even further sub-compartments within the SR lumen which could play a role in the proposed cross-talk communication between RyR1 channels and SERCA1 pumps in HSR membranes.

References

1. Aaron, B-M.B., Oikawa, K., Reithmeier, R.A.F., and Sykes, B.D. (1984) J. Biol. Chem. 259:11876-11881.
2. Adachi-Akahane, S., Cleeman, L., and Morad, M. (1996) J. Gen. Physiol. 108:435-454.
3. Adachi-Akahane, S., Lu, L., Li, Z., Frank, J.S., and Philipson, K.D. (1997) J. Gen. Physiol. 109:717-729.
4. Adams, B.A., Tanabe, T., Mikami, A., Numa, S., and Beam, K.G. (1990) Nature (Lond.) 346:569-572.
5. Alonso, G.L., Gonzalez, D.A., Takara, D., Ostuni, M.A., and Sanchez, G.A. (1998) Biochim. Biophys. Acta 1405:47-54.
6. Anderson, K., Lai, F.A., Liu, Q.Y., Rousseau, E., Erikson, H.P. and Meissner, G. (1989) J. Biol. Chem. 264:1329-1335.
7. Anderson, K. and Meissner, G. (1995) J. Gen. Physiol. 105:363-383.
8. Andersson-Cedergren, E. (1959) J. Ultrastruct. Research 1.
9. Ashley, C.C., and Ridgeway, E.B. (1970) J. Physiol. 209:105-130.
10. Beam, K.G., Tanabe, T., and Numa, S. (1989) Ann. N.Y. Acad. Sci. 560:127-137.
11. Bennet, H.S., and Porter, K.R. (1953) Am. J. Anat. 93:61.
12. Berman, M.C. (1999) Biochim. Biophys. Acta 1418:48-60.
13. Beuckelmann, D.J., and Wier, W.G. (1988) J. Physiol. (Lond.) 405:233-255.

14. Bigelow, D.J., Squier, T.C., and Inesi, G. (1992) J. Biol. Chem. 267:6952-6962.

15. Bishop, J.E., and Al-Shaw, M.K. (1988) J. Biol. Chem. 263:1886-1892.

16. Block, B.A., Imagawa, T., Cambell, K.P., and Franzini-Armstrong, C. (1988) J. Cell Biol. 107:2587-2600.

17. Brandl, C.J., Green, N.M., Korczak, B., and MacLennan, D.H. (1986) Cell 44:597-607.

18. Brandt, N.R., Caswell, A.H., Wen, S.R., and Talvenheimo, J.A. (1990) J. Membr. Biol. 113:237-251.

19. Brilliantes, A.M.B., Ondrias, K., Scott, A., Kobrinsky, E., Ondriasova, E., Moschella, M.C., Jayarman, T., Landers, M., Erlich, B.E., and Marks, A.R. (1994) Cell 77:513-523.

20. Buck, E.D., Nguyen, H.T., Pessah, I.N., and Allen, P.D. (1997) J. Biol. Chem. 272:7360-7367.

21. Buck, E., Zimanyi, I., Abramson, J.J., and Pessah, I.N. (1992) J. Biol. Chem. 267:23560-23567.

22. Bull, R., Marengo, J., Suarez-Isla, B., Donoso, P., Sutko, J., and Hidalgo, C. (1989) Biophys. J. 56:749-756.

23. Burmeister Getz, E.E., and Lehman, S.L. (1997) Am. J. Physiol. 272:C1087-C1098.

24. Cala, S.E., and Jones, L.R. (1983) J. Biol. Chem. 258:11932-11936.

25. Cala, S.E., and Jones, L.R. (1991) J. Biol. Chem. 266:391-398.

26. Callaway, C., Seryshev, A., Wang, J.P., Slevik, K.J., Needleman, D.H.,

Canter, C., Wu, Y., Jayarman, T., Marks, A.R., and Hamilton, S.L. (1994) J. Biol. Chem. 269:15876-15884.

27. Callewaert, G. (1992) Cardiovasc. Res. 26:923-932.

28. Cambell, K.P., Franzini-Armstrong, C., and Shamoo, A.E. (1980) Biochim. Biophys. Acta 602:97-116.

29. Cannell, M.B., Berlin, J.R., and Lederer, W.J. (1987) Science 238:1419-1423.

30. Carl, S.L., Felix, K., Caswell, A.H., Brandt, N.R., Ball Jr., W.J., Vaghy, P.L., Meissner, G., and Ferguson, D.G. (1995) J. Cell Biol. 129:672-682.

31. Carl, S.L., Felix, K., Caswell, A.H., Brandt, N.R., Brunschwig, J.P., Meissner, G., and Ferguson, D.G. (1995) Muscle Nerve 18:1232-1243.

32. Caswell, A.H., Brandt, N.R., Brunschwig, J.P., and Purkerson, S. (1991) Biochemistry 30:7507-7513.

33. Caswell, A.H., and Hutchinson, B. (1971) Biochem. Biophys. Res. Commun. 42:43-49.

34. Caswell, A.H., and Warren, S. (1972) Biochem. Biophys. Res. Commun. 46:1757-1763.

35. Chen, L., Sumbilla, C., Lewis, D., Zhong, L., Struck, C., Kirtley, M.E., and Inesi, G. (1996) J. Biol. Chem. 271:10745-10752.

36. Chen, S.R.W., Zhang, L., and MacLennan, D.H. (1992) J. Biol. Chem. 267:23318-23326.

37. Chen, S.R.W., Zhang, L., and MacLennan, D.H. (1994) Proc. Natl. Acad. Sci. USA 91:11953-11957.

38. Cheng, H., Fill, M., Valdivia, H., and Lederer, W.J. (1995) Science 267:2009-2010.

39. Chu, A., Diaz-Munoz, M., Hawkes, M.J., Brush, K., and Hamilton, S.L. (1990) Mol. Pharmacol. 37:735-741.

40. Chu, A., Dixon, M.C., Saito, A., Seiler, S., and Fleischer, S. (1988) Methods Enzym. 157:36-46.

41. Chu, A., Sumbilla, C., Inesi, G., Jay, S.D., and Cambell, K.P. (1990) Biochemistry 29:5899-5905.

42. Clarke, D.M., Loo, T.W., Inesi, G., and MacLennan, D.H. (!989) Nature 339:476-478.

43. Collins, J.H. (1991) Biochem. Biophys. Res. Commun. 178:1288-1290.

44. Coronado, R., Kawano, S., Lee, C.J., Valdivia, C., and Valdivia, H.H. (1992) Methods Enzymol. 207:699-707.

45. Coronado, R., Morrissette, J., Sukareva, M., and Vaughan, D.M. (1994) Am. J. Physiol. 266:C1485-C1504.

46. Costantin, L., Franzini-Armstrong, C., and Podolsky, R.J. (1965) Science 147:158-159.

47. Costello, B., Chadwick, C., Saito, A., Chu, A., Maurer, A., and Fleischer, S. (1986) J. Cell. Biol. 103:741-753.

48. Csernoch, L., Jacquemond, V., and Schneider, M.F. (1993) J. Gen. Physiol. 101:297-333.

49. Damiani, E., and Margreth, A. (1990) Biochem. Biophys. Res. Commun. 172:1253-1259.

50. Damiani, E., and Margreth, A. (1991) Biochem. J. 277:825-832.

51. Damiani, E., Picello, E., Saggin, L., and Margreth, A. (1995) Biochem. Biophys. Res. Commun. 209:457-465.

51a. Damiani, E., Tobaldin, G., Bortoloso, E., and Margreth, A. (1997) Cell Calcium 22:129-150.

52. Davidson, G.A., and Varhol, R.J. (1995) J. Biol. Chem. 270:11731-11734.

53. de Meis, L., and Carvalho, M.G.C. (1974) Biochemistry 13:5032-5038.

54. de Meis, L., and Sorenson, M.M. (1989) Biochim. Biophys. Acta 984:373-378.

54a. Dettbarn, C. and Palade, P. (1998) J. Pharm. Exp. Ther. 285:739-745.

55. Diaz-Munoz, M., Hamilton, S.L., Kaetzel, M.A., Hazarika, P., and Dedman, J.R. (1990) J. Biol. Chem. 265:15894-15899.

56. Donoso, P., Prieto, H., and Hidalgo, C. (1995) Biophys. J. 68:507-515.

57. Ebashi, S. (1961) Progr. Theoret. Phys.17:35-40.

58. Ebashi, S., and Lipmann, F. (1962) J. Cell Biol. 14:389-400.

59. Ebashi, S. (1980) Proc. R. Soc. Lond. B. 207:259-286.

60. Eckert, R. in Animal Physiology (third addition) W.H. Freeman and Company. 1988.

61. Endo, M. (1975) Proc. Jap. Acad. 51:467-472.

62. Endo, M. (1977) Physiol. Rev. 57:71-108.

63. Endo, M., Tanaka, M., and Ogawa, Y. (1970) Nature 228:34-36.

64. Escobar, A.L., Monck, J.R., Fernandez, J.M., and Vergara, J.L. (1994) Nature (Lond.) 367:739-741.

65. Fabiato, A. (1983) Am. J. Physiol. 245:C1-C14.

66. Fabiato, A. (1985) J. Gen. Physiol. 85:189-246.

67. Fabiato, A. (1985) J. Gen. Physiol. 85:247-289.

68. Fabiato, A. (1985) J. Gen. Physiol. 85:291-320.

69. Fabiato, A., and Fabiato, F. (1979) Nature 281:146-148.

70. Fairhurst, A.S., and Hasselbach, W. (1970) Eur. J. Biochem. 13:504-509.

71. Fan, H., Brandt, N.R., and Caswell, A.H. (1995) Biochemistry 34:14902-14908.

72. Fan, H., Brandt, N.R., Peng, M., Schwartz, A., and Caswell, A.H. (1995) Biochemistry 34:14893-14901.

73. Fan, J-S., and Palade, P. (1999) J. Physiol. 516:769-780.

74. Fano, G., Marsili, V., Angela, P., Aisa, M.C., Giambianco, I., and Donato, R. (1990) FEBS Lett. 255:381-384.

75. Fawcett, D.W., and Revel, J.P. (1961) J. Biophys. Biocem. Cytol. 10:89-109.

76. Feher, J.J., and Lipford, G.B. (1985) Eur. J. Biochem. 13:504-509.

77. Fernandez-Belda, F., Kurzmack, M., and Inesi, G. (1984) J. Biol. Chem. 259:9687-9698.

78. Fill, M., Coronado, R., Mickelson, J.R., Vilven, J., Ma, J., Jacobson, B.A., and Louis, C.F. (1990) Biophys. J. 57:471-475.

79. Fleischer, S., Ogunbunmi, E.M., Dixon, M.C., and Fleer, E.A.M. (1985) Proc. Natl. Acad. Sci. USA 82:7256-7259.

80. Fliegel, L., Onishi, M., Carpenter, M.R., Khanna, V.K., Reithmeier,

R.A.F., and MacLennan, D.H. (1987) Proc. Natl. Acad. Sci. USA 84:1167-1171.

81. Flucher, B.E., Andrews, S.B., Fleischer, S., Marks, A.R., Caswell, A., and Powell, J.A. (1993) J. Cell Biol. 123:1161-1174.

82. Ford, L.E. and Podolsky, R.J. (1970) Science 167:58-59.

83. Forge, V., Mintz, E., and Guillain, F. (1993) J. Biol. Chem. 268:10953-10960.

84. Frank, G.B. (1964) Proc. Roy. Soc. Ser. B 160:504-512.

85. Franzini-Armstrong, C. (1970) J.Cell Biol. 47:488-499.

86. Franzini-Armstrong, C. (1972) Tissue Cell 4:469-478.

87. Franzini-Armstrong, C., Kenney, L.J., and Varriano-Marston, E. (1987) J. Cell. Biol. 105:49-56.

88. Franzini-Armstrong, C., Pincon-Raymond, M., and Rieger, F. (1991) Dev. Biol. 146:364-376.

89. Froemming, G.R., Murray, B.E., and Ohlendieck, K. (1999) Biochim. Biophys. Acta 1418:197-205.

90. Gilchrist, J.S.C., Belcastro, A.N., and Katz, S. (1992) J. Biol. Chem. 267:20850-20856.

91. Gilchrist, J.S.C., Palahniuk, C., and Bose, R. (1997) Molec. Cell. Biochem. 172:159-170.

91a. Gilchrist, J.S.C., and Pierce, G.N. (1993) J. Biol. Chem. ??:4291-4299.

92. Goeger, D.E., Riley, R.T., Dorner, J.W., and Cole, R.J. (1988) Biochem. Pharmacol. 37:978-981.

93. Grunwald, R., and Meissner, G. (1995) J. Biol. Chem. 270:11338-11347.

94. Guo, W., and Cambell, K.P. (1995) J. Biol. Chem. 270:9027-9030.

95. Gyorke, I., and Gyorke, S. (1998) Biophys. J. 75:2801-2810.

96. Gyorke, S. and Fill, M. (1993) Science 260:807-809.

97. Gyorke, S. and Fill, M. (1994) Science 263:987-988.

98. Gyorke, S., Velez, P., Suare-Isla, B., and Fill, M. (1994) Biophys. J. 66:1879-1886.

98a. Hain, J., Nath, S., Mayrleitner, M., Fleicher, S., and Schindler, H. (1994) Biophys. J. 67:1823-1833.

99. Hakamata, Y., Nakai, J., Takeshima, H., and Imoto, K. (1992) FEBS Lett. 312:229-235.

100. Han, J.W., Thieleczek, R., Varsanyi, M., and Heilmeyer, L.M.G. (1992) Biochemistry 31:337-384.

101. Han, S., Schiefer, A., and Isenberg, G. (1994) J. Physiol. (Lond.) 480:411-421.

101a. Harrington, C.R. (1990) Anal. Biochem. 2:285-287.

102. Hasselbach, W. (1964) Fed. Proc. 23:900-912.

103. Hasselbach, W. (1979) Top. Curr. Chem. 78:1-56.

104. Hasselbach, W., and Migala, A. (1987) FEBS Lett. 221:119-123.

105. Heegaard, C.W., Le Maire, M., Gulik-Krywicki, T., and Moller, J.V. (1990) J. Biol. Chem. 265:12020-12028.

106. Heilbrunn, L.V., and Wiercinski, F.J. (1947) J. Cell. and Comp. Physiol. 29:15-32.

107. Herrmann-Frank, A., and Varsanyi, M. (1993) FEBS Lett. 332:237-242.

108. Hesketh, T.R., Smith, G.A., Houslay, M.D., McGill, K.A., Birdsall, N.J.M., Metcalfe, J.C., and Warren, G.B. (1976) Biochemistry 15:4145-4151.

109. Hollingworth, S., Harkins, A.B., Kurebayashi, N., Konishi, M., and Baylor, S.M. (1992) Biophys. J. 63:224-234.

110. Holmberg, S.R.M., and Williams, A.J. (1990) Biochim. Biophys. Acta 1022:187-193.

111. Hymel, L., Inui, M., Fleischer, S., and Schindler, H. (1988) Proc. Natl. Acad. Sci. USA 85:441-445.

112. Hymel, L., Schindler, H., Inui, M., and Fleischer, S. (1988) Biochem. Biophys. Res. Commun. 152:308-314.

113. Ikemoto, N. (1974) J. Biol. Chem. 249:649-651.

114. Ikemoto, N. (1982) Annu. Rev. Physiol. 44:297-317.

115. Ikemoto, N., Antoniu, B., Kang, J.J., Meszaros, L.G., and Ronjat, M. (1991) Biochemistry 30:5230-5237.

116. Ikemoto, N., Antoniu, B., and Meszaros, L.G. (1985) J. Biol. Chem. 260:14096-14100.

117. Ikemoto, N., Nagy, B., Bhatnagar, G.M., and Gergely, J. (1974) J. Biol. Chem. 249:2357-2365.

118. Ikemoto, N., Ronjat, M., Meszaros, L.G., and Koshita, M. (1989) Biochemistry 28:6764-6771.

119. Ikemoto, T., Iino, M., and Endo, M. (1995) J. Physiol. (Lond.) 487:573-582.

120. Imagawa, T., Smith, J.S., Coronado, R., and Cambell, K.P. (1987) J. Biol.

Chem. 262:16636-16643.

121. Imredy, J.P. and Yue, D.T. (1994) Neuron 12:1301-1318.

122. Inesi, G., and De Meis, L. (1989) J. Biol. Chem. 264:5929-5936.

123. Inesi, G., Lewis, D., and Murphy, A.J. (1984) J. Biol. Chem. 259:996-1003.

124. Inesi, G., and Sagara, Y. (1994) J. Membr. Biol. 141:1-6.

125. Inesi, G., Sumbilla, C., and Kirtley, M.E. (1990) Physiol. Rev. 70:749-760.

126. Inui, M., Saito, A., and Fleischer, S. (1987) J. Biol. Chem. 262:1740-1747.

127. Isenberg, G. and Han, S. (1994) J. Physiol. 480:423-438.

128. Jacquemond, V., Csernoch, L., Klein, M.G., and Schneider, M.F. (1991) Biophys. J. 60:867-873.

129. Jayaraman, T., Brillantes, A.M., Timerman, A.P., Fleischer, S., Erdjument-Bromage, H., Tempst, P., and Marks, A.R. (1992) J. Biol. Chem. 267:9474-9477.

130. Jencks, W.P. (1992) Ann. N.Y. Acad. Sci. 671:49-56.

131. Jones, L.R., Besch, H.R., Sutko, J.L., and Willerson, J.T. (1979) J. Pharmacol. Exp. Ther. 209:48-55.

132. Jones, L.R., Zhang, L., Sanborn, K., Jorgenson, A.O., and Kelley, J. (1995) J. Biol. Chem. 270:30787-30796.

133. Jorgenson, A.O., Arnold, W., Pepper, D.R., Kahl, S.D., Mandel, F., and Cambell, K.P. (1988) Cell. Motil. Cytoskeleton 9:164-174.

134. Jorgenson, A.O., Shen, A.C-Y., Arnold, W., McPherson, P.S., and Cambell, K.P. (1993) J. Cell. Biol. 120:969-980.

135. Jorgenson, A.O., Shen, A.C-Y., Cambell, K.P., and MacLennan, D.H. (1983) J. Cell. Biol. 97:1573-1581.

136. Kawasaki, T., and Kasai, M. (1994) Biochem. Biophys. Res. Commun. 199:1120-1127.

137. Kijima, Y., Ogunbunmi, E., and Fleischer, S. (1991) J. Biol. Chem. 266:22912-22918.

138. Kim, D.H., and Ikemoto, N. (1986) J. Biol. Chem. 261:11674-11679.

139. Kim, D.H., Ohnishi, S.T., and Ikemoto, N. (1983) J. Biol. Chem. 258:9662-9668.

140. Kim, K.C., Caswell, A.H., Talvenheimo, J.A., and Brandt, N.R. (1990) Biochemistry 29:9281-9289.

141. Kimura, Y., Kurzydlowski, K., Tada, M., and MacLennan, D.H. (1996) J. Biol. Chem. 271:21726-21731.

142. Kirino, Y., Osakabe, M., and Shimizu, H. (1983) J. Biochem. 94:1111-1118.

143. Klein, M.G., Simon, B.J., and Schneider, M.F. (1990) J. Physiol. 425:599-626.

144. Knudsen, C.M., Stang, K.K., Moomav, C.R., Slaughter, C.A., and Cambell, K.P. (1993) J. Biol. Chem. 268: 12646-12654.

145. Krause, K-H., Milos, M., Luan-Rilliet, Y., Lew, D.P., and Cox, J.A. (1991) J. Biol. Chem. 266:9453-9459.

146. Kurebayashi, N. and Ogawa, Y. (1998) Biophys. J. 74:1795-1807.

147. Lai, F.A., Erikson, H.P., Rousseau, E., Liu, Q.Y., and Meissner, G. (1988)

Nature (Lond.) 331:315-319.

148. Lai, F.A., and Meissner, G. (1989) J. Bioenerg. Biomembr. 21:227-246.

149. Lam, E., Martin, M.M., Timerman, A.P., Sabers, C., Fleischer, S., Lukas, T., Abraham, R.T., O'Keefe, S.J., O'Neil, E.A., and Wienderrecht, G.J. (1995) J. Biol. Chem. 270:26511-26522.

150. Lattanzio, F.A., Schlatterer, R.G., Nicar, M., Cambell, K.P., and Sutko, J.L. (1987) J. Biol. Chem. 262:2711-2718.

151. Leong, P. and MacLennan, D.H. (1998) J. Biol. Chem. 273:7791-7794.

152. London, B. and Krueger, J.W. (1986) J. Gen. Physiol. 88:475-505.

153. Lu, X, Xu, L., and Meissner, G. (1994) J. Biol. Chem. 269:6511-6516.

154. Lu, X., Xu, L. and Meissner, G. (1995) J. Biol. Chem. 270:18459-18464.

155. Lytton, J., and Zarain-Hertzberg, A. (1989) J. Biol. Chem. 264:7059-7065.

156. Lytton, J., Westlin, M., Burk, S.E., Shull, G.E., and MacLennan, D.H. (1992) J. Biol. Chem. 267:14483-14489.

157. Lytton, J., Westlin, M., and Hanley, M.R. (1991) J. Biol. Chem. 266:17067-17071.

158. Ma, J. (1995) Biophys. J. 68:893-899.

159. Ma, J., Bhat, M.B., and Zhao, J. (1995) Biophys. J. 69:2398-2404.

160. Ma, J., Fill, M., Knudson, C.M., Cambell, K.P., and Coronado, R. (1988) Science 242:99-102.

161. MacIntosh, D.B., and Ross, D.C. (1988) J. Biol. Chem. 263:12220-12223.

162. Mack, M.M., Zimanyi, I., and Pessah, I.N. (1992) J. Pharmacol. Exp. Ther. 262:1028-1037.

163. MacLennan, D.H. (1970) J. Biol. Chem. 245:4508-4518.

164. MacLennan, D.H., Cambell, K.P., and Reithmeier, R.A.F. (1983) Calcium and Cell Function 4:151-173.

165. MacLennan, D.H., Seeman, P., Iles, G.H., and Yip, C.C. (1971) J. Biol. Chem. 246:2702-2710.

166. MacLennan, D.H., Yip, C.C., Iles, G.H., and Seeman, P. (1972) Cold Spring Harbour Symp. Quant. Biol. 37:469-478.

167. MacLennan, D.L., and Wong, P.T.S. (1971) Proc. Natl. Acad. Sci. USA 68:1231-1235

168. Mahaney, J.E., Froehlich, J.P., and Thomas, D.D. (1995) Biochemistry 34:4864-4879.

169. Makinose, M. (1971) FEBS Lett. 12:269-270.

170. Makinose, M., and Hasselbach, W. (1971) FEBS Lett. 12:271-272.

170a. Marie, V., and Silva, J.E. (1998) J. Cell. Physiol. 175:283-294.

171. Marsili, V., Mancinelli, L., Menchetti, G., Fulle, S., Balgoni, F., and Fano, G. (1992) J. Muscle Res. Cell Motil. 13:511-515.

172. Martonosi, A.N. (1969) J. Biol. Chem. 244:613-620.

173. Marty, I., Robert, M., Villaz, M., De Jongh, K., Lai, Y., Catterall, W.A., and Ronjat, M. (1994) Proc. Natl. Acad. Sci. USA 91:2270-2274.

174. Mayrleitner, M., Timerman, A.P., Wiederrecht, G., and Fleischer, S. (1994) Cell Calcium 15:99-108.

175. McPherson, P.S., and Cambell, K.P. (1993) J. Biol. Chem. 268:19785-19790.

176. Meissner, G. (1975) Biochim. Biophys. Acta 389:51-68.

177. Meissner, G. (1984) J. Biol. Chem. 259:2365-2374.

178. Meissner, G. (1986) J. Biol. Chem. 261:6300-6306.

179. Meissner, G., Darling, E., and Eveleth, J. (1986) Biochemistry 25:236-244.

180. Michalak, M., Dupraz, P. and Shoshan-Barmatz, V. (1988) Biochim. Biophys. Acta 939:587-594.

181. Millman, M.S. and Haynes, D.H. (1979) Biophys. J. 25:26a.

182. Mintz, E., and Guillain, F. (1997) Biochim. Biophys. Acta 1318:52-70.

183. Mitchell, R.D., Palade, P., Saito, A., and Fleischer, S. (1988) Methods Enzym. 157:51-68.

184. Mitchell, R.D., Simmerman, H.K., and Jones, L.R. (1988) J. Biol. Chem. 263:1376-1381.

185. Miyamoto, H., and Racker, E. (1981) FEBS Lett. 133:235-238.

186. Morii, H., and Tonomura, Y. (1983) J. Biochem. 93:1271-1285.

187. Moutin, M.J., and Dupont, Y. (1988) J. Biol. Chem. 263:4228-4235.

188. Murayama, T. and Ogawa, Y. (1992) J. Biochem. 112:514-522.

188a. Murray, B.E., and Ohlendieck (1997) Biochem. J. 324:689-696.

189. Muscatello, U., Andersson-Cedergren, E., Azzone, G.F., and von der Decken, A. (1961) J. Biophysic. And Biochem. Cytol. 10:201.

190. Nabauer, M. and Morad, M. (1990) Am. J. Physiol. 258:C189-C193.

191. Nabauer, M., Callewaert, G., Cleeman, L., and Morad, M. (1989) Science 244:800-803.

192. Nagasaki, K., and Fleischer, S. (1988) Cell Calcium 9:1-7.

193. Nagasaki, K., and Kasai, M. (1983) J. Biochem. 94:1101-1109.

194. Nakai, J., Dirkson, R.T., Nguyen, H.T., Pessah, I.N., Beam, K.B., and Allen, P.D. (1996) Nature 380:72-75.

195. Nelson, T.E., and Nelson, K.E. (1990) FEBS Lett. 263:292-294.

196. Odermatt, A., Becker, S., Khanna, V.K., Kurzydlowski, K., Leisner, E., Pette, D., and MacLennan, D.H. (1998) J. Biol. Chem. 273:12360-12369.

197. Odermatt, A., Taschner, P.E.M., Khanna, V.K., Busch, H.F.M., Karpati, G., Jablecki, C.K., Breuning, M.H., and MacLennan, D.H. (1996) Nat. Genet. 14:191-194.

198. Odermatt, A., Taschner, P.E.M., Scherer, S.W., Beatty, B., Khanna, V.K., Cornblath, D.R., Chaudhry, V., Yee, W.C., Schrank, B., Karpati, G., Breuning, M.H., Knoers, N., and Maclennan, D.H., (1997) Genomics 45:541-553.

199. Ogawa, H., Stokes, D.L., Sasabe, H., and Toyoshima, C. (1998) Biophys. J. 75:41-52.

200. Ohkura, M., Furukawa, K-I., Fujimori, H., Kuruma, A., Kawano, S., Hiraoka, M., Kuniyasu, A., Nakayama, H., and Ohizumi, Y. (1998) Biochemistry 37:12987-12993.

201. Onishi, S.T. (1979) J. Biochem. (Tokyo) 86:1147-1150.

202. Orchard, C.H., Eisner, D.A., and Allen, D.G. (1983) Nature 304:735-738.

203. Orlova, E.V., Serysheva, I.I., vanHeel, M., Hamilton, S.L., and Chiu, W. (1996) Nat. Struct. Biol. 3:547-552.

204. Orr, I., and Shoshon-Barmatz, V. (1996) Biochim. Biophys. Acta 1283:80-88.

205. Otsu, K., Willard, H.F., Khanna, V.K., Zorzato, F., Green, N.M., and MacLennan, D.H. (1990) J. Biol. Chem. 265:13472-13483.

206. Palade, P. (1987) J. Biol. Chem. 262:6142-6148.

207. Palade, G.E. (1956) J. Biophysic. Biochem. Cytol. 2:85.

208. Pape, P.C., Jong, D.S., and Chandler, W.K. (1995) J. Gen. Physiol. 106:259-336.

209. Pessah, I.N., Francini, A.O., Scales, D.J., Waterhouse, A.L., and Casida, J.E. (1986) J. Biol. Chem. 261:8643-8648.

210. Pessah, I.N., Stambuk, R.A., and Casida, J.E. (1987) Mol. Pharmacol. 31:232-238.

211. Pessah, I.N., Waterhouse, A.L., and Casida, J.E. (1985) Biochem. Biophys. Res. Commun. 128:449-456.

212. Pessah, I.N., and Zimanyi, I. (1991) Mol. Pharmacol. 39:679-689.

213. Plenge-Tellechea, F., Soler, F., and Fernandez-Belda, F. (1997) J. Biol. Chem. 272:2794-2800.

214. Porter, K.R., and Palade, G.E. (1957) J. Biophysic. Biochem. Cytol. 3:269.

215. Radermacher, M., Rao, V., Grassucci, R., Frank, J., Timerman, A.P., Fleischer, S., and Wagenknecht, T. (1994) J. Cell Biol. 127:411-423.

216. Radermacher, M., Wagenknecht, T., Grassucci, R., Frank, J., Inui, M., and Fleischer, S. (1992) Biophys. J. 61:936-940.

217. Reinstein, J., and Jencks, W.P. (1993) Biochemistry 32:6632-6642.

218. Rice, W.J., and MacLennan, D.H. (1996) J. Biol. Chem. 271:31412-31419.

219. Rios, E., and Brum, G. (1987) Nature 325:717-720.

220. Rios, E., Karhanek, M., Ma, J., and Gonzalez, A. (1993) J. Gen. Physiol. 102:449-481.

221. Rios, E., and Pizarro, G. (1991) Physiol. Rev. 71:849-908.

222. Rousseau E., Smith, J.S., Henderson, J.S., and Meissner, G. (1986) Biophys. J. 50:1009-1014.

223. Rousseau, E., Smith, S.J., and Meissner, G. (1987) Am. J. Physiol. 253:C364-C368.

224. Sagara, Y., and Inesi, G. (1991) J. Biol. Chem. 266:13503-13506.

225. Saiki, Y., and Ikemoto, N. (1997) Biochem. Biophys. Res. Commun. 241:181-186.

226. Saiki, Y., and Ikemoto, N. (1999) Biochemistry 38:3112-3119.

227. Schafer, B.W., and Heizmann, C.W. (1996) Trends Biochem. Sci. 21:134-140.

228. Schiefer, A., Meissner, G., and Isenberg, G. (1995) J. Physiol. 489:337-348.

229. Schneider, M.F., and Chandler, W.K. (1973) Nature 242:244-246.

230. Scofano, H.M., Barrabin, H., Lewis, D., and Inesi, G. (1985) Biochemistry 24:1025-1029.

231. Scott, B.T., Simmerman, H.K.B., Collins, J.H., Nadal-Ginard, B., and Jones, L.R. (1988) J. Biol. Chem. 263:8958-8964.

232. Seidler, N.W., Jona, I., Vegh, M., and Martonosi, A. (1989) J. Biol. Chem. 264:17816-17823.

233. Seiler, S., Wegener, A.D., Whang, D.H., Hathaway, D.R., and Jones, L.R.

(1984) J. Biol. Chem. 259:8580-8587.

234. Serysheva, I.I., Orlova, E.V., Chiu, W., Sherman, M.B., Hamilton, S.L., and vanHeel, M. (1995) Nat. Struct. Biol. 2:18-24.

235. Sham, J.S.K., Cleeman, L., and Morad, M. (1995) Proc. Natl. Acad. Sci. USA 92:121-125.

236. Shoshan-Barmatz, V., Hadad, N., Feng, W., Shafir, I., Orr, I., Varsanyi, M., Heilmeyer, L.M.G. (1996) FEBS Lett. 386:205-210.

237. Shoshan-Barmatz, V., Orr, I., Weil, S., Meyer, H., Varsanyi, M., and Heilmeyer, L.M.G. (1996) Biochim. Biophys. Acta 1283:89-100.

238. Shoshan-Barmatz, V., and Zchent, S. (1993) J. Membr. Biol. 133:171-181.

239. Shouten, V.J.A. (1990) J. Physiol. 431:427-444.

240. Simon, B.J., and Hill, D.A. (1992) Biophys. J. 61:1109-1116.

241. Simon, B.J., Klein, M.G., and Schneider, M.F. (1989) Biophys. J. 55:793-797.

242. Sitsapesan, R., and Williams, A.J. (1990) J. Physiol. 423:425-439.

243. Sitsapesan, R., and Williams, A.J. (1995) J. Membr. Biol. 146:133-144.

244. Slupsky, J.R., Onishi, M., Carpenter, M.R., and Reithmeier, R.A.F. (1987) Biochemistry 26:6539-6544.

245. Smith, D.S. (1961) J. Biophysic. Biochem. Cytol. 10:61-87.

246. Smith, G.L., Valdeolmillos, M., Eisner, D.A, and Allen, D.G. (1988) J. Gen. Physiol. 92:351-368.

247. Smith, J.S., Coronado, R., and Meissner, G. (1986) Biophys. J. 50:921-928.

248. Smith, J.S., Coronado, R., and Meissner, G. (1986) J. Gen. Physiol. 88:573-588.

249. Smith, J.S., Imagawa, T., Ma, J., Fill, M., Cambell, K.P., and Coronado, R. (1988) J. Gen. Physiol. 92:1-26.

250. Smith, J.S., Rousseau, E., and Meissner, G. (1989) Circ. Res. 64:352-359.

251. Soler, F., Plenge-Tellechea, F., Fortea, I., and Fernandez-Belda, F. (1998) Biochemistry 37:4266-4274.

252. Spamer, C., Heilmann, C., and Gerok, W. (1987) J. Biol. Chem. 262:7782-7789.

253. Stern, M.D. (1992) Biophys. J. 63:497-517.

254. Strand, M.A., Louis, C.F., and Mickelson, J.R. (1993) Biochim. Biophys. Acta 1175:319-326.

255. Suko, J., Maurer-Fogy, I., Plank, B., Bertel, O., Wyskovsky, W., Hohenegger, M., and Hellman, G. (1993) Biochim. Biophys. Acta 1175:193-206.

256. Sumbilla, C., and Inesi, G. (1987) FEBS Lett. 210:31-36.

257. Sun, X.H., Protasi, F., Takahashi, M., Takeshima, H., Ferguson, D.G., and Franzini-Armstrong, C. (1995) J. Cell Biol. 129:659-671.

258. Sutko, J.L., Ito, K., and Kenyon, J.L. (1985) Fed. Proc. 44:2984-2988.

259. Szegedi, C., Sarkozi, S., Herzog, A., Jona, I., Varsanyi, M. (1999) Biochem. J. 337:19-22.

260. Szent-Gyorgyi, A. (1945) Acta Physiol. Scand. 9:XXV

261. Takasago, T., Imagawa, T., Furukawa, K.I., Ogurusu, T, and Shigekawa, M. (1991) J. Biochem. 109:163-170.

262. Takekura, H., Bennet, L., Tanabe, T., Beam, G., and Franzini-Armstrong, C. (1994) Biophys. J. 67:793-803.

263. Takekura, H., Nishi, M., Noda, T., Takeshima, H., and Franzini-Armstrong, C. (1995) Proc. Natl. Acad. Sci. USA 92:3381-3385.

264. Takeshima, H., Iino, M., Takekura, H., Nishi, M., Kuno, J., Minowa, O., Takano, H., and Noda, T. (1994) Nature 369:556-559.

265. Takeshima, H., Nishimura, S., Matsumoto, T., Ishida, H., Kangawa, K., Minamino, N., Matsuo, H., Ueda, M., Hanuoka, M., Hirose, T. (1989) Nature 339:439-445.

266. Tanabe, T., Mikama, A., Numa, S., and Beam, K.G. (1990) Nature (Lond.) 344:451-453.

267. Tanabe, T., Takeshima, H., Mikami, A., Flockerzi, V., Takehashi, H., Kangawa, K., Kojima, M., Matsuo, H., Hirose, T., and Numa, S. (1987) Nature 328:313-318.

268. Tanaka, M., Ozawa, T., Maurer, A., Cortese, J.D., and Fleischer, S. (1986) Arch. Biochem. Biophys. 251:369-378.

269. Timerman, A.P., Jayaraman, T., Wierderrecht, G., Marks, A.R., and Fleischer, S. (1994) Biochem. Biophys. Res. Commun. 198:701-706.

270. Timerman, A.P., Wiederrecht, G., Marcy, A., and Fleischer, S. (1995) J. Biol. Chem. 270:2451-2459.

271. Toyoshima, C., Sasabe, H., and Stokes, D.L. (1993) Nature 362:469-471.

272. Treves, S., Scutari, E., Robert, M., Groh, S., Ottolia, M., Prestipino, G., Ronjat, M., and Zorzato, F. (1997) Biochemistry 36:11496-11503.

273. Tripathy, A., and Meissner, G. (1996) Biophys. J. 70:2600-2615.

274. Tripathy, A., Xu, L., Mann, G., and Meissner, G. (1995) Biophys. J. 69:106-119.

275. Valdivia, H.H., Kaplan, J.H., Ellis-Davies, G.C., and Lederer, W.J. (1995) Science 267:1997-2000.

276. Varsanyi, M., and Heilmeyer, Jr, L.M.G. (1979) FEBS Lett. 103:85-88.

277. Varsanyi, M., and Heilmeyer, Jr, L.M.G. (1980) FEBS Lett. 122:227-230.

278. Veratti, E. (1902) Memorie Ist. Lomb., Cl. Di sc., e nat. 19:87-133.

279. Wagenknecht, T., Grassucci, R., Berkowitz, J., Wiederrecht, G.J., Xin, H.B., and Fleischer, S. (1996) Biophys. J. 70:1709-1715.

280. Wagenknecht, T., Grassucci, R., Frank, J., Saito, A., Inui, M., and Fleischer, S. (1989) Nature (Lond.) 338:167-170.

281. Wagenknecht, T., and Radermacher, M. (1995) FEBS Lett. 369:43-46.

282. Wang, J., and Best, P.M. (1992) Nature (Lond.) 359:739-741.

283. Wang, J.P., Needleman, D.H., and Hamilton, S.L. (1993) J. Biol. Chem. 268:20974-20982.

284. Weber, A., Herz, R. and Reiss, I. (1963) J. Gen. Physiol. 46:679-702.

284a. Wictome, M., and Khan, Y.M., East, J.M., and Lee, A.G. (1992) Biochem. J. 310:859-868.

285. Wier, W.G. and Yue, D.T. (1986) J. Physiol. (Lond.) 376:504-530.

286. Witcher, D.R., Kovacs, R.J., Schulman, H., Cefali, D.C., and Jones, L.R. (1991) J. Biol. Chem. 266:11144-11152.

287. Wu, K.D., Lee, W.S., Wey, J., Bungard, D., and Lytton, J. (1996) Am. J.

Physiol. 269:C775-C784.

288. Wyskovsky, W., Hohenegger, M., Plank, B., Hellman, G., Klein, S., and Suko, J. (1990) Eur. J. Biochem. 194:549-559.

289. Xu, L., and Meissner, G. (1998) Biophys. J. 75:2302-2312.

290. Yamada, S., and Ikemoto, N. (1980) J. Biol. Chem. 255:3108-3119.

291. Yamaguchi, M., and Kanazawa, T. (1984) J. Biol. Chem. 259:9526-9531.

292. Yamazawa, T., Takeshima, H., Shimulta, M., and Iino, M. (1997) J. Biol. Chem. 272:8161-8164.

293. Yu, X., Carrol, S., Rigaud, J.L., and Inesi, G. (1993) Biophys. J. 64:1232-1242.

294. Zhang, L., Kelley, J., Schmeisser, G., Kobayashi, Y.M., and Jones, L.R. (1997) J. Biol. Chem. 272:23389-23397.

295. Zorzato, F., Fuji, J., Otsu, K., Phillips, M., Green, N.M., Lai, F.A., Meissner, G., and MacLennan, D.H. (1990) J. Biol. Chem. 265:2244-2256.